Scuola Normale Superiore

Tesi di perfezionamento in Metodi e Modelli per le Scienze Molecolari

New integrated numerical approaches to the Smoluchowski equation for the interpretation of molecular properties in solution phase chemistry

***Candidate*:**
Andrea Piserchia

***Supervisor*:**
Prof. Vincenzo Barone

A.A. 2017/2018

a Maria Francesca e alla mia famiglia,

Abstract

The necessity of a proper modelization of molecular diffusion in solution phase chemistry in order to rationalize properties and observables of the same give rise to the question "which tools from the theoretical chemistry field can be used?". The most commonly used approaches in order to answer this question relies on the usage of stochastic models. Then, depending on the particular conformational dynamics of the studied systems and the time scale on which molecular relaxation phenomena occurs, different models and tools can fit the desired level of description. Among all these approaches I focused on the Smoluchowski equation since its wide application in the theoretical chemistry community and since it well adapts to many diffusion problems in solution phase chemistry. Smoluchowski equation is a partial derivative equation that describes how the probability density of a set of coordinates evolves along time. Once the equation is solved, the probability profiles enclose informations upon specific properties and observables. My research activity in this field focused on new and more general numerical approaches to the solution of Smoluchowski equation with the application to specific case studies of chemical interest.

Initially I have studied a class of methods apt to solve partial derivative differential equations. In particular, the chosen methodology is known as Discrete Variable Representation (DVR). Successively I have used this methodology in order to solve the one-dimensional Smoluchowski equation, in the stochastic processes framework applied to molecular systems. Comparing this method with preexisting ones I have validated this novel approach. This method has been implemented on a FORTRAN code with the aim of having an integrated approach for the solution of the one-dimensional Smoluchowski equation.

Then I focused my research activity on the enhancement of the several physicochemical ingredients that enter into the one-dimensional Smoluchowski equation. In particular I extended an earlier diffusion tensor model including the dependence of the same on a generalized coordinate. Then, applying DVR theory to one-dimensional Smoluchowski equation I gave a more complete and general theoretical scenario of the same. In the framework of stochastic processes applied to molecular systems I have implemented and validated this novel approach.

At last, for what concerns the Smoluchowski equation solved with DVR, I extended

the same formalism to coupled one-dimensional Smoluchowski equations along the same generalized coordinate where there is the possibility of reactive exchanges of population and/or sinking terms between different coupled states. This is of great interest for example in the context of photoexcitations, where one has a population evolving through a ground and an excited state, along a specific coordinate, *e.g.* a twisting coordinate. From the temporal evolution of the probability density of the excited state one can retrieve lifetimes and/or compute the time resolved spectra at different times, etc. This last implementation merge the use of DVR basis with product approximation and diffusion tensor calculation along a generalized coordinate. The result is an integrated computational "black-box" tool in the framework of Gaussian software that give access to the generic user the possibility to study these specific systems of interest.

Contents

List of Figures **v**

List of Tables **vi**

1 Introduction **1**

1.1 Basic concepts of stochastic dynamics and the Smoluchowski equation 1

1.2 Work plan 5

2 Discrete variable representation of Smoluchowski equation using a sinc basis set **7**

2.1 DVR of complicated operators 9

2.2 DVR applied to Smoluchowski equation 10

2.3 Case-study calculations 15

2.3.1 Harmonic potential 15

2.3.2 Bistable potential 17

2.3.3 A chemical case-study 27

2.4 Final remarks 34

3 Variable diffusion tensor along a generalized coordinate **37**

3.1 Computation of generalized coordinate 39

3.2 Modeling of the diffusion tensor 41

3.3 Implementation 46

3.4 Case-study calculations 46

3.5 Final remarks 58

4 General Approach to Coupled Reactive Smoluchowski Equations: Integration and Application of DVR and Generalized Coordinate Methods to Diffusive Problems **61**

4.1 Coupled reactive Smoluchowski equations 64

4.2 Test-case 67

4.3 Application 69

4.4 Final remarks 80

5 Conclusions **83**

A General theory of DVR **85**

B Finite difference scheme **89**

C Rate of internal conversion using adiabatic and diabatic electronic states **91**

D Time resolved emission spectra calculation **95**

List of Figures

2.1 Plot of the harmonic potential 16
2.2 Sketch of a generic bistable potential 19
2.3 Plot of the quartic potential and of the periodic potential . . . 22
2.4 Plot of a general non-symmetric potential 26
2.5 Surface plot of the probability density profile for a specific non-symmetric diffusive problem and check of the convergence to the right equilibrium distribution 28
2.6 Plot of the tristable potentials for the different examined dihaloethanes 30

3.1 Sketch of a generic molecular system used in the diffusion tensor model construction 42
3.2 Sketch of n-butane and cyclopentene molecules 48
3.3 Calculated generalized contributions to diffusion tensor for n-butane molecule performing both a relaxed and a non-relaxed scan 49
3.4 Calculated potential and diffusion for n-butane molecule . . . 51
3.5 Calculated potential and diffusion for cyclopentene molecule . 53
3.6 Sketch of 3-chloro-2-(chloromethyl)toluene and 2,2'-bifuran molecules 54
3.7 Calculated potential and diffusion for 3-chloro-2-(chloromethyl)toluene molecule 55
3.8 Calculated potential and diffusion for 2,2'-bifuran molecule . . 56

4.1 Plot of the survival probability for the examined test-case . . . 68
4.2 Sketch of (N,N-dimethylamino)benzonitrile (DMABN) molecule and starting conformation 70

4.3 Calculated potential energies of ground end excited states of DMABN molecule and oscillator strength 72
4.4 Calculated generalized contribution to diffusion for DMABN molecule and variation of the dipole moment of the excited state 74
4.5 Calculated radiative and non-radiative constants from the excited state to the ground state for DMABN molecule 75
4.6 Surface plot of the probability density profile for DMABN molecule and the same extrapolated at several times 77
4.7 Calculated time resolved emission spectra for DMABN molecule and the same extrapolated at several times 78
4.8 Calculated peak intensities of the DMABN time resolved spectrum along time and mono-exponential fit 79

List of Tables

2.1 Convergence of diffusion operator eigenvalues for the harmonic potential 18
2.2 Convergence of diffusion operator eigenvalues for the symmetric bistable potentials 23
2.3 Convergence of diffusion operator eigenvalues for the non-symmetric bistable potential 25
2.4 Potential parameters used for the different tristable potentials and convergence of the diffusive operator eigenvalues 30
2.5 Calculated equilibrium populations and rate constants for the different examined dihaloethanes 33

Chapter 1

Introduction

1.1 Basic concepts of stochastic dynamics and the Smoluchowski equation

An important class of methods apt to describe molecular processes in condensed phases is that of stochastic methods. The understanding of stochastic dynamics and formal methods for the solution of mathematical equations that describe them are of fundamental importance when dealing with the modelization of solution phase chemistry. In this class of dynamics enters various processes of interest for the generic chemist, such as roto-translational molecular motions in liquid phases, conformational dynamics, collective fluctuations in "soft" materials (*e.g.* biomembranes, liquid crystals), etc. In this view, a simple example of stochastic process can be thought as the conformational dynamics of simple molecules (*e.g.* n-butane) considered as a diffusive motion over a specific torsion angle, taken as the only stochastic variable of the problem. [1, 2]

Given a dynamical system, a stochastic process is the time evolution of an ensemble of variables $\boldsymbol{X}(t)$ (characteristics of the system) under the eventual action of deterministic forces and "stochastic" forces due to the random interaction with the surrounding. In the chemist's practice, $\boldsymbol{X}(t)$ is typically a collection of positional, orientational, internal degrees of freedom of single molecules, and the stochastic component is modeled as a "Gaussian

white noise" resulting from the collisions with surrounding molecules (thermal bath). Such dynamics is named Brownian motion and it is described by Langevin equation. This equation is the prototype of differential stochastic equations, where the force experienced by the system under study is given by the sum of three main contributes: two deterministic contributes, one arising from the potential that generates a force field and the other of dissipative kind coming from the friction that damps the motion and then a stochastic contribution given by the fluctuating forces.

The numerical integration of Langevin equation generates a stochastic trajectory for the $\boldsymbol{X}(t)$ variables that it is different each time even when starting from the same initial conditions. This loss of determinism is such that in order to describe the dynamical process it is preferable to adopt a probabilistic treatment, where the quantity of interest is the non-equilibrium probability distribution (or density) $p(\boldsymbol{X}, t)$; the product $p(\boldsymbol{X}, t)\ \delta\boldsymbol{X}$ gives the probability that the system is in a state $\boldsymbol{X}(t)$, when it is observed at time t, included in the interval of amplitude $\delta\boldsymbol{X}$ and centered in $\boldsymbol{X}$. Obviously, it is necessary to give an initial condition, that is the time-zero distribution $p(\boldsymbol{X}, 0)$ that specifies how the system has been "prepared" (or that says in which configuration it has been "seen" at such initial moment).

Along time, $p(\boldsymbol{X}, t)$ evolves under a specific law. Hereafter we shall consider a particular category of physical systems, and precisely the systems that are macroscopically at thermal equilibrium. In this case, the stochastic process is of stationary kind, that is, $p(\boldsymbol{X}, t)$ admits limit-profile reached over infinitely long times, and this limit-profile is unique and corresponds to the Boltzmann equilibrium distribution $\lim_{t\to+\infty} p(\boldsymbol{X}, t) = p_{eq}(\boldsymbol{X})$. Other than stationary, we shall assume that the process is of Markov type, *i.e.* in order to know the actual state of the system, it is necessary to know the state just at the previous instant. In other words, dynamics is assumed to have no memory effects. It can be shown that this is coherent with the adopted stochastic noise (the white noise) [3, 4]. Finally we shall further restrict the field considering a stationary Markov diffusive process. In order to consider a stochastic as diffusive, it is necessary that:

- the local friction must be sufficiently high (this is known as "over-

damped" regime);

- the system is observed at sufficiently long time intervals.

the first two conditions are equivalent to assume that inertial effects of dynamics are negligible (*i.e.* we ignore momenta and angular momenta). The second condition corresponds in practice to use a "slow" investigative experimental technique to observe dynamics; from here it can be understood that the transition from a dynamical regime to the other (from non-diffusive to diffusive) is related with the time scale between two consecutive observations of the system. In case of diffusive regime of motion, that is legitimately adoptable for molecular dynamics in condensed fluid phases at ordinary temperatures, the only relevant coordinates $\boldsymbol{X}$ are configurational ones (positions, orientations, internal conformations of molecules, etc.). Indeed, using projective methods [5] conjugated momenta are eliminated treating them as fast variables that rapidly lose correlation with the values assumed in previous instants, while the configurational variables are slow because of correlation loss over longer time scales. Evolution of $p(\boldsymbol{X}, t)$ is governed by the Smoluchowski equation [5], introduced in the following. Diffusion description of stochastic processes via the Smoluchowski equation has found widespread application in chemistry, in particular to describe kinetic processes that are diffusive in nature where fluctuations play an important role, and proper probabilistic modelization is needed [6]. This time-dependent partial derivative equation belongs to the wider class of Fokker-Planck equations that are used to model numerous systems in physics, chemistry, biology, finance and other research fields [3].

From hereafter we shall treat our case of interest that is the one-dimensional Smoluchowski equation where $\boldsymbol{X}$ reduces to a single variable x. In this case the Smoluchowski equation reads

$$\frac{\partial}{\partial t}\, p(x,t) = -\Gamma\, p(x,t) \tag{1.1}$$

with

$$\Gamma = -\frac{\partial}{\partial x}\, D(x)\, p_{eq}(x)\, \frac{\partial}{\partial x}\, p_{eq}^{-1}(x) \tag{1.2}$$

This is a partial derivative differential equation: of the first order with respect to time t and of the second order with respect to x. Derivatives with respect to x appear in the evolution operator Γ, in which enter two fundamental physical ingredients: the energetics of the system, that is introduced with the equilibrium distribution $p_{eq}(x)$ and the dissipative term, that is represented by the diffusion coefficient $D(x)$, typically coordinate dependent. This last one is related to local friction by the Einstein's fluctuation-dissipation Theorem [5]

$$D(x) = \frac{k_B T}{\xi(x)} \tag{1.3}$$

in which $\xi(x)$ is the friction coefficient dependent itself by medium viscosity and from molecular geometry. We point out that Smoluchowski equation can be intended as the extension of the "common" translational diffusion equation that regulates the matter transport in fluid phases at rest (Fick's Law) to generic stochastic variables cases. We also point out that eqn. (1.1) is isomorphic to Schrödinger equation concerning wave functions in quantum mechanics, *i.e.* the two equations have an analogous mathematical structure. This suggests that also solution methods can have affinities.

As a last remark, we stress that Smoluchowski equation is valid in the limit of high friction regime. This is a valid assumption for chemical systems presented throughout the next Chapters. By the way, this assumption is not always valid and other equations must be invoked in order to properly describe the time evolution of the probability density, *e.g.* Fokker-Planck, Kramers-Klein, generalized Langevin equations. As stated before, both the selected timescale Δt, on which the dynamics is observed and friction play an important role in discriminating whether the dynamics is diffusive or not. In particular, the dynamics of the system must be observed at "sufficiently long" time intervals. This means not too long time intervals to undermine the mathematical approximation that underlies Fokker-Planck and Smoluchowski equations, that is $\Delta t \to 0$, and not too short, otherwise the evolution of "fast" variables wouldn't be negligible. In other words, given a set of stochastic variables $\boldsymbol{X}$, only if a particular subset of "slow" variables $\boldsymbol{X}^{\mathrm{S}} \subseteq \boldsymbol{X}$ is isolated and their dynamics is observed at "sufficiently

long" time intervals, the dynamics appears diffusive with good approximation. The other variables of the set $\boldsymbol{X}^{\mathrm{F}}$, are the so called "fast" ones, and they can be eliminated in order to describe the probabilistic evolution of the system if observed in such timescale, because they are "redundant"[1]. The formal method in order to operate such $\boldsymbol{X}^{\mathrm{F}}$ variables elimination, passing from the Fokker-Planck equation to the Smoluchowski equation[2], is the so called Mori-Zwanzig projective method [5]. In the common practice, the choice of the "slow" variables subset is driven by chemical intuition. Whenever the diffusive regime and/or the Markovian properties of the stochastic variables are no longer verified, the validity of the Smoluchowski equation breaks down. This is evident by numerical anomalies that arise when solving the correspondent Smoluchowski equation in non diffusive regime and/or with non Markovian variables. Several examples of the application of the Smoluchowski equation apt to describe femtosecond dynamics probed with fast experimental techniques are present in the literature starting from the earlier works of the eighties on femtosecond dynamics of geminate pair recombination, internal twisting of fluorescent species, etc. [7, 8, 9, 10, 11].

1.2 Work plan

In this introductive Chapter we made a rapid overview over the basic concepts of stochastic dynamics. Based on these premises on the next Chapter we shall start with the presentation of a new general framework for solving the one-dimensional Smoluchowski equation using a discrete variable repre-

[1] As an example, for the Brownian motion of a particle of mass m that experiences a translational friction ξ it can be shown that if the dynamics is observed over a timescale $\Delta t \gg \frac{m}{\xi}$, the dynamics is diffusive on the positional variable $\boldsymbol{r}$ (that is $\boldsymbol{X}^{\mathrm{S}} \equiv \boldsymbol{r}$), while the velocity ($\boldsymbol{X}^{\mathrm{F}} \equiv \boldsymbol{v}$) can be eliminated because it is "redundant". In the time interval Δt the velocity loses memory (time correlation) of its initial conditions. In other words $\boldsymbol{r}$ is a variable that evolves slowly, while $\boldsymbol{v}$ is subjected to rapid fluctuations (with $\boldsymbol{r}$ essentially fixed) due to the stochastic noise because of the interaction with the thermal bath and such to produce a memory loss of the initial state. If $\boldsymbol{X}^{\mathrm{F}} \equiv \boldsymbol{v}$ is relevant, we are in the so called "underdamped regime" or "low friction regime", and in this situation Kramers-Klein equation must be used in order to describe the system dynamics.

[2] And so passing from the original Fokker-Planck operator $\Gamma_{\boldsymbol{X}}$ to the reduced Smoluchowski operator $\Gamma_{\boldsymbol{X}^{\mathrm{S}}}$.

sentation (DVR) based on the so called sinc basis set. The reliability of our implementation is assessed by comparing the convergence of diffusive operator eigenvalues calculated using our method and using a simple finite difference scheme for some model diffusive problems. Then in Chapter 3 a generalization to arbitrary large amplitude motions of a recent approach to the evaluation of diffusion tensors is presented and is implemented in a widely available package for electronic structure computations. A fully black-box tool is obtained, which, starting from the generation of geometric structures along different kinds of paths, proceeds toward the evaluation of an effective diffusion tensor and to the solution of the one-dimensional Smoluchowski equations by means of DVR numerical approach presented in Chapter 2. Application to a number of case studies shows that the results issuing from our approach are identical to those delivered by previous software (in particular DiTe) for rigid scans along a dihedral angle, but can be improved by employing relaxed scans (*i.e.*, constrained geometry optimizations) or even more general large amplitude paths. In Chapter 4 a new and more general approach to diffusion problems with the inclusion of reactivity among different coupled diffusional states is rationalized and presented. The result is a system of coupled Smoluchowski equations. The two main developments presented in the previous Chapters are combined and implemented in a software package tool allowing the generic user to set up and run diffusional calculations along a generalized coordinate with very low efforts. We show the applicability of the whole framework to a generic diffusional case of chemical interest that is the study case of (N, N-dimethylamino)benzonitrile (DMABN) fluorescence, whose excited state undergoes twisted intramolecular charge transfer (TICT) relaxation. The population dynamics of the excited state coupled to the ground state is followed, and fluorescence decay spectrum is calculated. Finally in Chapter 5 some perspectives for further advancements are provided.

Chapter 2

Discrete variable representation of Smoluchowski equation using a sinc basis set

The mathematical structure of the Smoluchowski equation (1.1) is similar to Schrödinger's equation and this suggests analogous solution methods to solve it. The most common approaches in current use are finite-difference methods in space and time [12], and basis set expansions [13]. In the first kind of approaches one follows the evolution of the probability density $p(x,t)$ using finite difference approximations in x and t. On the other hand, the second class of methods is based on the projection of the time evolution operator upon a conventional basis of orthogonal functions, typically referred to as a spectral basis. Once constructed, the matrix representation of the operator Γ is diagonalized in order to find the eigenvalues spectrum and then to calculate the time propagation.

A third class of methods that seems to straddle the boundary between grid discretization and basis function expansion are the so called pseudospectral methods which use functions that are localized on a grid in coordinate space. Among these methods, discrete variable representation (DVR) has enjoyed great success as highly accurate representation for the solution of a variety of problems in molecular vibration-rotation spectroscopy, reactive scatter-

ing, etc... [14, 15, 16, 17, 18] It is a well known numerical method within the quantum chemistry community for solving time-dependent Schrödinger's equation [19], while, to the best of our knowledge, this method has not yet seen widespread use in the "classical" community.

To construct a DVR, a finite basis of orthonormal functions, typically classical orthogonal polynomials or Fourier basis, is transformed to another orthonormal basis set (the DVR) in which each basis function is localized about one point of a coordinate space grid [20]. Those points are their associated grids of Gaussian quadrature points that, in the case of classical orthonormal polynomials, coincide with their roots. The advantages of using DVRs are the fact that they solve the problem of integral evaluation, because there are no integrals to evaluate, and the fact that they produce diagonal representations of coordinate functions (like the potential in Schrödinger's equation); while for derivative operators (such as kinetic energy) they usually produce analytical representations, depending on the starting basis set [14, 21].

The real power of DVRs becomes evident in multidimensional problems, where the calculation of the operator's matrix representation is very cheap and for complicated operators, *i.e.* operators whose terms involve both (non-commuting) derivatives and functions of coordinate, where it is possible, in some instances, to use the product approximation [16, 20].
This last aspect, as it will be pointed out in the next Section, is especially significant in connection with the Smoluchowski diffusion operator. In this first exploration we shall focus our attention on one-dimensional problems of the general coordinate x, and we shall treat only bound potentials. DVR is used to approximate $p(x,t)$ and the time evolution operator, using a uniform grid in the coordinate x for which the corresponding basis set is a Fourier basis (also known as sinc methods).

In the next Section we provide both a rapid overview of the theory behind DVR of complicated operators, and the details on how to apply it to Smoluchowski equation; in Section 2.3 we show the application of the method to some specific familiar diffusion problems, and we make a comparison with another method, a simple finite difference (FD) scheme. After we have val-

idated the new method we apply it to a chemical case-study represented by the diffusive torsion dynamic of some simple molecules. A short review of DVR theory is proposed in Appendix A, and the FD scheme that will be employed is reported in Appendix B.

2.1 DVR of complicated operators

DVRs are representations in bases of continuous functions which are in some sense localized "on a grid" in coordinate space. They are usually obtained by transformation from a truncated global basis, *i.e.* to construct a DVR, a finite basis of "global" orthonormal functions (typically orthogonal polynomials or Fourier basis) is transformed to another orthonormal basis set (the DVR) in which each basis function is "localized" about one point of a coordinate space grid $\{x_i\}$. The mathematical theory that underlies DVR and how they are constructed is well reported in the classical works of Light, Bačić and coworkers [20, 22, 23]. In order to not make heavier the reading, we have summarized this theory in Appendix A, where we address the interested Reader which might be unfamiliar with the general theory of DVR.

The essential feature of DVR is that we have a set of N basis functions $\{\theta_i(x)\}$ with the properties

$$\theta_i(x_j) = \sqrt{w'_j}\,\delta_{ij} \tag{2.1}$$

for a set of N points x_j and weights w'_j ($w'_j \equiv \sqrt{\frac{w(x_j)}{w_j}}$, cfn. eqn. (A.13) in Appendix A), and

$$\langle\theta_i|\theta_j\rangle = \int_a^b dx\,\theta_i(x)\,\theta_j(x) = \delta_{ij} \tag{2.2}$$

for an interval $[a, b]$ that contains all of the x_j.
DVRs are generally used with the approximation that the matrix representation of a general function of the coordinate is diagonal and the diagonal matrix elements are simply the values of the function at the DVR points (see

eqn. (A.14) in Appendix A).

For simple operators as $\frac{d^n}{dx^n}$, the DVR matrix $\mathbf{D}^{(n)\,\mathrm{DVR}}$ (with elements $D_{ij}^{(n)\,\mathrm{DVR}} = \langle\theta_i|\frac{d^n}{dx^n}|\theta_j\rangle$) is determined from transformation matrices and exact matrix representations of one-dimensional operators in the original "delocalized" polynomial basis set. Of course, changing the global starting basis set (*e.g.* Legendre, Laguerre, Hermite polynomials, Fourier basis, etc...) will result in different $\mathbf{D}^{(n)\,\mathrm{DVR}}$. For $n = 1, 2$ see refs. [14, 21]. However, for complicated operators, *e.g.* $\Xi = \frac{d}{dx}F(x)\frac{d}{dx}$, with $F(x)$ a rational function, for which matrix elements of terms or factors with derivatives must be calculated numerically, defining a DVR is harder.

A DVR can be defined from a finite basis representation (FBR) where matrix elements of terms or factors in the complicated operator are computed by quadrature, but this step undermines the simplicity and convenience of the DVR. One may bypass quadrature by replacing the matrix representation of the whole operator with a product of matrix representations, making use of approximate resolution of the identity. This approach is usually referred to as *product approximation* and it reads:

$$\langle\theta_i|\Xi|\theta_j\rangle = \sum_{k,l=1}^{N} \langle\theta_i|\frac{d}{dx}|\theta_k\rangle\langle\theta_k|F(x)|\theta_l\rangle\langle\theta_l|\frac{d}{dx}|\theta_j\rangle \tag{2.3}$$

or in matrix form

$$\mathbf{\Xi}^{\mathrm{DVR}} = \mathbf{D}^{(1)\,\mathrm{DVR}}\,\mathbf{F}^{\mathrm{DVR}}\,\mathbf{D}^{(1)\,\mathrm{DVR}} \tag{2.4}$$

where $\mathbf{F}^{\mathrm{DVR}}$ is diagonal, $(\mathbf{F}^{\mathrm{DVR}})_{ij} = F(x_i)\,\delta_{ij}$. In some instances this approximation can spoil the Hermiticity of the operator; this will be seen in the next Section.

2.2 DVR applied to Smoluchowski equation

In the high-friction regime (also called *overdamped* regime) the Fokker-Planck equation simplifies into the Smoluchowski equation (eqns. (1.1, 1.2)).

Here, for convenience, we recall it for one spatial dimension x,

$$\frac{\partial}{\partial t}\, p(x,t) = \frac{\partial}{\partial x}\, D(x)\, p_{eq}(x)\, \frac{\partial}{\partial x}\, p_{eq}^{-1}(x)\, p(x,t) = -\Gamma\, p(x,t) \tag{2.5}$$

As stated in the Introduction, $D(x)$ is a space-dependent diffusion coefficient and $p(x,t)$ is the probability density of finding a value of x at time t, with stationary limit $\lim_{t\to+\infty} p(x,t) = p_{eq}(x)$. In this case

$$p_{eq}(x) = \frac{e^{-\beta V(x)}}{Z} \tag{2.6}$$

is the canonical (Boltzmann) distribution, for the potential $V(x)$; with $\beta = 1/k_B T$ the Boltzmann factor and $Z = \int dx\, e^{-\beta V(x)}$ the partition function; Γ is the *diffusion operator*. In particular, we shall take in consideration only bound potentials, *i.e.* $V(x)$ goes to infinity at the endpoints of the domain, such that it's always possible to define $p_{eq}(x)$. Consequently we shall treat only cases with reflective or periodic boundary conditions.

It is more convenient to deal with Hermitian operators, so we will consider the symmetrized form of the diffusion operator Γ. To this scope we multiply both members of eqn. (2.5) by $p_{eq}^{-1/2}(x)$; defining $\widetilde{p}(x,t) = p_{eq}^{-1/2}(x)\, p(x,t)$

$$\frac{\partial}{\partial t}\, \widetilde{p}(x,t) = -\widetilde{\Gamma}\, \widetilde{p}(x,t) \tag{2.7}$$

and

$$\begin{aligned} \widetilde{\Gamma} &= p_{eq}^{-1/2}(x)\, \Gamma\, p_{eq}^{1/2}(x) \\ &= -p_{eq}^{-1/2}(x)\, \frac{\partial}{\partial x}\, D(x)\, p_{eq}(x)\, \frac{\partial}{\partial x}\, p_{eq}^{-1/2}(x) \end{aligned} \tag{2.8}$$

The eigenvalues $\{\lambda_i\}$ associated to $\widetilde{\Gamma}$ are all real and the fact that diffusion $D(x)$ is a positive function, assures that they are all positive. They regulate the time evolution of $p(x,t)$, describing the correct relaxation till the equilibrium state for a given initial distribution $p(x,0)$. In particular, the presence of a unique null eigenvalue $\lambda_0 = 0$ guarantees the existence of the equilibrium state while the positivity of the others guarantees to reach it; in

fact λ_0 is associated to the eigenfunction $p_{eq}^{1/2}(x)$, indeed $\widetilde{\Gamma}\, p_{eq}^{1/2}(x) = 0$. The eigenvalues $\{\lambda_i\}$ have physical dimension of rates (inverse of time), and in the case of diffusive dynamics under the influence of a potential $V(x)$ that presents sufficiently deep wells separated by an energy gap, we can associate to small λ_i values "jump" processes between wells (*i.e.* slow activated processes where it is required to overpass the energy gap); high λ_i values can be associated, instead, to fluctuation processes inside the wells (fast processes). This aspect will be examined in Section 2.3.2, when we treat the bistable potential.

At this point we can construct $\widetilde{\mathbf{\Gamma}}^{\mathrm{DVR}}$ matrix using an ordinary product approximation (as seen in Section 2.1); considering for brevity $M(x) = D(x)\, p_{eq}(x)$

$$\widetilde{\mathbf{\Gamma}}^{\mathrm{DVR}} = -\mathbf{P}_{eq}^{-1/2\,\mathrm{DVR}}\, \mathbf{D}^{(1)\,\mathrm{DVR}}\, \mathbf{M}^{\mathrm{DVR}}\, \mathbf{D}^{(1)\,\mathrm{DVR}}\, \mathbf{P}_{eq}^{-1/2\,\mathrm{DVR}} \tag{2.9}$$

As already mentioned, in some instances use of the product approximation can spoil the Hermiticity of the operator and of course, this problem may arise also in many dimensions. In this case we can see that depending on the chosen DVR basis functions, if $\mathbf{D}^{(1)\,\mathrm{DVR}}$ is not anti-Hermitian, $\widetilde{\mathbf{\Gamma}}^{\mathrm{DVR}}$ will not be Hermitian. In order to obtain an Hermitian DVR of the symmetrized diffusion operator by invoking the product approximation one must write $\widetilde{\mathbf{\Gamma}}^{\mathrm{DVR}}$ in the explicitly Hermitian form [16]

$$\check{\Gamma} = p_{eq}^{-1/2}(x)\, \left(\frac{\partial}{\partial x}\right)^{\dagger}\, M(x)\, \frac{\partial}{\partial x}\, p_{eq}^{-1/2}(x) \tag{2.10}$$

where $(\frac{\partial}{\partial x})^{\dagger} = \overleftarrow{\frac{\partial}{\partial x}}$ and the arrow denotes differentiation to the left. With this last expedient we have guaranteed Hermiticity to the operator, and in DVR it will be:

$$\check{\mathbf{\Gamma}}^{\mathrm{DVR}} = \mathbf{P}_{eq}^{-1/2\,\mathrm{DVR}}\, (\mathbf{D}^{(1)\,\mathrm{DVR}})^{\dagger}\, \mathbf{M}^{\mathrm{DVR}}\, \mathbf{D}^{(1)\,\mathrm{DVR}}\, \mathbf{P}_{eq}^{-1/2\,\mathrm{DVR}} \tag{2.11}$$

On the other hand, even if this procedure looks easy and straightforward, at the computational level it may cause some problems. In particular, when

dealing with bound potentials (as in our case), the high values of $V(x)$ at the endpoints and inside the x domain (if present) generate numerical instability with great ease, due to the computation of $p_{eq}(x) \propto \exp(-\beta V(x))$. It is more convenient to consider the alternative form of the symmetrized operator

$$\widetilde{\Gamma} = -D(x)\left[\frac{\partial^2}{\partial x^2} + \frac{1}{2}\frac{\partial^2 V(x)}{\partial x^2} - \frac{1}{4}\left(\frac{\partial V(x)}{\partial x}\right)^2\right] - \frac{\partial D(x)}{\partial x}\frac{\partial}{\partial x} - \frac{1}{2}\frac{\partial D(x)}{\partial x}\frac{\partial V(x)}{\partial x} \tag{2.12}$$

obtained from eqn. (2.8) using eqn. (2.6) and setting out derivatives. Employing again the product approximation is straightforward, because derivatives of the potential and diffusion are simple functions of x and consequently their DVR matrices are diagonal. One has only to carry about DVR of derivative operators terms, $\mathbf{D}^{(1)\,\mathrm{DVR}}$ and $\mathbf{D}^{(2)\,\mathrm{DVR}}$ in this case. The great advantage of using this way, instead of eqn. (2.11), is that one can manage great values of $V(x)$ with no numerical problems, but the drawback is that both $\mathbf{D}^{(1)\,\mathrm{DVR}}$ and $\mathbf{D}^{(2)\,\mathrm{DVR}}$ must be Hermitian in order to have $\widetilde{\mathbf{\Gamma}}^{\mathrm{DVR}}$ to be Hermitian as well. This requirement is fulfilled using sinc-DVR (that is constructed in turn on Fourier basis, see Subsection "sinc-DVR" in Appendix A) [14, 15], but not using other DVRs [21].

Following Colbert and Miller [14], we consider probability densities $p(x,t)$ that are defined on a grid consisting of $N-1$ equally spaced grid points $\{x_i\}$ on the range $[a,b]$

$$x_i = a + i\frac{(b-a)}{N}, \qquad i = 1, \ldots, N-1 \tag{2.13}$$

In this case the weights coincide simply with $\Delta x = \frac{b-a}{N}$, the grid spacing and the corresponding DVR-functions are sinc functions

$$\theta_i(x) = \frac{1}{\sqrt{\Delta x}}\,\mathrm{sinc}\left[\frac{\pi\,(x-x_i)}{\Delta x}\right] = \sqrt{\Delta x}\,\frac{\sin(\pi\,(x-x_i)/\Delta x)}{\pi\,(x-x_i)} \tag{2.14}$$

These functions are "localized" on the grid points; indeed they are equal to $\frac{1}{\sqrt{\Delta x}}$ for $x = x_i$ and zero for $x = x_j$, $j \neq i$.

In the case of reflective boundary conditions the associated $N-1$ (FBR) functions for a uniform grid are the particle-in-a-box eigenfunctions

$$\phi_m(x) = \sqrt{\frac{2}{b-a}} \sin\left[\frac{m\pi(x-a)}{b-a}\right], \qquad m = 1, \ldots, N-1 \tag{2.15}$$

where the range has to be taken in the mathematical limit $a \to -\infty, b \to +\infty, N \to +\infty$. The DVR elements of the two derivative operators are given by [14, 15]

$$(\mathbf{D}^{(1)})_{ij} = \begin{cases} 0 & i = j \\ \frac{1}{\Delta x} \frac{(-1)^{i-j}}{i-j} & i \neq j \end{cases} \tag{2.16}$$

$$(\mathbf{D}^{(2)})_{ij} = \begin{cases} -\frac{1}{3}\frac{\pi^2}{\Delta x^2} & i = j \\ -\frac{2}{\Delta x^2} \frac{(-1)^{i-j}}{(i-j)^2} & i \neq j \end{cases} \tag{2.17}$$

On the other hand, in the case of periodic boundary conditions in the generic range $[a, b]$, the appropriate basis functions are [2]

$$\phi_m(x) = \frac{e^{\frac{i2mx}{b-a}}}{\sqrt{b-a}}, \qquad m = 0, \pm 1, \pm 2, \ldots, \pm N \tag{2.18}$$

and the $2N+1$ grid points are

$$x_i = i\frac{b-a}{2N+1}, \qquad i = 1, \ldots, 2N+1 \tag{2.19}$$

The matrix elements for the first and second derivatives has been derived and evaluated using procedures analogous to those presented by Colbert and Miller [14], and the expressions are

$$(\mathbf{D}^{(1)})_{ij} = \begin{cases} 0 & i = j \\ \frac{\pi}{b-a} \frac{(-1)^{j-i}}{\sin[\pi(j-i)/(2N+1)]} & i \neq j \end{cases} \tag{2.20}$$

$$(\mathbf{D}^{(2)})_{ij} = \begin{cases} -\frac{4\pi^2}{(b-a)^2} \frac{N(N+1)}{3} & i = j \\ -\frac{2\pi^2}{(b-a)^2} \frac{(-1)^{j-i} \cos[\pi(j-i)/(2N+1)]}{\sin^2[\pi(j-i)/(2N+1)]} & i \neq j \end{cases} \tag{2.21}$$

Using these expressions, once the bound potential $V(x)$ and the diffusion coefficient $D(x)$ are given, $\widetilde{\mathbf{\Gamma}}^{\mathrm{DVR}}$ is easily constructed using product approx-

imation on eqn. (2.12). Then, eigenvalues and eigenfunctions are calculated from the numerical diagonalization of $\widetilde{\mathbf{\Gamma}}^{\mathrm{DVR}}$. Given the initial distribution $p(x,0)$, the profile $p(x,t)$ is built expanding upon DVR functions calculated at DVR points $\{x_i\}$ for which θ_i's are equal to $\frac{1}{\sqrt{\Delta x}}$, cfn. eqns. (2.1, 2.14).

2.3 Case-study calculations

In this Section, we apply the methodology sketched in the preceding Section to some diffusive test problems described with Smoluchowski equation, considering different potentials and the effect of a constant or variable diffusion coefficient. Our objective is to determine the eigenvalues (λ^{DVR} in the following) of the DVR diffusion operator matrix $\widetilde{\mathbf{\Gamma}}^{\mathrm{DVR}}$, calculated using sinc-DVR with product approximation on eqn. (2.12) as shown in the previous Section. In particular we shall focus on three different kinds of potentials, namely the analytic case of harmonic potential and the well known case of bistable potential with equivalent and nonequivalent minima that is usually adopted in the modelization of numerous chemical problems. In order to illustrate the validity of the method we concentrate on the eigenvalue convergence, *i.e.* how many grid points (N_{points} in the following) are necessary for sinc-DVR to provide accurate first eigenvalues in order to have a reliable description of the system. We compare them with analytic results (where possible) or with values calculated by other methods, in particular, a simple finite difference (FD) scheme (reported in Appendix B), λ^{FD} in the following. We remark that for reflective boundary conditions $N_{\mathrm{points}} \equiv N - 1$ while for periodic ones $N_{\mathrm{points}} \equiv 2N + 1$ (see Section 2.2); from now on the potential $V(x)$ is expressed in $k_B T$ units.

2.3.1 Harmonic potential

It is always convenient to make reference to analytic cases when a new method is tested. One of these is the one-dimensional diffusion problem over a parabolic potential, shown in Figure 2.1, with a constant diffusion

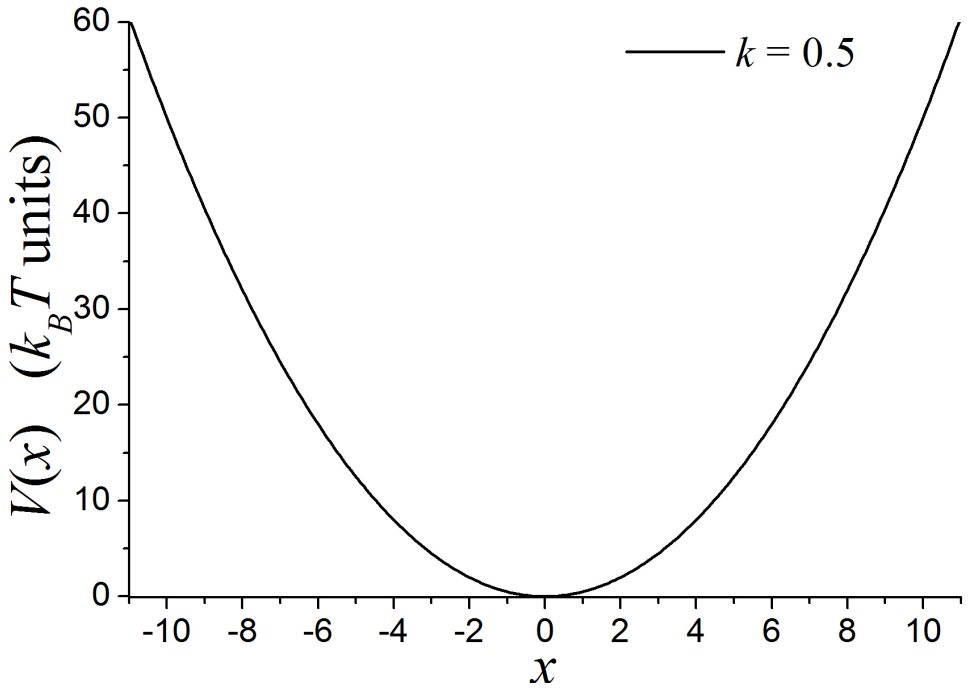

Figure 2.1: Plot of the harmonic potential used in our calculations, eqn. (2.22).

coefficient $D(x) = D$, also known as Ornstein-Uhlenbeck process [24, 25]

$$V(x) = \frac{1}{2}kx^2 \tag{2.22}$$

Here, x is defined over the entire real axis and k denotes the force constant; the axes origin is chosen such as to coincide with the potential minimum. Physically this case can be used to describe the local oscillatory dynamic of molecules in a certain phase (*e.g.* a molecule fluctuating in a layer of a smectic liquid crystal phase). Boundary conditions are reflective and eigenvalues are simply[1]

$$\lambda_m = mkD, \qquad m = 0, 1, 2, \ldots \tag{2.23}$$

with the null eigenvalue λ_0 associated to the stationary solution

[1]The diffusion operator eigenfunctions in this case are simply given by Hermite polynomials multiplied by the equilibrium distribution.

$$p_{eq}(x) = \frac{e^{-V(x)}}{\int_{-\infty}^{+\infty} dx\ e^{-V(x)}} = \sqrt{\frac{k}{2\pi}} e^{-\frac{kx^2}{2}} \tag{2.24}$$

The x range for calculations is chosen following the proposal of Colbert and Miller [14], that is, introducing an energy cutoff V_{cutoff} for the potential energy and discarding grid points for which:

$$V(x_i) > V_{\text{cutoff}} \tag{2.25}$$

i.e. where the probability density $p(x,t)$ would be negligibly small. Practically, we accomplish this by choosing a range for which the gap: potential at the endpoints/potential at the global minima is less than 50 $k_B T$ units. Convergence of the calculation can also be checked by increasing the energy cutoff, but for the sake of simplicity and since we have chosen a large enough V_{cutoff}, this will not be discussed.

In Table 2.1 we report the convergence of the first ten nonzero eigenvalues calculated with DVR method, given in diffusion coefficient units (that is equivalent to have taken $D = 1$, *i.e.* D is a scaling factor for the eigenvalues) and shown up to five significant figures, for $k = 1.0$ and x range $[-10.0, 10.0]$. We compare them with the ones calculated using the FD scheme. As it can be easily seen, the convergence is more rapid using DVR instead of FD; in particular for $N_{\text{points}} > 26$ we are just at convergence, while for FD, more than 65 and more than 210 grid points are required in order to have respectively λ_1^{FD} and λ_{10}^{FD} converged up to five significant figures.

2.3.2 Bistable potential

Another suitable model to test the DVR method, is the well known bistable potential, that has the general shape sketched in Figure 2.2: two minima a and c respectively, separated by a potential maximum b and bound at the endpoints. There are several examples of bistable systems, those analyzed most often in the literature being the laser, the tunnel diode [26], and more generally activated reactions, *e.g.* hindered rotations. A more recent example currently studied and continuously under intensive investiga-

Table 2.1: Convergence of the first ten nonzero eigenvalues, given in diffusion coefficient units and shown up to five significant figures, for the harmonic potential, eqn. (2.22), with $k = 1.0$ and x range $[-10.0, 10.0]$, calculated with DVR method and FD scheme, respectively, λ^{DVR} and λ^{FD}.

N_{points}	λ_1^{DVR}	λ_2^{DVR}	λ_3^{DVR}	λ_4^{DVR}	λ_5^{DVR}	λ_6^{DVR}	λ_7^{DVR}	λ_8^{DVR}	λ_9^{DVR}	$\lambda_{10}^{\mathrm{DVR}}$
6	0.63371	4.4689	4.5375	12.655	12.677					
8	0.76420	2.9013	3.0612	7.8742	7.9163	15.303	15.323			
10	0.92271	2.2799	2.6542	5.6605	5.7480	10.624	10.658	17.280	17.300	
12	0.98723	2.0638	2.7630	4.6092	4.8203	8.1653	8.2305	12.892	12.923	18.909
14	0.99876	2.0094	2.9385	4.1662	4.6719	6.8699	7.0204	10.406	10.463	14.835
16	0.99992	2.0008	2.9928	4.0288	4.8753	6.2616	6.6567	9.0108	9.1386	12.437
18	1.0000	2.0000	2.9995	4.0028	4.9829	6.0493	6.8302	8.3163	8.6640	11.037
20	1.0000	2.0000	3.0000	4.0002	4.9988	6.0051	6.9750	8.0608	8.8133	10.323
22	1.0000	2.0000	3.0000	4.0000	5.0000	6.0003	6.9983	8.0061	8.9731	10.060
24	1.0000	2.0000	3.0000	4.0000	5.0000	6.0000	6.9999	8.0003	8.9983	10.006
26	1.0000	2.0000	3.0000	4.0000	5.0000	6.0000	7.0000	8.0000	9.0000	10.000
28	1.0000	2.0000	3.0000	4.0000	5.0000	6.0000	7.0000	8.0000	9.0000	10.000
30[a]	1.0000	2.0000	3.0000	4.0000	5.0000	6.0000	7.0000	8.0000	9.0000	10.000

N_{points}	λ_1^{FD}	λ_2^{FD}	λ_3^{FD}	λ_4^{FD}	λ_5^{FD}	λ_6^{FD}	λ_7^{FD}	λ_8^{FD}	λ_9^{FD}	$\lambda_{10}^{\mathrm{FD}}$
6	0.72186	93.365	93.365	24150	24150					
8	0.69747	7.9693	7.9708	181.03	181.03	4120.2	4120.2			
10	0.80433	3.1002	3.1203	22.513	22.513	166.29	166.29	1228.7	1228.7	
12	0.91504	2.1594	2.2633	8.2333	8.2333	32.869	32.869	131.78	131.78	528.49
14	0.96955	1.9344	2.2284	4.9808	4.9821	13.544	13.544	37.479	37.479	103.94
16	0.98603	1.9112	2.4633	3.9550	3.9730	8.2174	8.2174	17.758	17.758	38.701
18	0.99180	1.9350	2.7130	3.6684	3.7885	6.2576	6.2581	11.289	11.289	20.764
20	0.99470	1.9569	2.8430	3.6731	4.0490	5.5100	5.5196	8.6252	8.6252	13.955
22	0.99640	1.9708	2.8989	3.7574	4.4227	5.3311	5.4241	7.4555	7.4561	10.880
24	0.99747	1.9796	2.9299	3.8302	4.6483	5.4200	5.7815	7.0293	7.0429	9.4068
26	0.99817	1.9852	2.9496	3.8786	4.7570	5.5702	6.2318	7.0302	7.1653	8.7705
28	0.99864	1.9891	2.9628	3.9108	4.8229	5.6873	6.4848	7.2247	7.6825	8.6494
30	0.99897	1.9917	2.9719	3.9328	4.8672	5.7670	6.6225	7.4226	8.1307	8.8386

[a] For $N_{\mathrm{points}} = 30$ convergence up to 5 significant figures is reached till λ_{15}.

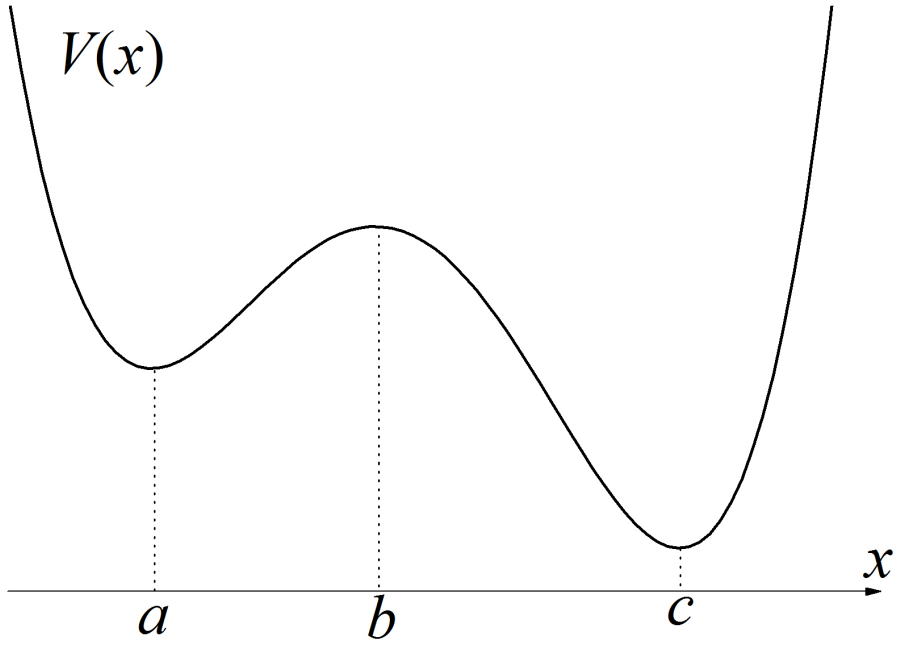

Figure 2.2: Sketch of a generic bistable potential; b individuates the maximum that separates the two minima a, c.

tion is the folding-unfolding of proteins along a single effective coordinate. The energy landscape involved in this process presents a bistable like profile [27], and protein folding trajectories can be described qualitatively by one-dimensional diffusion over this energy landscape [28].

As anticipated in Section 2.2, when the barrier that separates the two minima is sufficiently high, the diffusion process from a to c and vice versa is said to be activated. In this situation, the lowest nonzero eigenvalue λ_1 is associated with the "jump" process between the two wells and its value is generally separated by several orders of magnitude from the the others. When the barrier height increase, λ_1 gets smaller, showing an Arrhenius law behaviour, and in this limit it can be identified as [4]

$$\lambda_1 = r_{ac} + r_{ca} \tag{2.26}$$

where r_{ac} and r_{ca} are the escape rates from well a towards well c and vice versa. Kramers in his pioneering work [29] has shown that for the dynamics

in a bistable potential, with constant diffusion coefficient ($D(x) = D$), these rates can be approximated as

$$r_{ac}^{\mathrm{K}} = \frac{D\sqrt{V^{(2)}(a)\,|V^{(2)}(b)|}}{2\pi}\; e^{-V(b)+V(a)} \tag{2.27}$$

where the vertical bars indicate the absolute value and $V^{(n)}$ indicates the nth-order derivative $\frac{d^n V(x)}{dx^n}$. To calculate r_{ca} one has simply to exchange a with c in the previous equation.
This asymptotic result has been refined many years later by Edholm and Leimar [30] who calculated an improved expression for the escape rate

$$r_{ac}^{\mathrm{E}} = r_{ac}^{\mathrm{K}}\left[1 - D\left(\frac{1}{8}\frac{V^{(4)}(b)}{\left[V^{(2)}(b)\right]^2} - \frac{1}{8}\frac{V^{(4)}(a)}{\left[V^{(2)}(a)\right]^2} + \frac{5}{24}\frac{\left[V^{(3)}(b)\right]^2}{\left|V^{(2)}(b)\right|^3} + \frac{5}{24}\frac{\left[V^{(3)}(a)\right]^2}{\left[V^{(2)}(a)\right]^3}\right) + O([V(b) - V(a)]^2)\right] \tag{2.28}$$

which gives a better approximation to eqn. (2.27). This result is important for a first comparison between the calculated λ_1^{DVR} and λ_1^{FD}, for different functional forms of the bistable potential (see below), where analytic expressions are not available for the eigenvalues.
In the following we take in consideration the two different cases of symmetric and non-symmetric bistable potentials in order to provide a more complete picture; for the last case we discuss also the situation of a non-constant diffusion coefficient.

Symmetric case

A symmetric potential ($V(x) = V(-x)$) is characterized by equivalent minima $V(a) = V(c)$, and with a constant diffusion coefficient D we also have that $r_{ac} = r_{ca}$. By calling $V(b) - V(a) = V_0$ the energy barrier height, we take in consideration two different functional forms for $V(x)$, respectively

$$V(x) = V_0\left(x^2 - 1\right)^2 \tag{2.29}$$

for which we apply reflective boundary conditions and

$$V(x) = \alpha \cos x + 2\alpha \cos 2x \tag{2.30}$$

for which we apply periodic boundary conditions. In the last equation α is a parameter and the energy barrier will be $V_0(\alpha)$. Just to mention, the potential in eqn. (2.29) is also known as the quartic potential or "Landau-Ginzburg potential" and is a popular model for bistable systems [4]. On the other hand, the potential of eqn. (2.30) can be used to describe the diffusive problem involving a torsion angle. The potentials and the parameters used in our calculations are reported in Figure 2.3 where the profiles are shifted to the origin in order to have a direct comparison of the barrier heights.

In Table 2.2 we report the convergence of the first three nonzero eigenvalues calculated with the DVR method, given in diffusion coefficient units and shown up to five significant figures, for different values of the barrier heights V_0, and $V_0(\alpha)$. We compare our results with those issuing from a FD calculation and with the λ_1's obtained with the Edholm's approximation

$$\lambda_1^{\mathrm{E}} = 2\, r_{ac}^{\mathrm{E}} \tag{2.31}$$

using eqn. (2.28). We want to stress that eqns. (2.26, 2.27, 2.28) are only good approximations to λ_1 and one should not take λ_1^{E} as the *true* value to be reached. Finally, for the periodic potential eqn. (2.30) we also report the first three nonzero eigenvalues obtained using the orthonormal representation (OR) method with a Fourier basis, for which the matrix elements of the diffusion operator are analytical.

As anticipated above, λ_1's always differs by several orders of magnitude from λ_2's and λ_3's and this gap increases as V_0 becomes larger, implying different time scales for the diffusive relaxation processes.

Secondly, in all cases, λ_1's converge collectively to values slightly different from λ_1^{E}, confirming the fact that these last ones should not be taken as exact reference values. Finally, we see that for the two cases of lowest energy barriers, λ_1^{FD} converge up to five significant figures more slowly than λ_1^{DVR},

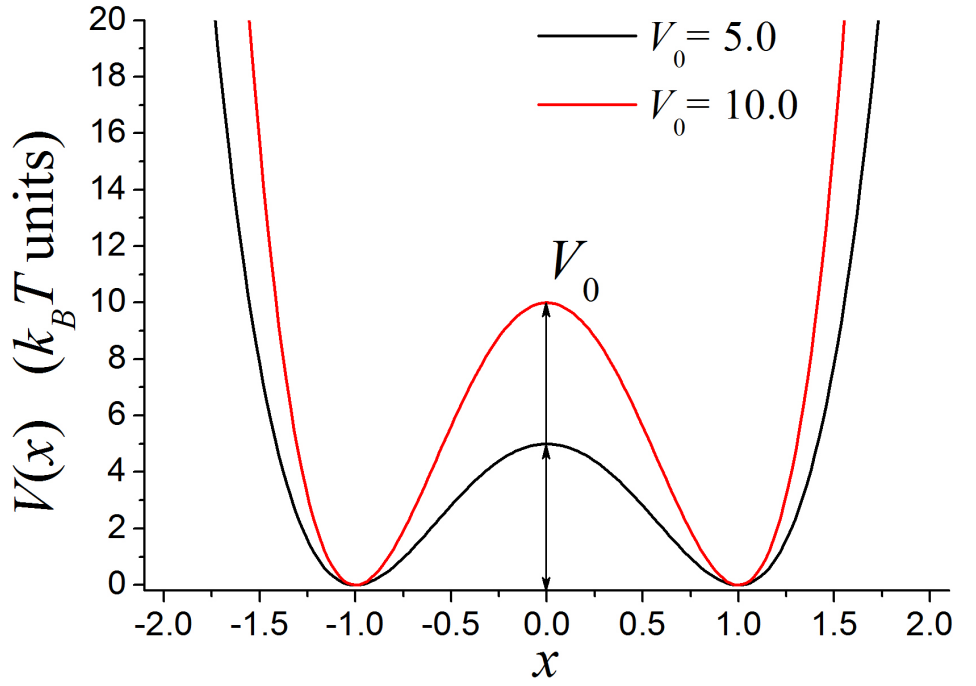

(a)

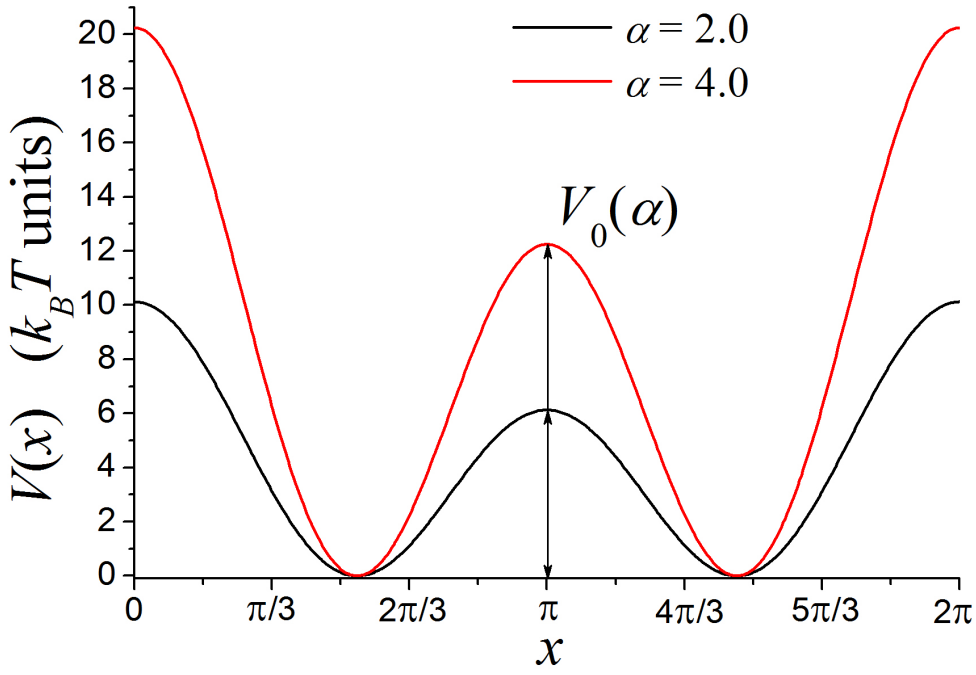

(b)

Figure 2.3: Plot of the quartic potential, eqn. (2.29) (panel a), and of the periodic potential, eqn. (2.30) (panel b). Both profiles are shifted with respect to the origin in order to emphasize the energy barriers involved, V_0 and $V_0(\alpha)$ respectively.

Table 2.2: Convergence of the first three nonzero eigenvalues, given in diffusion coefficient units and shown up to five significant figures, for the bistable potentials, eqns. (2.29, 2.30), for different values of V_0, and $V_0(\alpha)$, calculated with DVR method and FD scheme. Comparison is also shown for Edholm λ_1^{E}, calculated with eqn. (2.31).

N_{points}	λ_1^{DVR}	λ_1^{FD}	λ_1^{E}	λ_2^{DVR}	λ_2^{FD}	λ_3^{DVR}	λ_3^{FD}
$V_0 = 5.0$[a]			5.6113×10^{-2}				
20	7.9016×10^{-2}	5.5459×10^{-2}		16.448	16.462	26.287	25.943
25	5.5693×10^{-2}	5.5491×10^{-2}		16.445	16.460	26.282	26.082
30	5.5505×10^{-2}	5.5501×10^{-2}		16.445	16.457	26.283	26.146
35	5.5523×10^{-2}	5.5506×10^{-2}		16.445	16.454	26.283	26.184
40	5.5523×10^{-2}	5.5510×10^{-2}		16.445	16.452	26.283	26.208
$V_0 = 10.0$[a]			7.8683×10^{-4}				
35	4.8909×10^{-4}	7.8357×10^{-4}		36.170	36.325	58.181	59.439
40	7.7788×10^{-4}	7.8357×10^{-4}		36.170	36.297	58.181	59.165
45	7.8386×10^{-4}	7.8357×10^{-4}		36.170	36.275	58.181	58.970
50	7.8368×10^{-4}	7.8357×10^{-4}		36.170	36.257	58.181	58.826
55	7.8368×10^{-4}	7.8357×10^{-4}		36.170	36.244	58.181	58.717
$\alpha = 2.0$, $V_0 = 6.125$[b,c]			9.6862×10^{-3}				
21	1.1167×10^{-2}	9.6731×10^{-3}		10.426	10.624	12.867	12.952
25	9.7230×10^{-3}	9.6744×10^{-3}		10.426	10.572	12.871	12.940
31	9.6771×10^{-3}	9.6753×10^{-3}		10.426	10.524	12.871	12.922
35	9.6772×10^{-3}	9.6757×10^{-3}		10.426	10.504	12.871	12.913
41	9.6772×10^{-3}	9.6761×10^{-3}		10.426	10.484	12.871	12.903
$\alpha = 4.0$, $V_0 = 12.25$[b,d]			4.3806×10^{-5}				
35	4.8442×10^{-5}	4.3487×10^{-5}		25.244	25.418	28.800	28.938
41	4.3282×10^{-5}	4.3487×10^{-5}		25.244	25.393	28.800	28.931
45	4.3462×10^{-5}	4.3487×10^{-5}		25.244	25.376	28.800	28.920
51	4.3484×10^{-5}	4.3487×10^{-5}		25.244	25.353	28.800	28.903
55	4.3487×10^{-5}	4.3487×10^{-5}		25.244	25.341	28.800	28.892
61	4.3487×10^{-5}	4.3487×10^{-5}		25.244	25.341	28.800	28.892

[a] The selected x range is $[-2.0, 2.0]$.

[b] The selected x range is $[0, 2\pi]$.

[c] Using orthonormal representation method with a Fourier basis, at convergence: $\lambda_1^{\mathrm{OR}} = 9.6772 \times 10^{-3}, \lambda_2^{\mathrm{OR}} = 10.426, \lambda_3^{\mathrm{OR}} = 12.871$.

[d] Using orthonormal representation method with a Fourier basis, at convergence: $\lambda_1^{\mathrm{OR}} = 4.3487 \times 10^{-5}, \lambda_2^{\mathrm{OR}} = 25.244, \lambda_3^{\mathrm{OR}} = 28.800$.

while the same cannot be said doubling V_0. However, in all instances, for the other two eigenvalues (λ_2, λ_3) FD shows a very slow convergence compared to DVR, and in order to have the first three nonzero eigenvalues all equal to DVR ones, up to the fifth significant figure, we have to use a huge number of grid points. Indeed, in order of potential appearance as in Table 2.2, we need respectively more than 450, 1500, 750 and 1500 grid points to reach convergence with FD to the same values calculated with DVR; which need fewer points. So, as an example, for the quartic potential with $V_0 = 10.0$ using FD we need 1500 grid points in order to have λ_i^{FD} $(i = 1, 2, 3)$ equal to the ones calculated with DVR; this shows the slow convergence of FD as opposed to DVR. These simple examples (together with the harmomic potential) show how DVR can be used to reproduce accurately the eigenvalue spectrum of the diffusion operator and consequently to describe the correct relaxation dynamics till the equilibrium with a low computational effort.

Non-symmetric case

Finally we consider a non-symmetric bistable potential with nonequivalent minima $V(a) \neq V(c)$, and with non-constant diffusion coefficient. In particular we analyze a periodic potential of the form

$$V(x) = \alpha_1 \cos x + 2\alpha_1 \cos 2x - \alpha_2 \sin x \tag{2.32}$$

with fixed parameters $\alpha_1 = 2.0$, $\alpha_2 = 1.5$, shown in Figure 2.4. This potential could describe the energetics of a torsion angle that identifies, for example, the relative orientation between two parts of a molecule and it has been shown how to compute well sound variable diffusion coefficients for this kind of situations [31]. Starting from constant diffusion coefficient, it is clear that a change in the coefficient would produce only a scaling of the eigenvalues (as stated previously); in particular, as D increases, the friction that damps the motion while keeping it alive at the same time [5] gets smaller, and the eigenvalues get increased accelerating the relaxation dynamics; of course, the opposite behaviour is observed when D decreases. However, when the diffusion coefficient is no longer constant, it is difficult to predict a priori its

Table 2.3: First three converged eigenvalues calculated with DVR method and shown up to five significant figures, for the non-symmetric bistable potential eqn. (2.32) with different diffusion functions eqns. (2.33, 2.34).

Diffusion function	λ_1^{DVR}	λ_2^{DVR}	λ_3^{DVR}
$D(x) = D^{\mathrm{a}}$	1.9435×10^{-2}	9.8592	13.418
$D(x) = \cos x + 2.0$	2.1135×10^{-2}	12.467	20.132
$D(x) = -\cos x + 2.0$	5.6454×10^{-2}	17.145	23.545
$D(x) = \sin x + 2.0$	3.5715×10^{-2}	11.949	19.751
$D(x) = -\sin x + 2.0$	4.0402×10^{-2}	15.321	22.124

[a] For a constant diffusion, we can use eqns. (2.26, 2.28) to calculate estimated $r_{ac}^{\mathrm{E}} = 1.1381 \times 10^{-3}, r_{ca}^{\mathrm{E}} = 2.0473\times^{-2}, \lambda_1^{\mathrm{E}} = 2.1611 \times 10^{-2}$.

effect on the eigenvalues; to this purpose, here we treat four different cases

$$D(x) = \pm \cos x + c \tag{2.33}$$

and

$$D(x) = \pm \sin x + c \tag{2.34}$$

with fixed shift $c = 2.0$. These four functions are chosen in order to see the effect of locally increasing the diffusion around respectively the two endpoints and around the maximum, eqn. (2.33); and respectively around the left and right minima of the potential, eqn. (2.34).

In Table 2.3 we report the first three converged eigenvalues for the non-symmetric bistable potential eqn. (2.32) with different diffusion coefficients eqns. (2.33, 2.34), calculated with the DVR method. Also FD converges to the same DVR values, but more slowly; indeed to reach convergence with constant diffusion (first entry in Table 2.3) we just need 35 grid points with DVR method, while more than 800 grid points are required using FD. In the case of variable diffusion function (last four entries in Table 2.3) we just need 45 grid points with DVR method, while more than 1300 grid points are required using FD to reach the same λ_i^{DVR} $(i = 1, 2, 3)$.

Taking as reference the constant diffusion case (first entry), we can see that increasing the diffusion around the maximum (third entry) has the effect to give the greatest acceleration, *i.e.* greatest eigenvalues, compared to the

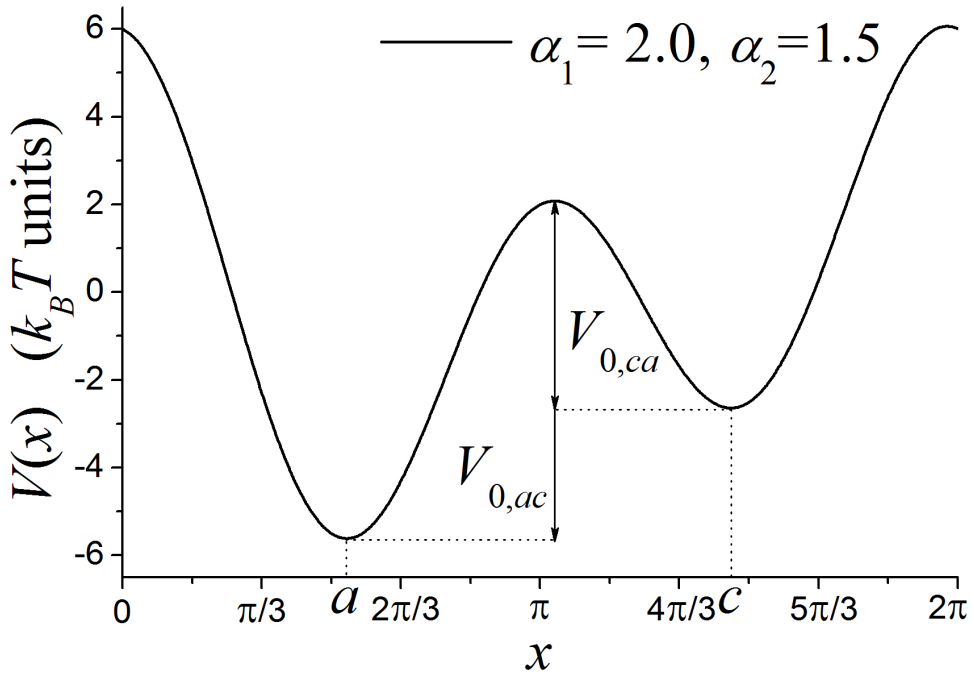

Figure 2.4: Plot of the non-symmetric potential, eqn. (2.32); a, c individuate the two minima separated by the energy barriers $V_{0,ac} = 7.4670$ and $V_{0,ca} = 4.3543$ $k_B T$ units going respectively from a to c, and vice versa.

others. One can qualitatively imagine that increasing the diffusion (and so, lowering friction) around the maximum has the same effect of directly lowering the energy barrier, by the way, we remark that further insights would be only speculative at this point.

Finally, in Figure 2.5 (panel a) we report the relaxing profile till the equilibrium state, built using 101 DVR points at each time propagation step with constant diffusion and a gaussian initial distribution centered at $x = 4.5$ and with standard deviation $\sigma = 0.05$. It can be noted the initial rapid broadening of the profile $p(x, t)$ due to the fast "fluctuation" processes inside the potential well; these are related to large eigenvalues. As time progresses, the other deeper minimum starts to become populated; this slow population movement between wells is a low activated process related to λ_1. Finally the profile reaches the equilibrium distribution, that matches perfectly the analytic one (see panel b).

2.3.3 A chemical case-study

As a final example, in order to show the applicability of DVR method to case-studies of chemical interest we consider here the specific case of conformational dynamics of *n*-butane and three dihaloethanes, in particular 1-chloro-2-fluoroethane, 1-bromo-2-fluoroethane, 1-bromo-2-chloroethane (from now on respectively abbreviated as CFE, BFE, BCE). We treat the dynamic as a diffusive motion upon the torsion angle γ of the central C–C bond, taken as the only variable for this problem. This choice has been dictated by the renewed interest for such kind of dynamics, indeed, recent developments in the field of pulsed-IR spectroscopy allowed the experimental determination of kinetic constants of isomerization between conformers [32]. Since time scale is very short (some ten ps), these processes are indeed too fast to be investigated with the conventional spectroscopical techniques, and since few years ago the only possibility to study them was to recover to molecular dynamics simulations.

For each molecule above mentioned we solve the Smoluchowski equation using DVR method (as seen before) and we calculate the rate constants for

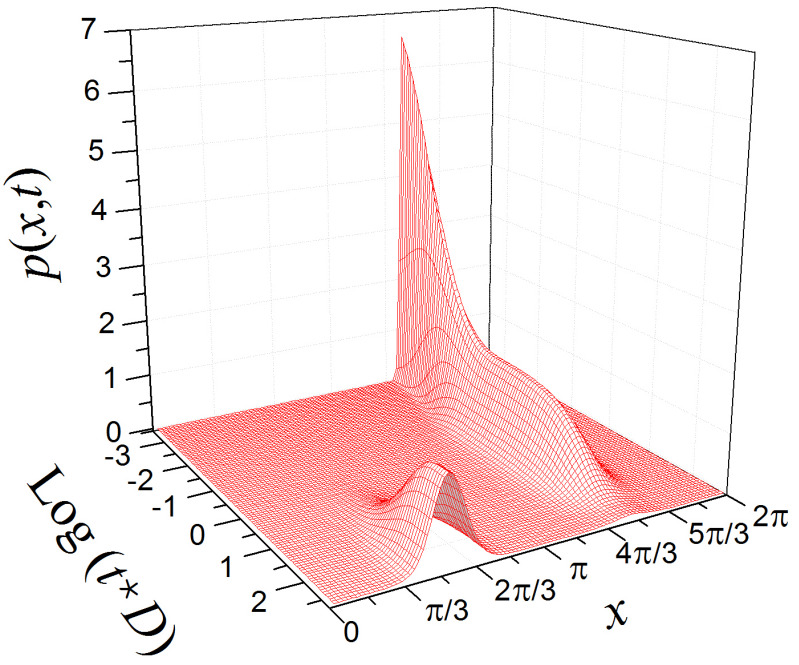

(a)

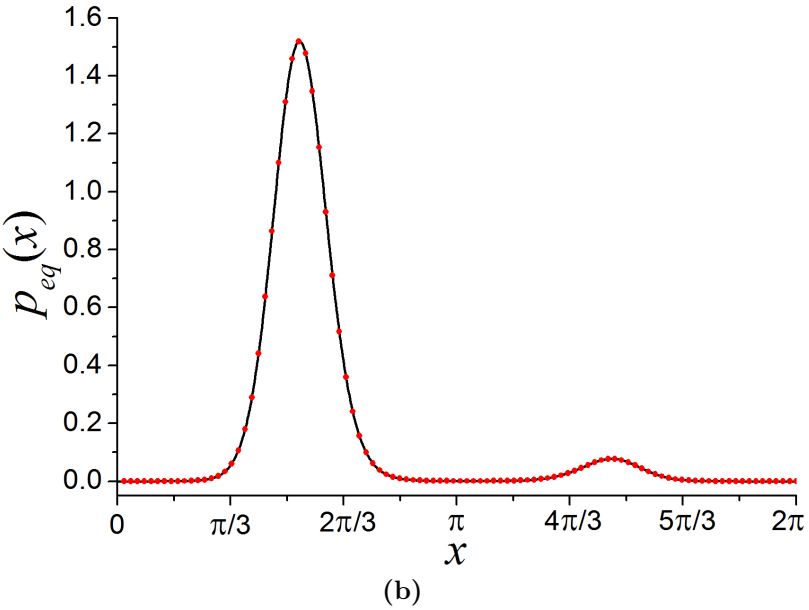

(b)

Figure 2.5: (a) Surface plot for the relaxation profile $p(x,t)$ of the non-symmetric diffusive problem eqn. (2.32) with constant diffusion and an initial gaussian distribution centered at $x = 4.5$ and $\sigma = 0.05$. The profile is calculated using 101 DVR grid points at each step of time propagation; this last is expressed in decimal logarithm units. (b) Analytic equilibrium distribution $p_{eq}(x)$ for the non-symmetric problem (black line), and extrapolated from relaxation profile (red dots).

gauche $\longleftrightarrow$ *trans* transitions given in diffusion coefficient units.The internal dynamic is regulated by the conformational energetics that in this case is represented by the torsion potential $V(\gamma)$, generally different for each molecule and by the friction, of viscous nature, that damps the motion. With regard to the friction, that determines the torsion diffusion coefficient, here we shall assume a constant diffusion D, thus independent from the conformation. This approximation is valid till we have small molecules in which the two external rotating groups don't have big size as in this case. From the physical point of view we are assuming that hydrodynamic interactions between the atoms considered as beads are negligible. This is a valid assumption at this stage of the thesis, where the focus is on numerical methods apt to solve the Smoluchowski equation, in Section 3.4 we shall show the relevance of the angular dependence of diffusion constant and the hydrodynamic interactions between beads for n-butane, here omitted. As seen before, as long as D will not have a specific value, it will be only a scaling factor.
The torsion potential for the considered molecules is expressed as

$$V(\gamma) = \alpha_1 \cos\gamma + \alpha_2 \cos 2\gamma + \alpha_3 \cos 3\gamma \tag{2.35}$$

a tristable potential, where each well corresponds to a particular molecule conformation, namely the two equivalent *gauche* and the *trans* (from now on respectively abbreviated as g_+, g_- and t); see Figure 2.6, where the profiles has been shifted to the origin. The potential parameters α_i are taken from ref. [33] for n-butane and ref. [34] for dihaloethanes; they are all reported in Table 2.4 in k_BT units, where $T = 298$ K.

In Table 2.4 we also report the first three converged eigenvalues calculated with the DVR method (the convergence is reached using only 41 grid points), given in diffusion coefficient units and shown up to five significant figures, for the examined molecules. These eigenvalues have the same values of the ones obtained using OR method with a Fourier basis, for which the matrix elements of the diffusion operator are once again analytical.
It can be readily noticed the presence of two lowest eigenvalues λ_1^{DVR} and λ_2^{DVR} related (in a not straightforward way) to slow "jump" processes and

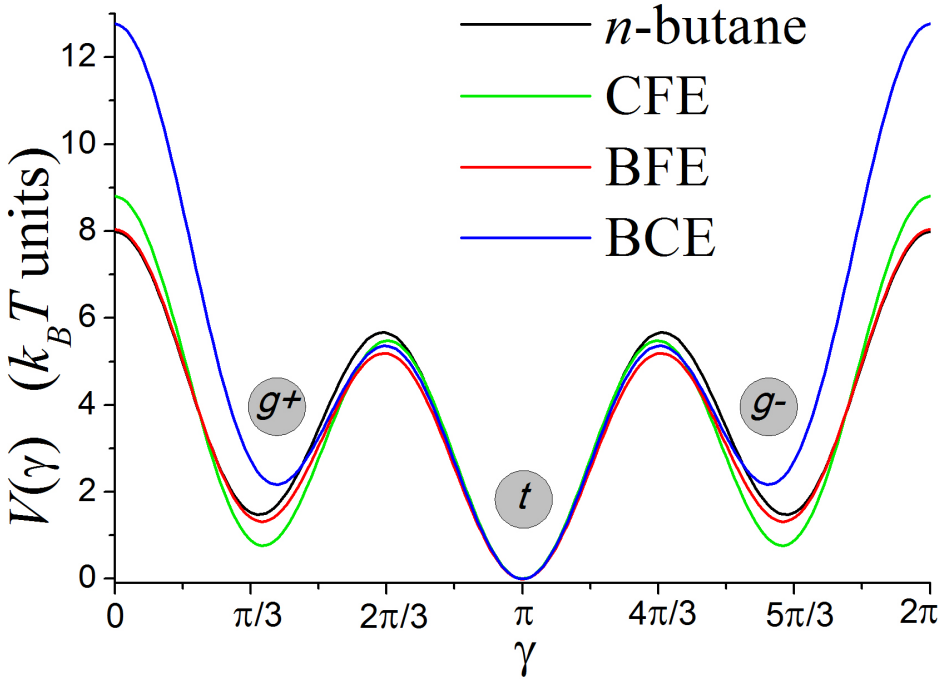

Figure 2.6: Plot of the torsion potential $V(\gamma)$, eqn. (2.35), for the examined molecules; profiles are shifted with respect to the origin in order to emphasize the energy barriers involved. The parameters employed to build the profiles are reported in Table 2.4.

Table 2.4: Potential parameters (in k_BT units, $T = 298$ K) used for the potential profiles $V(\gamma)$ shown in Figure 2.6, taken from refs. [33, 34] and first three converged eigenvalues given in diffusion coefficient units calculated with DVR method and shown up to five significant figures.

Molecule	α_1	α_2	α_3	λ_1^{DVR}	λ_2^{DVR}	λ_3^{DVR}
n-butane	1.285	0.266	2.708	0.060936	0.073656	15.508
CFE	1.402	0.811	2.997	0.035881	0.062864	16.585
BFE	1.419	0.481	2.601	0.073566	0.10030	14.379
BCE	3.377	1.562	3.006	0.13863	0.17044	15.306

clearly separated by λ_3^{DVR} by two/three orders of magnitude. In all these cases the jump processes are four (the direct transition $g_+ \to g_-$ is kinetically forbidden because of the too high energy barrier involved, and here it will not be considered), even if only two are distinguished, namely $t \to g_\pm$ and $g_\pm \to t$, due to the impossibility to discriminate between g_+ and g_-.

Now the problem is how to relate these two lowest eigenvalues with the rate constants $k_{t\to g_\pm}$ and $k_{g_\pm \to t}$ associated to the "jump" transitions between potential wells. For the chemist used to think in terms of activated processes, indeed, these rate constants are precisely the ones to assume relevance and to constitute phenomenological parameters to be determined from experimental data (or from molecular dynamics simulation of these systems). In phenomenological terms, the transitions between the two *gauche* and the *trans* conformation are described adopting a first order kinetic scheme for the *site populations* evolution. By generic n-th "site" we mean the "potential well" inside which there is the n-th minimum of the potential profile ($n \equiv t, g_\pm$ in our case); the population of this site is naturally defined integrating the nonequilibrium distribution $p(\gamma, t)$ inside the site domain delimited by the neighbours maxima γ_{n-} and γ_{n+}

$$P_n(t) := \int_{\gamma_{n-}}^{\gamma_{n+}} d\gamma \, p(\gamma, t) \tag{2.36}$$

in particular, the equilibrium populations are given by

$$P_{eq,n} = \int_{\gamma_{n-}}^{\gamma_{n+}} d\gamma \, p_{eq}(\gamma) \tag{2.37}$$

The kinetic model regulates the relaxation $P_n(t) \to P_{eq,n}$ starting from generic initial conditions. As anticipated before, for our specific case we adopt the following scheme based on four elementary steps (two by two one

the inverse of the other one)

$$\begin{aligned} g_+ &\xrightarrow{k_{g_+\to t}} t \\ t &\xrightarrow{k_{t\to g_+}} g_+ \\ g_- &\xrightarrow{k_{g_-\to t}} t \\ t &\xrightarrow{k_{t\to g_-}} g_- \end{aligned} \tag{2.38}$$

with $k_{g_+\to t} = k_{g_-\to t}$ and $k_{t\to g_+} = k_{t\to g_-}$ because of the symmetry of potential and considering the principle of microscopic reversibility

$$k_{g_\pm\to t}\, P_{eq,g_\pm} = k_{t\to g_\pm}\, P_{eq,t} \tag{2.39}$$

in order to guarantee the reaching of the correct equilibrium state.

Kinetic schemes like the one in eqn. (2.38) can be written as a set of differential equations of the kind

$$\frac{d\boldsymbol{P}(t)}{dt} = -\boldsymbol{K}\boldsymbol{P}(t) \tag{2.40}$$

with $\boldsymbol{P}$ and $\boldsymbol{K}$, respectively, the populations vector and the kinetic matrix. The crucial point is to find a meeting point between the discretized description (kinetic approach for the transitions between the "sites") and the continuous one (diffusive model for the generalized coordinate), *i.e.* to look for a possible connection between $\boldsymbol{K}$ and $\widetilde{\boldsymbol{\Gamma}}$. Intuitively the two descriptions are interfaced if a neat separation between the time scales of fast processes (fluctuations inside the wells) and slow processes exists (jumps between wells). This problem has been formally faced by Moro and Nordio [35, 36] using "localized site functions". Briefly, the starting point is to construct a basis set of functions of the stochastic variable, called "localized site functions", that in the limit of high potential barriers tends to become an orthonormal basis upon which it is possible to represent in matrix form the diffusion operator. The resulting matrix has the same dimensions of the kinetic matrix $\boldsymbol{K}$ and it is possible to establish an univocal connection amongst its eigenvalues

Table 2.5: Equilibrium populations calculated by numerical integration of eqn. (2.37) and rate constants given in diffusion coefficient units calculated with eqns. (2.39, 2.42), using $\lambda_1^{\mathrm{DVR}}, \lambda_2^{\mathrm{DVR}}$ reported in Table 2.4.

Molecule	$P_{eq,t}$ [a]	$P_{eq,g_\pm}$ [a]	$k_{t\to g_\pm}$	$k_{g_\pm\to t}$
n-butane	0.682	0.159	0.0130	0.0556
CFE	0.529	0.235	0.0154	0.0346
BFE	0.651	0.174	0.0186	0.0694
BCE	0.818	0.0911	0.0155	0.139

[a] Populations are normalized, in fact $P_{eq,t} + 2P_{eq,g_\pm} = 1$.

and the kinetic constants. In the end, one discovers that the eigenvalues of the symmetrized kinetic matrix $\widetilde{\boldsymbol{K}}$ must be equal to the eigenvalues (both in ascending order) of the symmetrized diffusion representation $\widetilde{\boldsymbol{\Gamma}}$. The final result is the following expressions for the two kinetic constants

$$\begin{aligned} k_{t\to g_\pm} &= \lambda_1 \frac{P_{eq,g_\pm}}{P_{eq,t}} \\ k_{t\to g_\pm} &= \lambda_2 P_{eq,g_\pm} \end{aligned} \tag{2.41}$$

The two values of $k_{t\to g_\pm}$ would be certainly different, but it can be shown that their difference decrease as the barriers between minima get increased. Consequently the best estimate that we can produce is the arithmetic average of the two rate values

$$k_{t\to g_\pm} = \frac{1}{2}\left(\lambda_1 \frac{P_{eq,g_\pm}}{P_{eq,t}} + \lambda_2 P_{eq,g_\pm}\right) \tag{2.42}$$

while the rate constant for the back transitions $k_{g_\pm\to t}$ is calculated using microscopic reversibility, eqn. (2.39).

In Table 2.5 we report the equilibrium populations calculated by numerical integration of eqn. (2.37) and the rate constants given in diffusion coefficient units for the examined molecules, calculated with eqns. (2.39, 2.42) and using $\lambda_1^{\mathrm{DVR}}, \lambda_2^{\mathrm{DVR}}$ reported in Table 2.4.

2.4 Final remarks

In this Chapter we have presented how to setup a reliable framework to solve the one-dimensional Smoluchowski equation making use of sinc-DVR methods in conjunction with product approximation. We have demonstrated the efficiency of the approach calculating the eigenvalues of the diffusion operator for some simple and familiar test-cases and reaching convergence with the use of few grid points. The reliability of the results has been assessed through the comparison with a simple finite difference scheme, which has shown in some cases much poorer performances with respect to DVR. Another strength point of the DVR pseudospectral method is its simplicity, especially concerning code implementation.
We really believe that both the difficulties encountered with a simple FD scheme, where the convergence is reached more slowly, or orthonormal representation, where analytic matrix elements are not always available, can effectively be overcame by use of a discrete variable representation coupled with product approximation. Also, there are very encouraging perspectives concerning the application of this approach to multidimensional problems (where FD becomes often unfeasible), or more complicated Smoluchowski equations that contain other coordinate dependent terms, *e.g.* a reactive term. This last point will be discussed in Chapter 4.
Indeed, in multidimensional problems if the diffusion operator has no mixed second derivatives and if a direct product basis is used for the multidimensional system, the basis for each dimension may be separately transformed to the DVR. The resulting DVR matrix for the diffusion operator will be very sparse [14], simplifying and speeding-up its construction and diagonalization. For more complicated diffusion operators, direct product DVR's in conjunction with product approximation are still highly advantageous leading to straightforward simplifications of the matrix representation of the operator [16, 20]. Despite the simplicity of these approaches, it is difficult to predict *a priori* their numerical limit.

As a final consideration, in order to have a proper modelization of the diffusion function $D(x)$ it is necessary to construct reliable hydrodynamical

models, a task that it not always straightforward. In the next Chapter we will cover these important aspects; starting from the past works that has been done in this field [31, 37, 38], in order to have sound variable diffusion functions, even for multidimensional problems (where diffusion becomes a tensor). Once reliable information upon diffusion are achieved (in conjunction with the energetics of the system under study) one can complete the picture of the diffusive problem, *e.g.* calculating absolute kinetic constants for the molecules examined in Section 2.3.3 and comparing them with their estimates available in literature.

Chapter 3

Variable diffusion tensor along a generalized coordinate

Interpretation of experimental (especially spectroscopic) data in terms of structural and dynamical characteristics of molecular systems of increasing complexity is of paramount interest, but remains often not straightforward. In this connection, the role of computational simulations is constantly increasing in parallel with the improvement of hardware and, especially, of theoretical models and of the corresponding software. In several cases motions of the whole molecular system (*e.g.* global tumbling of the solute in a solvent) and internal degrees of freedom can be defined as diffusive parameters, which, in turn, can be effectively described in terms of an effective tensorial quantity, the diffusion tensor.

Several proposals have been published in recent years, which employ different general assumptions and hydrodynamic models. A comprehensive review of the most interesting approaches has been recently published by de la Torre and Bloomfield [39]. The main limitation of these models is that they can be applied either to rigid molecules (*e.g.* the HYDRONMR software [40]) or offer a quite limited choice of large amplitude internal motions (essentially torsions like, *e.g.*, in the DiTe approach [31]). However, chemists are often faced with diffusive problems involving motion along more general paths, which can be parametrized only in terms of a generalized coordinate lacking

an overall analytical expression, but rather described only numerically by a non-linear combination of local (curvilinear) coordinates.

A general approach for building such a generalized coordinate involves three main steps. The first one is the generation of an ordered series of geometrical structures visited by the system under study. The simplest way of obtaining these structures involves a rigid or relaxed (*i.e.* constrained optimization of all the other variables) scan along a predefined internal coordinate. More refined strategies range from steepest-descent paths originating from first-order saddle points (the length along this path is the well-known intrinsic reaction coordinate, IRC) [41] to principal component analyses (PCA) of molecular dynamics (MD) simulations [42]. In the second step, the variation of angular momentum between pairs of successive structures must be minimized, in order to minimize the coupling between the generalized coordinate and the overall rotations of the molecular system. Note that this step leads also to the minimization of the corresponding couplings in the diffusion tensor. Finally, the generalized coordinate is computed as the distance in mass-weighted Cartesian coordinates between successive structures. This choice leads to kinematic computations characterized by a unitary reduced mass. Once the generalized coordinate has been computed, it can be used, for instance, in a quantum mechanical (QM) context to compute vibrationally averaged values of observables solving an effective one-dimensional Schrödinger equation.

Several applications of this approach have been reported for different spectroscopies mostly employing a relaxed scan definition of the generalized coordinate [43, 44, 45, 46]. Of course, the IRC route has been pioneered by Fukui and further developed by Miller in terms of the so-called reaction path Hamiltonian [41, 47, 48]. Much less work has been performed along these lines in a classical mechanical context, especially in connection with diffusion problems.

We have implemented in the context of the Gaussian package [49] an extension to generalized coordinates of the diffusion tensor approach proposed in previous works [31, 37, 38]. Although the specific applications presented in the following employ rigid or relaxed scans, the implementation permits also

the use of IRC or PCA [42] paths. The final goal is to build a reliable framework for setting up and solving the one-dimensional Smoluchowski equation along any generalized coordinate, making use of the quite powerful solution method based on Discrete Variable Representation (DVR) [1] presented in the previous Chapter. Once both the main pieces of information (dissipation and energetics) are given and after the diffusive problem solved, some specific quantities (*e.g.* time correlation functions) can be connected to the dynamical quantities of interest (*e.g.* magnetic relaxation times). Furthermore, in some cases, it becomes possible to establish a connection between the continuum diffusive process along a generalized coordinate and the discrete kinetic process between well separated potential energy minima, thus enabling the calculation of rate constants [36, 37, 38, 1], which have a close connection with the phenomenological parameters extracted from experimental data.

In our opinion the diffusion tensor approach sketched above can be applied, in addition to the Smoluchowski equation, also in the context of the stochastic Liouville equation (SLE), which is at the heart of the most refined integrated models for the simulation of electronic paramagnetic resonance (EPR) spectra [50, 51, 52, 53, 54, 55] or in connection with the Fokker-Planck equation, which plays a comparable role in the simulation of nuclear magnetic resonance (NMR) spectra [56, 57, 58].

In the next two Sections we shall provide a short description of the approach used to compute the generalized coordinate and the diffusion tensor along the same. Then in Sections 3.3 and 3.4 we shall give essential details about the actual numerical implementation of the approach and the main results obtained for a couple of specific cases of chemical interest.

3.1 Computation of generalized coordinate

A straightforward strategy for calculating the generalized coordinate is to perform a relaxed potential energy scan along a predefined internal coordinate and obtain the generalized coordinate as the distance between mass-weighted Cartesian coordinates of the successive geometries obtained by the scan. The angular momentum between the pairs of consecutive structures

should be minimized in order to minimize the coupling between the rotations of the system and the generalized coordinate. For this we have used an approach based on the IRC [41, 47]. A closed curve representing the minimum energy path in the mass-weighted Cartesian space $\mathbf{C}$ of the motion along the internal rotation, is generated [46]. The space $\mathbf{C}$ contains the coordinates of a point $\mathbf{c}$ which are the elements of the set $\mathbf{c}_i : i = [1, 2, \ldots, 3N]$. $\mathbf{c}$ is defined as a function of s, the parameter corresponding to the generalized coordinate; in the following way

$$\frac{d\mathbf{c}(s)}{ds} = \frac{\mathbf{g}}{\sqrt{\mathbf{g}^\dagger \mathbf{g}}} \tag{3.1}$$

Here $\mathbf{g}$ is the energy gradient in mass-weighted Cartesian coordinates. Each value of s is associated with a point $\mathbf{c}$ in $\mathbf{C}$ by a map $\mathbf{a}(s)$, according to the Reaction Path Hamiltonian (RPH) of Miller and coworkers [48]

$$\mathbf{c}_i = \mathbf{a}_i(s) + \sum_{k=1}^{3N-7} \mathbf{L}_{i,k}(s)\, Q_k \tag{3.2}$$

Here we have taken into consideration the fact that eqn. (3.1) has seven solutions which are zero: six corresponding to translations and external rotations and one related to the curve as the energy along the internal rotation is expected to vary slowly. In eqn. (3.2), $\mathbf{L}_k(s)$ contains the eigenvectors corresponding to the nonzero eigenvalue of the Hamiltonian and Q_k are the vibrational normal modes.

Imposing the Eckart conditions to two consecutive optimized geometries and then superimposing their Eckart frames, we are able to minimize the roto-translational displacement between them. More precisely, Eckart conditions minimize the Coriolis coupling between the external and internal motions of a molecule, *i.e.*, separation of the roto-translational motion from internal motions or vibrations [59]. The origin of the coordinate system for the first geometry (usually the equilibrium geometry) is shifted to the center of mass and subsequently, the successive geometries obtained by the scan are shifted with respect to the same. The normalized coordinates of the molecule at the

successive geometries are then calculated from the transformation matrix which imposes the so-called rotational and translational Eckart conditions.[1] The numerical algorithm that carries out this operation is based on quaternions [60]. Finally, the map $\mathbf{a}(s)$ is calculated as the distance between two consecutive points in $\mathbf{C}$ in terms of mass-weighted coordinates

$$|ds|^2 = |\mathbf{a}_{i+1}(s) - \mathbf{a}_i(s)|^2 = |\mathbf{c}_{i+1} - \mathbf{c}_i|^2 \tag{3.3}$$

Considering that two consecutive points (*i.e.* two consecutive geometries) in the configurational space $\mathbf{C}$ are close enough to neglect the vibrational displacement (*i.e.* the second part in RHS of eqn. (3.2)).

The reduced mass has been taken to be unity and the information about kinematic coupling is stored as the discrepancy between the curve s, parameterized by the map $\mathbf{a}(s)$ in a point to point basis and the corresponding internal coordinate along which the scan is performed.

3.2 Modeling of the diffusion tensor

A molecular system made of N material points (see Figure 3.1) is considered, representing the atoms of a molecule without constraints, immersed in a continuous medium with viscosity η. The Cartesian positions $\mathbf{r}_\alpha$ ($\alpha = 1, \ldots, N$) of the atoms are referred to a Laboratory Frame (LF) and the associated velocities $\mathbf{v}_\alpha = \dot{\mathbf{r}}_\alpha$ as well. Also a Molecular Frame (MF) is defined and placed on the center of mass of the system, with new atom coordinates $\mathbf{c}_\alpha$. The Cartesian forces acting on the material points are associated to velocities via the $3N \times 3N$ friction matrix $\boldsymbol{\Xi}$

[1] The minimization of vibro-rotational coupling is necessary to minimize the coupling between the large amplitude motion and rotations, because the goal when calculating the movement from one point to the next one is to have a generalized coordinate "uncontaminated" from the fact that the moluecule is simultaneously rotating.

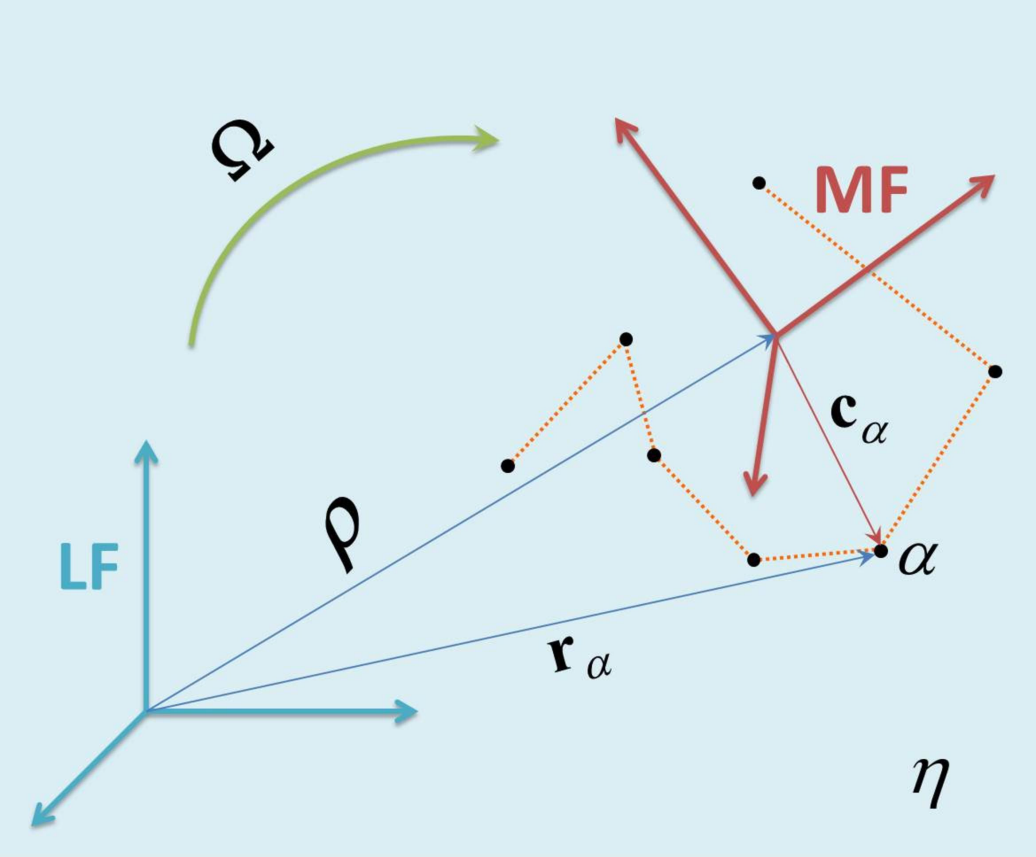

Figure 3.1: Sketch of an (un)constrained molecular system and physical quantities involved in the model construction. The dashed orange lines highlight the constraints, while the light blue background indicates the solvent.

$$\begin{pmatrix} \mathbf{F}_1 \\ \vdots \\ \mathbf{F}_\alpha \\ \vdots \\ \mathbf{F}_N \end{pmatrix} = - \boldsymbol{\Xi} \begin{pmatrix} \mathbf{v}_1 \\ \vdots \\ \mathbf{v}_\alpha \\ \vdots \\ \mathbf{v}_N \end{pmatrix} \tag{3.4}$$

For the constrained system an external coordinate set $[\boldsymbol{\rho}, \boldsymbol{\Omega}, \boldsymbol{q}]$ is defined, where $\boldsymbol{\rho}$ represents the distance of the system center of mass from the LF, $\boldsymbol{\Omega}$ collects the three Euler angles that bring the LF to the MF and $\boldsymbol{q}$ are the $3N-6$ internal coordinates. Now a subset of the internal coordinates $\boldsymbol{x} : x_1, \ldots, x_n$ with $n < 3N-6$ is selected and the remaining ones, $\boldsymbol{y} : y_1, \ldots, y_{3N-6-n}$ are kept frozen; a new set of external coordinates $\boldsymbol{\mathcal{R}} = [\boldsymbol{\rho}, \boldsymbol{\Omega}, \boldsymbol{x}]$ is now considered. Associated to the external coordinates there is the velocity set $\boldsymbol{\mathcal{V}} = [\boldsymbol{v}, \boldsymbol{\omega}, \dot{\boldsymbol{x}}]$, including, the translational velocity, the angular velocity and the internal moments. The total force is composed as well of three contributions $\boldsymbol{\mathcal{F}} = [\boldsymbol{f}, \boldsymbol{\tau}, \boldsymbol{\tau}_{\boldsymbol{x}}]$, namely, the translational force, the torque and the internal forces. Now, the new relation is

$$\begin{pmatrix} \boldsymbol{f} \\ \boldsymbol{\tau} \\ \boldsymbol{\tau}_{\boldsymbol{x}} \end{pmatrix} = - \boldsymbol{\xi} \begin{pmatrix} \boldsymbol{v} \\ \boldsymbol{\omega} \\ \dot{\boldsymbol{x}} \end{pmatrix} \tag{3.5}$$

with $\boldsymbol{\xi}$ the $(6+n) \times (6+n)$ friction matrix for the constrained system.

It can be easily shown [38, 61] that $\boldsymbol{\mathcal{F}} = \mathbf{A}\,\mathbf{F}$ and $\mathbf{v} = \mathbf{B}\,\boldsymbol{\mathcal{V}}$, where $\mathbf{A}$ and $\mathbf{B}$ are matrices of dimension, $(6+n) \times 3N$ and $3N \times (6+n)$ respectively that depend only on instantaneous molecular geometry. Also it can be shown that $\mathbf{B} = \mathbf{A}^{\mathrm{tr}}$ and after some algebra we arrive to

$$\boldsymbol{\xi} = \mathbf{B}^{\mathrm{tr}}\,\boldsymbol{\Xi}\,\mathbf{B} = \begin{pmatrix} \boldsymbol{\xi}_{TT} & \boldsymbol{\xi}_{TR} & \boldsymbol{\xi}_{TI} \\ \boldsymbol{\xi}_{RT} & \boldsymbol{\xi}_{RR} & \boldsymbol{\xi}_{RI} \\ \boldsymbol{\xi}_{IT} & \boldsymbol{\xi}_{IR} & \boldsymbol{\xi}_{II} \end{pmatrix} \tag{3.6}$$

where the subscripts T, R, I stand, respectively, for translational, rotational, internal contributions. In order to find the expression for the $\mathbf{B}$ matrix the

Cartesian velocities $\mathbf{v}_\alpha$ are expressed with respect to the external coordinates, using simple classical mechanics relations [62]

$$\mathbf{v}_\alpha = \boldsymbol{v} + \mathbf{E}^{\mathrm{tr}}(\boldsymbol{\Omega}) \cdot \left(\boldsymbol{\omega} \times \mathbf{c}_\alpha + \sum_{\mu=1}^{n} \frac{\partial \mathbf{c}_\alpha}{\partial x_\mu} \dot{x}_\mu \right) \tag{3.7}$$

with $\mathbf{E}(\boldsymbol{\Omega})$ the Euler matrix that brings the LF into the MF. Therefore,

$$\begin{pmatrix} \mathbf{v}_1 \\ \vdots \\ \mathbf{v}_\alpha \\ \vdots \\ \mathbf{v}_N \end{pmatrix} = \underbrace{\begin{pmatrix} \mathbf{1}_3 & -\mathbf{E}^{\mathrm{tr}}(\boldsymbol{\Omega})\, \mathbf{c}_1^{\times} & \mathbf{E}^{\mathrm{tr}}(\boldsymbol{\Omega})\, \frac{\partial \mathbf{c}_1}{\partial x_1} & \cdots & \mathbf{E}^{\mathrm{tr}}(\boldsymbol{\Omega})\, \frac{\partial \mathbf{c}_1}{\partial x_n} \\ \vdots & \vdots & \vdots & & \vdots \\ \mathbf{1}_3 & -\mathbf{E}^{\mathrm{tr}}(\boldsymbol{\Omega})\, \mathbf{c}_\alpha^{\times} & \mathbf{E}^{\mathrm{tr}}(\boldsymbol{\Omega})\, \frac{\partial \mathbf{c}_\alpha}{\partial x_1} & \cdots & \mathbf{E}^{\mathrm{tr}}(\boldsymbol{\Omega})\, \frac{\partial \mathbf{c}_\alpha}{\partial x_n} \\ \vdots & \vdots & \vdots & & \vdots \\ \mathbf{1}_3 & -\mathbf{E}^{\mathrm{tr}}(\boldsymbol{\Omega})\, \mathbf{c}_N^{\times} & \mathbf{E}^{\mathrm{tr}}(\boldsymbol{\Omega})\, \frac{\partial \mathbf{c}_N}{\partial x_1} & \cdots & \mathbf{E}^{\mathrm{tr}}(\boldsymbol{\Omega})\, \frac{\partial \mathbf{c}_N}{\partial x_n} \end{pmatrix}}_{\mathbf{B}} \begin{pmatrix} \boldsymbol{v} \\ \boldsymbol{\omega} \\ \dot{\boldsymbol{x}} \end{pmatrix} \tag{3.8}$$

where $\mathbf{c}_\alpha^{\times}$ is the 3×3 matrix with elements $\left(\mathbf{c}_\alpha^{\times}\right)_{mn} = \sum \varepsilon_{mln} \left(\mathbf{c}_\alpha\right)_l$ and where ε_{mln} is the Levi-Civita symbol.
It can be readily noticed that $\mathbf{B}$ is dependent only on the instantaneous geometry and, in principle, knowledge of the derivatives $\frac{\partial \mathbf{c}}{\partial x}$ is required. In the case one wants to deal just with natural internal coordinates, as dihedrals [31], bond angles and/or bond lengths, analytical expressions [63] for the derivatives $\frac{\partial \mathbf{c}}{\partial x}$ are well known.

In our treatment the subset $\boldsymbol{x}$ is reduced to a single generalized coordinate s, calculated from eqn. (3.3) with the method sketched in the previous Section. Equation (3.8) still holds; the derivatives will be now $\frac{\partial \mathbf{c}}{\partial s}$.

Once $\mathbf{B}$ is constructed, the remaining task is to model the unconstrained friction tensor $\boldsymbol{\Xi}$. The simplest model is that of independent beads, *i.e.*

$$\boldsymbol{\Xi} = \Xi_0\, \mathbf{1}_N \tag{3.9}$$

with $\Xi_0 = C R_e\, \eta\, \pi$, R_e being the hydrodynamical radius and $C = 4, 6$ the slip or stick, respectively, boundary condition coefficient. The constrained friction tensor is so

$$\boldsymbol{\xi} = \Xi_0 \, \mathbf{B}^{\mathrm{tr}} \, \mathbf{B} \tag{3.10}$$

and the requested diffusion tensor is easily calculated using Einstein relation

$$\mathbf{D} = k_B T \boldsymbol{\xi}^{-1} = \begin{pmatrix} \mathbf{D}_{TT} & \mathbf{D}_{TR} & \mathbf{D}_{TG} \\ \mathbf{D}_{RT} & \mathbf{D}_{RR} & \mathbf{D}_{RG} \\ \mathbf{D}_{GT} & \mathbf{D}_{GR} & \mathbf{D}_{GG} \end{pmatrix} \tag{3.11}$$

where G now stands for generalized. Since we are dealing with just one generalized coordinate, $\mathbf{D}_{GG}$ is a scalar function of s, and hereafter we shall name it simply $D_{GG}(s)$.

More sophisticated models can be chosen in order to take into account the effects of hydrodynamic interactions among the beads, using for example the Oseen [64, 65] or the Rotne-Prager [66] model. When evaluating the friction exerted by the medium over a generic bead, these models account for the perturbative effect of the other particle motion over the fluid velocity field. Here, we adopt the Rotne-Prager model because it has the advantage to always provide positive-definite diffusion tensors. Considering two generic atoms α, β the 3×3 blocks of the unconstrained diffusion tensor (here called $\boldsymbol{\Delta}$) are then given by

$$\begin{cases} \boldsymbol{\Delta}_{\alpha\alpha} = \frac{k_B T}{\Xi_0} \, \mathbf{1}_3 & \\ \boldsymbol{\Delta}_{\alpha\beta} = \frac{k_B T}{8\pi\eta r_{\alpha\beta}} \left[\left(1 + \frac{2R_e^2}{3r_{\alpha\beta}^2} \right) \mathbf{1}_3 + \left(1 - \frac{2R_e^2}{r_{\alpha\beta}^2} \right) \frac{\mathbf{r}_{\alpha\beta} \otimes \mathbf{r}_{\alpha\beta}}{r_{\alpha\beta}^2} \right] & \text{if } r_{\alpha\beta} \geq 2R_e \\ \boldsymbol{\Delta}_{\alpha\beta} = \frac{k_B T}{8\pi\eta r_{\alpha\beta}} \left[\frac{r_{\alpha\beta}}{2R_e} \left(\frac{8}{3} - \frac{3r_{\alpha\beta}}{4R_e} \right) \mathbf{1}_3 + \frac{\mathbf{r}_{\alpha\beta} \otimes \mathbf{r}_{\alpha\beta}}{8R_e^2} \right] & \text{if } r_{\alpha\beta} \leq 2R_e \end{cases} \tag{3.12}$$

where $\mathbf{r}_{\alpha\beta} = \mathbf{r}_\alpha - \mathbf{r}_\beta$, $r_{\alpha\beta} = |\mathbf{r}_{\alpha\beta}|$ and $\otimes$ the dyadic product. From eqn. (3.10) using again Einstein relation (eqn. (3.11)), $\mathbf{D}$ is easily found as

$$\mathbf{D} = \left(\mathbf{B}^{\mathrm{tr}} \, \boldsymbol{\Delta}^{-1} \, \mathbf{B} \right)^{-1} \tag{3.13}$$

3.3 Implementation

Here we just provide a short overview about the implementation. In a separate code embedded in the framework of the Gaussian package we have merged the computation of the potential (or free, *vide infra*) energy along the generalized coordinate with the calculation of the diffusion tensor along the same path. In particular during the scan along the internal coordinate, the molecular geometry can be optimized or not (relaxed and non-relaxed scan). In both cases at each step of the scan, the generalized coordinate s is calculated and the new Cartesian coordinates referred to the MF are given. The MF is chosen at the initial geometry to be fixed on the molecule center of mass and in Eckart orientation; all the following coordinates $\mathbf{c}$ are referred to this MF; in the present version of the code the derivatives $\frac{\partial \mathbf{c}}{\partial s}$ are calculated numerically, although implementation of analytical derivatives is under way. Several checks have been anyways performed to verify the stability of the numerical approach.

After the boundary conditions are chosen, the only free-parameter is the hydrodynamic radius of the beads R_e. Following ref. [31] we chose an effective sphere radius as the weighted arithmetic mean

$$R_e = \frac{\sum_X n_X R_X}{\sum_X n_X} \tag{3.14}$$

where n_X is the number of atoms of type X and R_X is the associated van der Waals (vdW) radius (we use the UFF set of vdW radii [67]). From this computation and the whole diffusion tensor calculation we only take into account non-hydrogen atoms, because the hydrogen ones are negligible from the consideration of exposed surface "wetted" by the solvent and typically they end up only with numerically negligible contributions.

3.4 Case-study calculations

In this Section we apply the method sketched above in Section 3.2 to some case-study molecules. Our goal is to determine $D_{GG}(s)$ from the integrated

calculation of the potential scan along the generalized coordinate with the calculation of the diffusion tensor along the same path. In some cases we shall use these two pieces of information to set up and solve a one-dimensional Smoluchowski equation for the generalized coordinate treated as a diffusive one and making use of the novel DVR solving approach illustrated in Chapter 2.

We shall examine three test cases of chemical interest in order to illustrate the applicability of the method, starting from the internal rotation around the central C-C bond of n-butane and we shall compare our results with those delivered by the DiTe software [31] showing the reliability of the novel approach. Next, we investigate the inversion motion (envelope twist) of cyclopentene that couldn't be treated with the previous softwares and finally the internal rotation of 3-chloro-2-(chloromethyl)toluene and 2,2'-bifuran. The hydrodynamic boundary constant has been always set equal to $C = 6$, (stick boundary conditions). Since the examined potential and diffusion profiles along s will result periodic, periodic boundary conditions for a generic range are used, eqns. (2.20, 2.21).

n-butane

The generalized coordinate s is calculated along the internal rotation of the central C-C bond θ, starting from the optimized geometry of n-butane, and performing both a non-relaxed and a relaxed scan of 100 steps in the range $0° < \theta < 360°$; where $\theta = 0°$ corresponds to the eclipsed conformation (see Figure 3.2, panel a). Initially we have performed a non-relaxed scan that is useful in order to compare our results with DiTe ones for the same system. In fact, we can retrieve $D_{II}(\theta)$ (quantity calculated by DiTe) from the knowledge of $D_{GG}(s)$ and of the variations of s with θ, *i.e.* $\frac{ds}{d\theta}$, and this can be done inside our program, again carried out numerically. As it can be seen in panel a of Figure 3.3 the two profiles are identical, confirming the consistency of our approach and the linear variation of s with respect to θ (panel b), as expected from a non-relaxed scan. This is no more true when a relaxed scan is performed, indeed s shows a curvilinear dependence from θ.

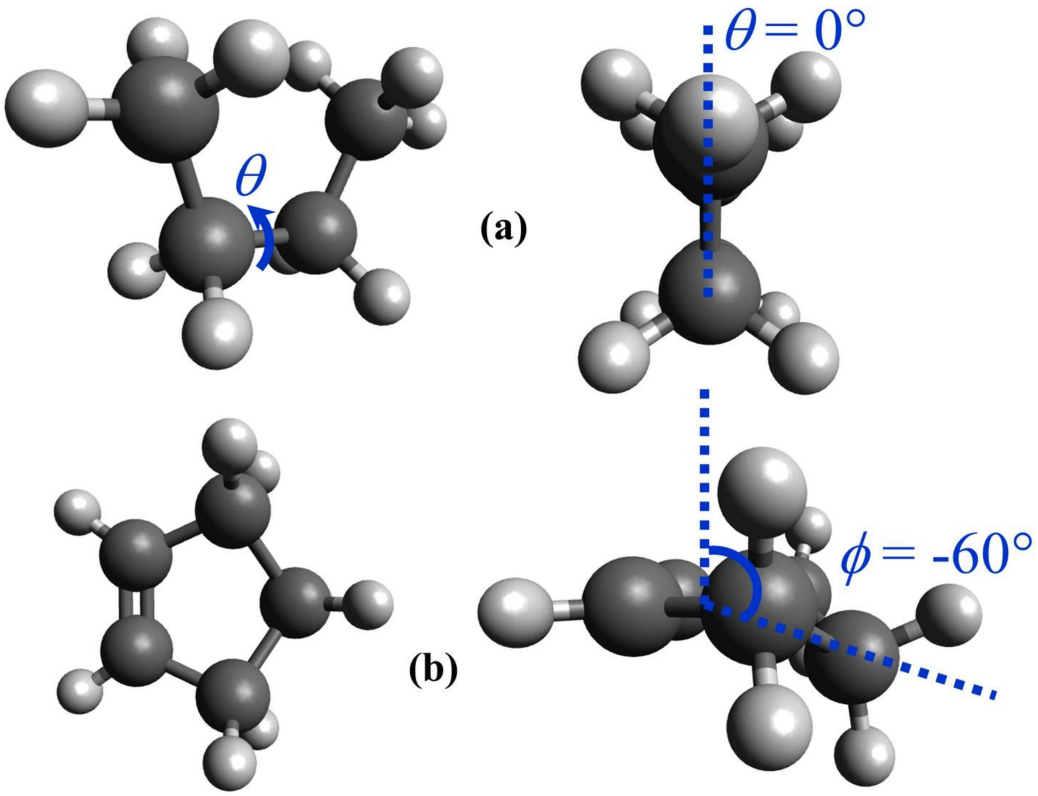

Figure 3.2: Sketch of *n*-butane (panel a) and cyclopentene (panel b) starting conformations for the scans along the highlighted internal coordinate.

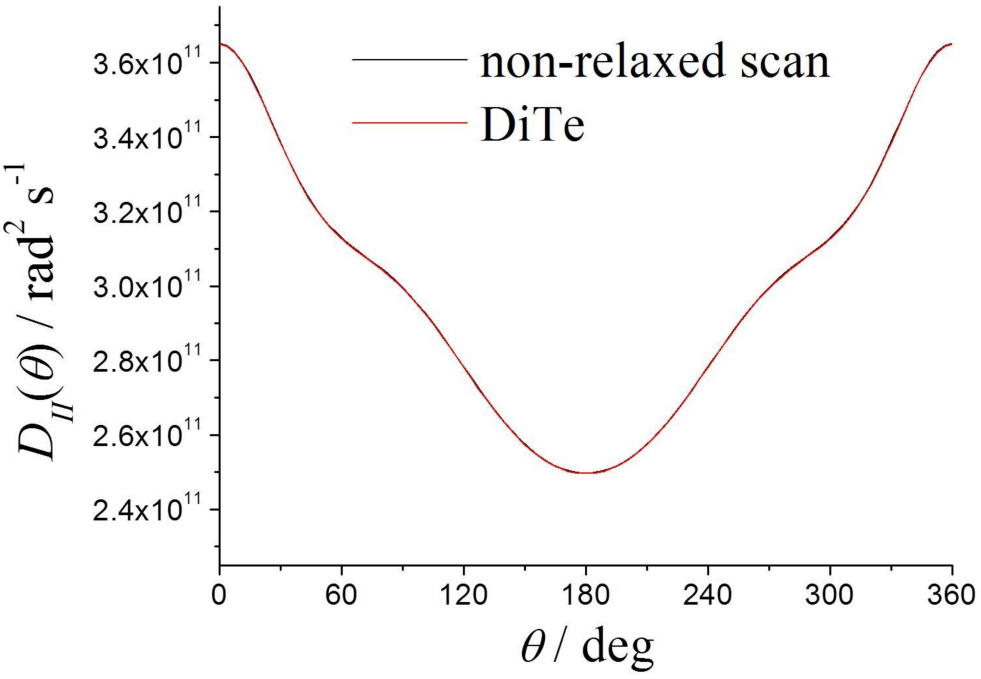

(a)

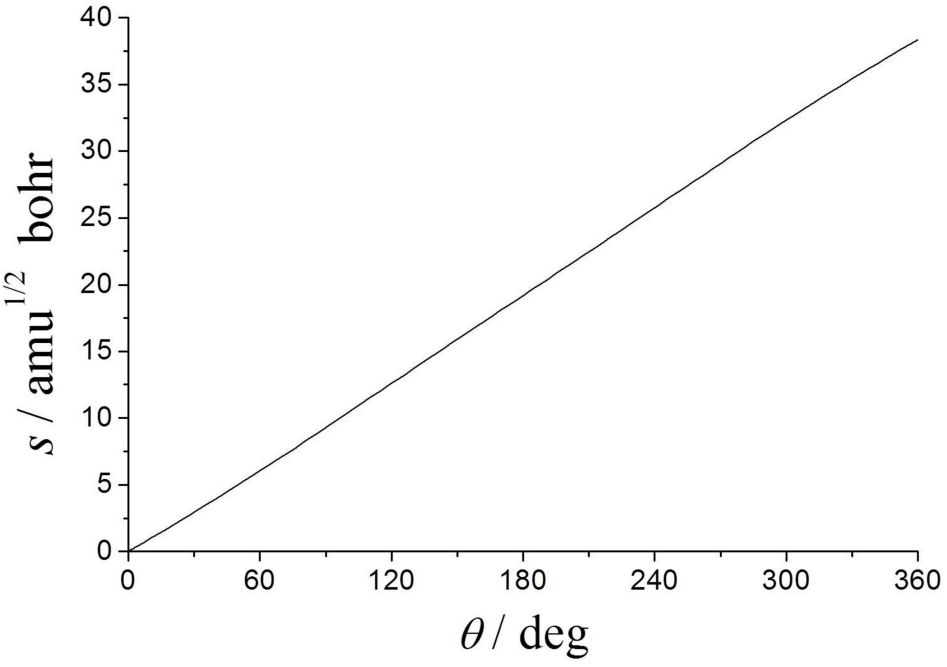

(b)

Figure 3.3: Panel a; calculated internal component of the diffusion tensor of n-butane from the non-relaxed scan (black line) and from DiTe (red line) at $T = 292$ K; the two curves are coincident. Panel b; variation of the generalized coordinate s with respect to the internal rotation θ.

Then we have performed a relaxed scan for the same system at the B2PLYP level [68, 69] using the aug-cc-pVTZ basis [70], adding dispersion corrections by the D3 empirical model [71] and including bulk solvent effects of *n*-butane by the conductor version of the polarizable continuum model (C-PCM) [72]. Note that the energy issuing from this treatment has the status of a free energy [73] and the only significant approximation (which can be lifted if needed) is to consider constant the frequencies of small amplitude motions perpendicular to the large amplitude path. The calculated energetics $V(s)$ and diffusion $D_{GG}(s)$ profiles are shown in Figure 3.4. The angular dependence of diffusion coefficient shows significant variations implying that the choice of a constant diffusion as in Subsection 2.3.3 is not recommended in order to properly describe diffusion properties and retrieve reliable observables (*vide infra*). We want to stress that there is no direct link between potential and diffusion. As stated before, they are essential ingredients to set up and solve the Smoluchowski equation for the generalized coordinate treated as a stationary diffusive process. Similarly to what we have done in Subsection 2.3.3, we use the two first lowest and non zero eigenvalues and the equilibrium populations in order to calculate the kinetic constants for the transitions between the three stable conformations, eqn. (2.42). These conformations can be identified with the three wells (marked with an asterisk in panel a of Figure 3.4) separated by a sufficiently high energy gap and they geometrically correspond to the two equivalent *gauche* and the *trans* conformation (from now on respectively abbreviated as $g_\pm$ and t). Edberg and coworkers [74] have calculated the kinetic constant $k_{t\to g_\pm} = 1.9 \times 10^{10}$ s^{-1} and $k_{g_\pm\to t} = 2.9 \times 10^{10}$ s^{-1} performing a nonequilibrium molecular dynamics simulation of bulk *n*-butane at $T = 292$ K. At the same temperature and using the viscosity of the medium as the one of *n*-butane [75] we obtain $k_{t\to g_\pm} = 3.75 \times 10^9$ s^{-1} and $k_{g_\pm\to t} = 1.17 \times 10^{10}$ s^{-1}, while assuming the same potential in the $[0°, 360°]$ range but using $D_{II}(\theta)$ calculated from DiTe we obtain $k_{t\to g_\pm} = 3.41 \times 10^9$ s^{-1} and $k_{g_\pm\to t} = 1.07 \times 10^{10}$ s^{-1}. The kinetic constants calculated with our method and with Dite are very similar, confirming the reliability of our approach and showing that the relaxation effects of a small molecule like *n*-butane are quite irrelevant. With respect to the values

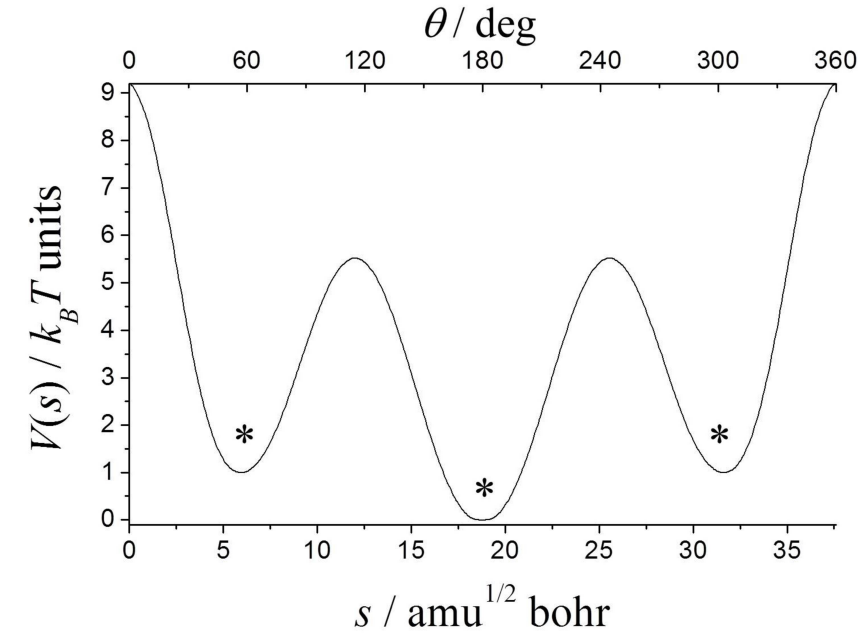

(a)

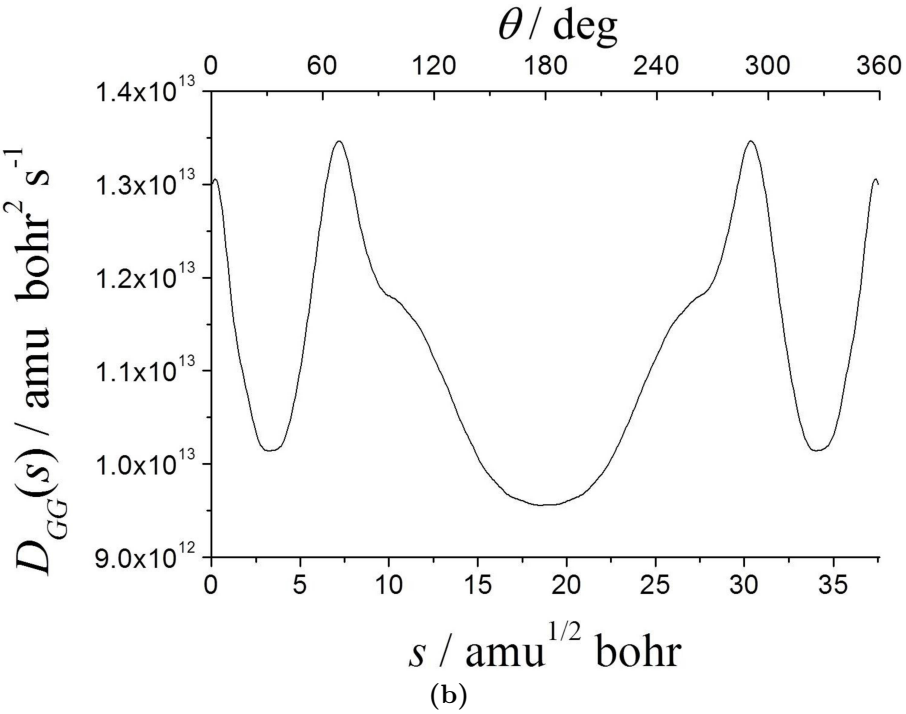

(b)

Figure 3.4: Calculated potential energy of n-butane from the relaxed scan (panel a) and diffusion along the generalized coordinate (panel b). The asterisks on the potential wells highlight the stable conformations. The upper axis shows the corresponding internal coordinate upon which the scan is performed. ($T = 292$ K)

reported in the work of Edberg and coworkers, our $k_{t\to g_\pm}$ in both cases are one order of magnitude smaller, while $k_{g_\pm\to t}$ are very close. We believe that this difference is mainly due to the fact that in our kinetic model we are not accounting for the solvent fluctuations around the molecule, in other words, we are considering the surrounding solvent molecules as if they are at equilibrium. Finally, the importance of including hydrodynamic interactions and the angular dependence of diffusion coefficient (differently from Subsection 2.3.3) is evident if we calculate $k_{t\to g_\pm}$ and $k_{g_\pm\to t}$ with a constant diffusion coefficient. Indeed, in this specific situation $k_{t\to g_\pm} = 5.1 \times 10^{11}$ s^{-1} and $k_{g_\pm\to t} = 2.2 \times 10^{12}$ s^{-1} obtaining an overestimation of the kinetic constant values because of the simple hydrodynamical model adopted (*i.e.* constant diffusion).

cyclopentene

The generalized coordinate s is calculated along the envelope movement regulated by a properly defined bending angle ϕ (see Figure 3.2, panel b), performing a relaxed scan of 100 steps in the range $-60° < \phi < 60°$ where $\phi = 0°$ correspond to the situation in which the envelope is completely opened (the energy minimum). We want to stress that this kind of computation was unfeasible using previous softwares like HYDRONMR and/or DiTe. The relaxed scan for the same system is performed at the B3LYP level [76] adding the D3 dispersion corrections and 6-31++G** basis including bulk solvent effects of carbon tetrachloride by the C-PCM. The potential and $D_{GG}(s)$ are shown in Figure 3.5 and, as expected, it can be seen that $V(s)$ is just a parabola inside which the system oscillates around the minimum along s. This is also confirmed after solving the Smoluchowski equation where there is no neat separation (in terms of orders of magnitude) between the eigenvalues, and consequently they can only be associated to fast processes of fluctuations inside the well.

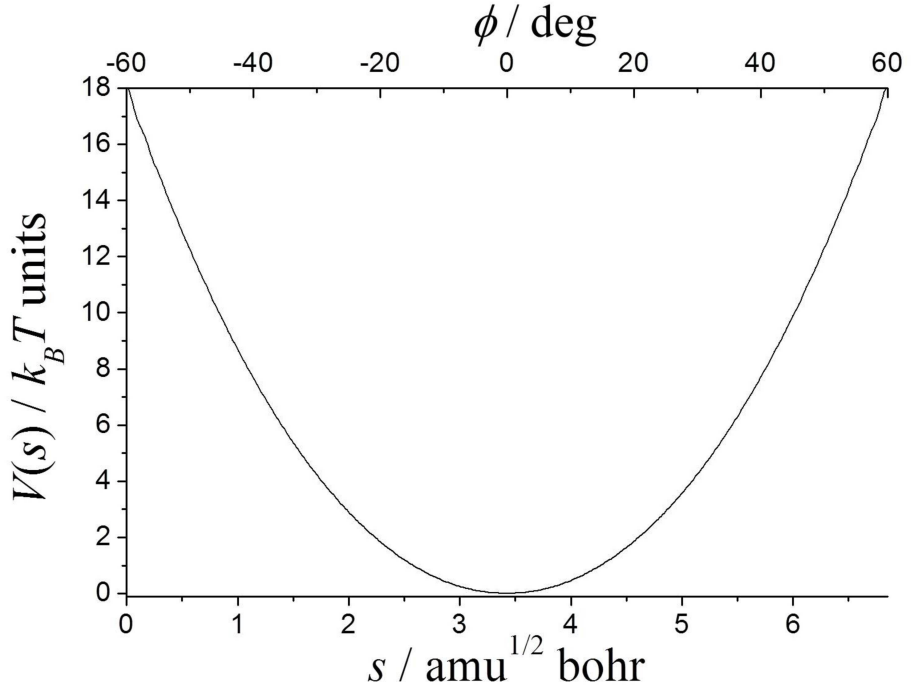

(a)

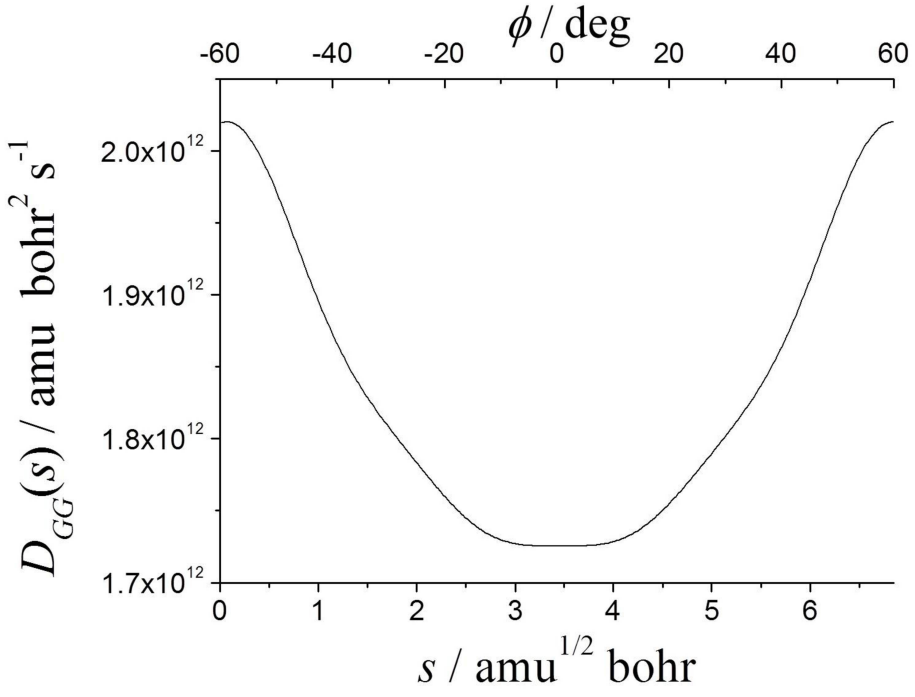

(b)

Figure 3.5: Calculated potential energy of cyclopentene from the relaxed scan (panel a) and diffusion along the generalized coordinate (panel b). The upper axis shows the corresponding internal coordinate upon which the scan is performed. ($T = 298.15$ K)

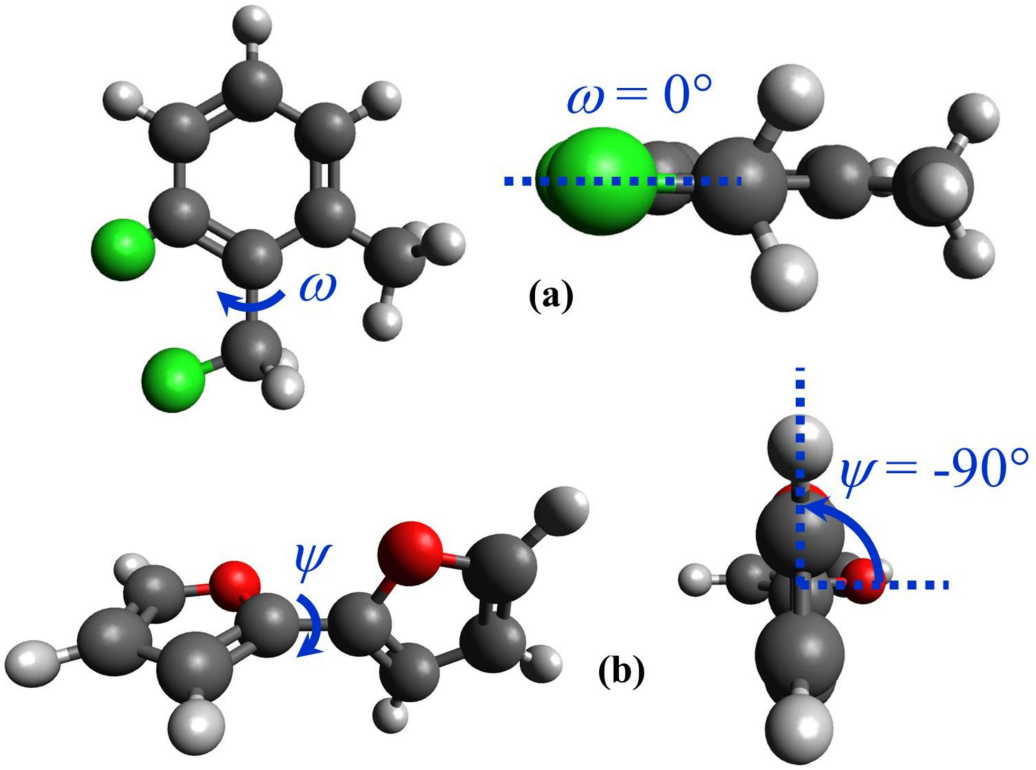

Figure 3.6: Sketch of 3-chloro-2-(chloromethyl)toluene (panel a) and 2,2'-bifuran (panel b) starting conformations for the scans along the highlighted internal coordinate.

3-chloro-2-(chloromethyl)toluene and 2,2'-bifuran

The generalized coordinate s is calculated along the internal rotation of 3-chloro-2-(chloromethyl)toluene C-C bond and the central one in 2,2'-bifuran (see Figure 3.6), performing a relaxed scan of 100 steps in the range $0° < \omega < 360°$ and $-90° < \psi < 270°$ for 3-chloro-2-(chloromethyl)toluene and 2,2'-bifuran molecules respectively. The relaxed scan for both systems is conducted at B3LYP level adding the D3 dispersion corrections and 6-31++G** basis including bulk solvent effects of carbon tetrachloride by the C-PCM. The potential and the generalized part of the diffusion tensor $D_{GG}(s)$ are shown in Figure 3.7 and Figure 3.8, as it can be seen they are both bistable with equivalent and nonequivalent minima respectively. Again, it is not possible to make direct inferences between the potential and diffusion

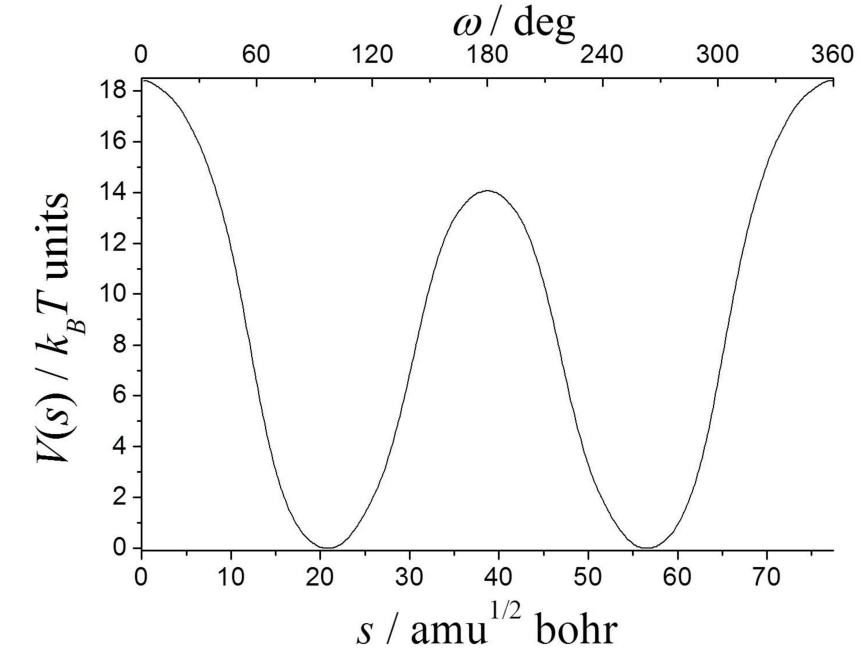

(a)

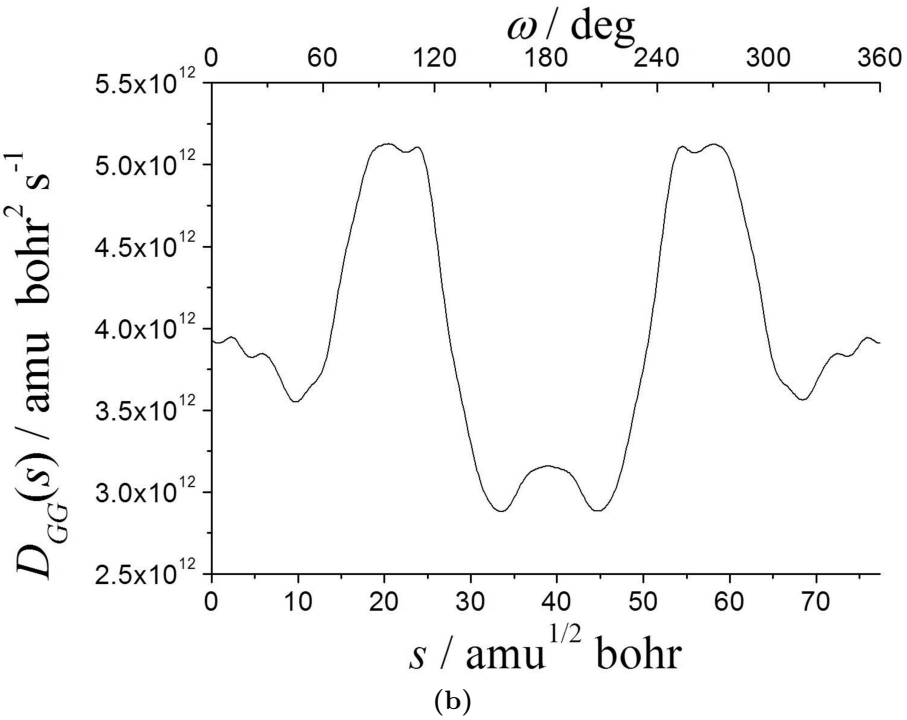

(b)

Figure 3.7: Calculated potential energy of 3-chloro-2-(chloromethyl)toluene from the relaxed scan (panel a) and diffusion along the generalized coordinate (panel b). The upper axis shows the corresponding internal coordinate upon which the scan is performed. ($T = 298.15$ K)

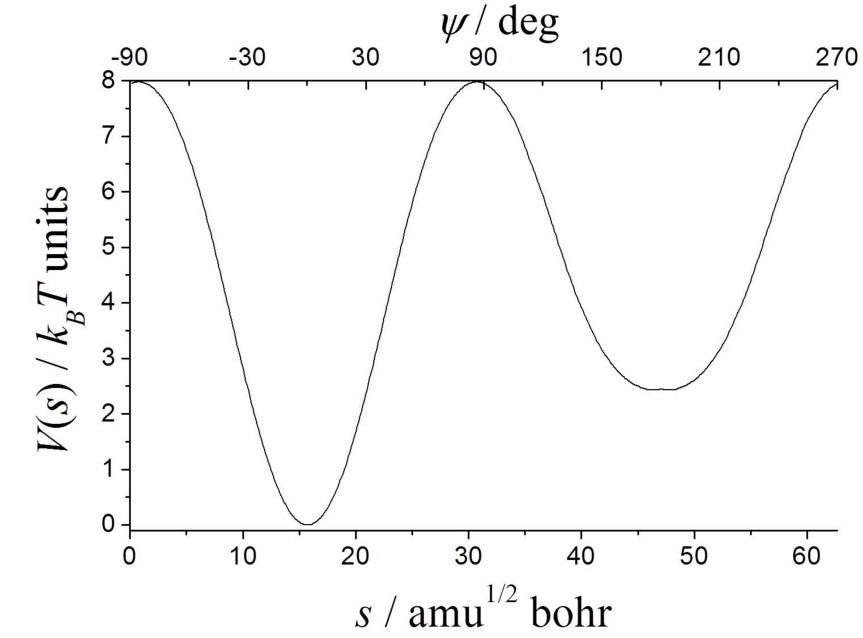

(a)

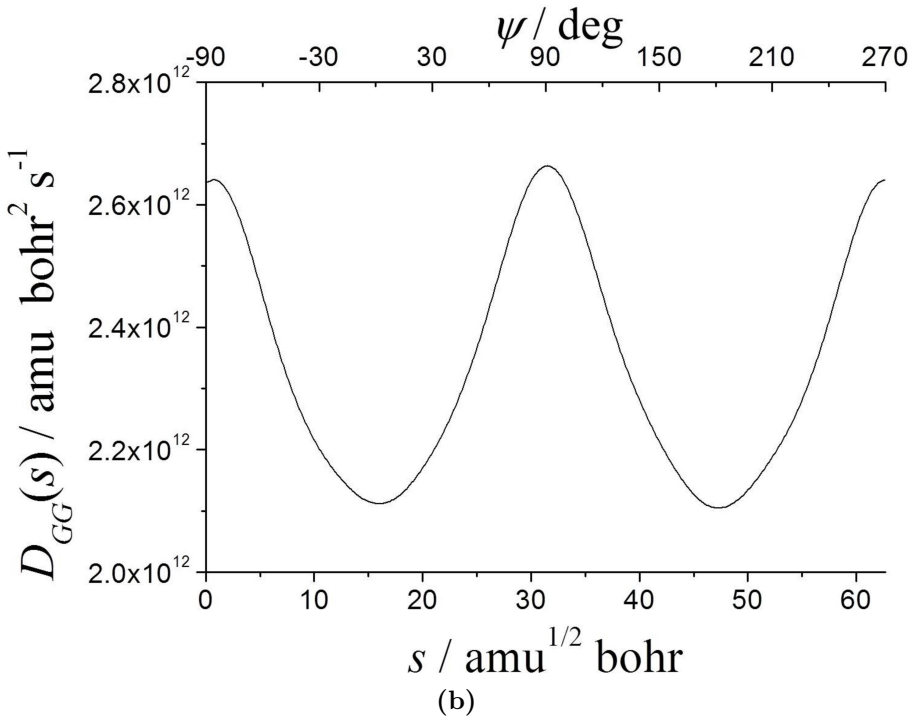

(b)

Figure 3.8: Calculated potential energy of 2,2'-bifuran from the relaxed scan (panel a) and diffusion along the generalized coordinate (panel b). The upper axis shows the corresponding internal coordinate upon which the scan is performed. ($T = 298.15$ K)

profiles. We use them both to set up and solve the Smoluchowski equation for the generalized coordinate treated as a stationary diffusive process and, as in the n-butane case, we calculate the kinetic constant for the transitions between the wells. Since this time the number of possible jumps is reduced (the forward and backward jump between the two wells), the kinetic model is different than for the n-butane case and this is also the case for the expression that links the eigenvalues to the kinetic constants, k_f and k_b respectively. In fact, in the case of a bistable potential we adopt a 2 elementary reactions mechanism between the two stable conformations (here labeled as "1" and "2")

$$\begin{aligned} 1 &\xrightarrow{k_f} 2 \\ 2 &\xrightarrow{k_b} 1 \end{aligned} \tag{3.15}$$

related by microscopic reversibility

$$k_f \, P_{eq,1} = k_b \, P_{eq,2} \tag{3.16}$$

In the case of equivalent minima (3-chloro-2-(chloromethyl)toluene case) $k_f = k_b$. The resulting expressions for the rate constants are

$$k_f = \frac{\lambda_1}{\frac{P_{eq,1}}{P_{eq,2}} + 1} \tag{3.17}$$

for the 2,2'-bifuran case and

$$k_f = k_b = \frac{\lambda_1}{2} \tag{3.18}$$

for the 3-chloro-2-(chloromethyl)toluene case. At room temperature $T = 298.15$ K and using the viscosity of the medium as the one of carbon tetrachloride [75] we obtain $k_f = k_b = 3.18 \times 10^6$ s^{-1} for the first molecule and $k_f = 4.30 \times 10^7$ s^{-1}, $k_b = 2.67 \times 10^8$ s^{-1} for the second one. As expected, the huge barrier for 3-chloro-2-(chloromethyl)toluene gives the smallest kinetic constant, while for 2,2'-bifuran, considering that the backward jump faces an

energy barrier similar to the ones of n-butane jumps, the lower magnitude of diffusion gives globally lower kinetic constants.

3.5 Final remarks

In this Chapter we have constructed and implemented an effective approach for computing diffusion tensors depending on a generalized large amplitude coordinate. The proposed approach is obtained by the integration of previous proposals for diffusive processes (mainly the HYDRONMR and DiTe approaches) with the intrinsic reaction coordinate and reaction path Hamiltonian descriptions of general large amplitude motions. The analysis of some case studies involving medium-size molecular systems shows that the new implementation fully agrees with the DiTe results for non relaxed scans, whereas it allows to improve the agreement with experimental results due to its ability of including full relaxation along directions perpendicular to the generalized large amplitude coordinate.

A number of extensions of the approach is possible. The first step is the solution of systems of coupled Smoluchowski equations including reactive terms [6, 7, 8, 77, 78, 79], of particular interest for the study of time resolved fluorescence experiments or, more generally, of photochemical processes. This will be the main topic of the next Chapter. In parallel, methods for solving stochastic Liouville or Fokker-Planck [3] equations can be implemented along the same lines and can be of remarkable interest for instance in connection with magnetic (EPR and NMR) spectroscopies.

A more ambitious target is the extension of the approach to more than one internal generalized coordinate. Among the main difficulties encountered in this purpose there is the computational cost of performing a relaxed scan simultaneously along two internal coordinates, implying a large number of optimizations steps. Then the selection of internal coordinates upon which the scan is performed in order to construct multiple generalized coordinates is not trivial. To the best of our knowledge this choice is still subjective and related to chemical intuition. After the generalized coordinates are computed, calculation of hypothetical correlations between them is also a problem. A

final drawback concerns the usage of diffusion tensor in the Smoluchowski equation context. Indeed, this usage requires that the dynamics over these generalized coordinates still constitutes a Markov process. This is surely true for one-dimensional systems, but the same cannot be said for multidimensional ones.

By the way, work along the extension of the approach to more than one internal generalized coordinate has already been performed in the quantum mechanical community, leading to the so-called reaction surface Hamiltonian, in which all the remaining internal coordinates are optimized at selected values of two or three large amplitude coordinates [80, 81]. An alternative is to perform a principal component analysis of a trajectory obtained from *e.g.* molecular dynamics and to select a reduced number of eigenvectors of the covariance matrix (the so-called essential dynamics) as large amplitude coordinates [42]. The theoretical machinery for all these approaches is well known and the corresponding stochastic equations can be solved by multidimensional extensions of the DVR approach, which are also well known in the quantum mechanical community [82, 83].

Numerical stability of the approach presented in this Chapter is guaranteed by the replacement of numerical derivatives by their analytical counterparts along the same lines recently followed in connection with vibronic contributions to electronic spectra [84, 85]. Numerical stability is also guaranteed by the reliability and the efficiency of DVR approach to one-dimensional problems [1] presented in Chapter 2 and, in different contexts, also for multidimensional problems [82, 83].

A final issue concerns the use of electronic energies in place of (the correct) free energies. From the one side, free-energies can be obtained by computing harmonic frequencies at different values of the large amplitude coordinate for all the remaining orthogonal (small amplitude) motions and employing well known statistical thermodynamics equations. Even leading anharmonicities can be included for those transverse motions by means of *e.g.* second order vibrational perturbation theory (VPT2) [46, 69, 86, 87]. From another side true dynamical techniques like *e.g.* the so called dynamic reaction coordinate [88] or metadynamics [89] can be employed to obtain free energies as a

function of the large amplitude generalized coordinate. Another recent and relevant alternative is represented by the construction of free-energy profiles along a specific coordinate using non-equilibrium sampling methods based on Jarzinsky's equality and Crook's theorem [90, 91]. The essence of Jarzinsky's equality is to put in relation the free-energy difference between two states of the coordinate of interest with the statistical distribution of the amounted work done in order to bring the system from the first state to the second one by following an arbitrary transformation protocol. [92, 93, 94]

Chapter 4

General Approach to Coupled Reactive Smoluchowski Equations: Integration and Application of DVR and Generalized Coordinate Methods to Diffusive Problems

The chemist is often faced with several microscopic processes that are diffusive in nature, for example solution phase chemical processes, biochemical kinetics or configurational dynamics of fluorophores in liquid solution. For such microscopic systems in solution, apart from pure diffusion, reactive phenomena involving one or more species can also be included. As an example, problems such as recombination of isolated ion pairs [77], fluorescence quenching [6, 78, 79], and intramolecular electron transfer [95, 9, 96] have been considered in the past. The picture of the whole process must include the coupling between the reactant species and in this view the description and theoretical modeling of such complicated systems become difficult and in many cases is not trivial.

The main problems that emerge are the selection of reliable tools from the theoretical chemistry and how they can be used in order to properly model the reactivity; in particular how to face and include the coupling of the different reactant species to diffusion and between them. This problem has been faced in the past by many scientific groups using chemical kinetics and in many cases the most robust theoretical tools from stochastic processes field. [3, 4] Here we take into consideration this last branch that has paved the road to a proper modeling of several microscopic processes which are diffusive in nature, adopting the Smoluchowski or more complicated Fokker-Planck equations.

For such systems diffusion can be thought of as occurring along one or more relevant coordinates. Then, reactivity can be taken into account by adding a coordinate dependent rate constant to the equation that is coupled to diffusion. Just to mention, in the last four decades, several works that have used this approach have adopted the so called reactive Smoluchowski equation; *e.g.* the pioneering works of Agmon and Hopfield on geminate recombination in excited-state proton transfer reactions [7, 8, 10], the diffusive dynamics of CO binding to heme proteins [11, 97], the barrierless isomerization in solution [77], the twisted-intramolecular charge transfer (TICT) from singlet excited state [6, 98], etc.

By the way, all these problems still lack a general and solid approach. In many cases the coupling that describes the population exchange between different diffusional states is absent and/or not directly explicit. In fact, the chemist is often faced with such diffusional problems and in the presence of reversible reactions, two or more coupled Smoluchowski equations are needed in order to describe completely the time evolution of the probability density. From this information, after proper modeling, observables can be retrieved; just to mention, computed time resolved emission spectra, rates, binding constants and survival probabilities.

We propose a general approach to a system of coupled reactive Smoluchowski equations capable to properly describe reactive systems in solution. We set down the main equations that govern the microscopical evolution of the system where we include the possibility of population exchange or dis-

appearance; calculating and considering respectively, coordinate dependent rate constants and sink contributions. We merge in a modular code all our previous developments on the solution of the one-dimensional Smoluchowski equation and molecular diffusion field seen in previous Chapters. So we merge the robust numerical approach rooted in the discrete variable representation (DVR) in order to solve the equation [1] and the variable diffusion tensor along a one-dimensional generalized coordinate considered as a diffusive process [2].
We briefly recall that the advantage in using DVR, instead of classical numerical methods such as finite difference methods and/or spectral methods, is the higher performances in terms of rapid eigenvalues convergence with the use of few grid points.
While the advantage in using a generalized coordinate is to treat diffusive problems involving motion along more general paths, this motion is parameterized by the generalized coordinate that lacks an absolute analytical expression, but is rather described only by a nonlinear combination of local (curvilinear) coordinates.

The final goal is to have a reliable framework with which it is possible to set up and solve two or more coupled Smoluchowski equations along a generalized coordinate with reactive and/or sink coordinate dependent contributions. In this view we propose a novel and reliable machinery different from the previous one proposed by Krissinel' and Agmon [77], surpassing the problems found in the past and integrating the combined effect of our two novel approaches. The code is embedded in the previously implemented framework for the diffusion tensor, in a development version of the Gaussian code [49].

A specific test case is used in order to verify the reliability of the code. Then we apply our integrated tool to the study case of TICT state fluorescence of (N, N-dimethylamino)benzonitrile (DMABN) molecule in water.

In the next Section we provide the mathematical background underlying the implemented code for an arbitrary number of coupled diffusive and reactive states; in Sections 4.2 and 4.3 we give some details about the reliability of the implemented code and its application to a specific case of chemical

interest.

4.1 Coupled reactive Smoluchowski equations

We consider n coupled states upon which diffusion and reaction take place along the same generalized coordinate s. The reactive one-dimensional Smoluchowski equation for the i-th state reads

$$\frac{\partial p_i(s,t)}{\partial t} = -\Gamma_i\, p_i(s,t) - \left[l_i(s) + \sum_{j \neq i}^{n} k_{ij}(s) \right] p_i(s,t) + \sum_{j \neq i}^{n} k_{ji}(s)\, p_j(s,t) \quad (4.1)$$

where again, $p_i(s,t)$ is the probability density of finding a value of s at time t, while Γ_i is the diffusion operator, eqn. (1.2), for the i-th state here reported for convenience,

$$\Gamma_i = -\frac{\partial}{\partial s}\, D_i(s)\, p_{i,eq}(s)\, \frac{\partial}{\partial s}\, p_{i,eq}^{-1}(s) \quad (4.2)$$

This operator, under the potential $V_i(s)$ and diffusion function $D_i(s)$ of the i-th state, regulates the population relaxation till the stationary limit represented by the Boltzmann distribution, eqn. (2.6).

The term $k_{ij}(s)$ physically represents the rate at which the population of the i-th state at a specific value of s migrates towards the j-th state, while the sink term $l_i(s)$ physically represents the rate of population depletion from the i-th state at a specific value of s. The combined effect of potential and diffusion governs the population dynamics starting from an initial distribution and widening it till the equilibrium state. But in the presence of reactive terms that are respectively, the reaction rate $k_{ij}(s)$ from level i to level j and the sink term $l_i(s)$, the achievement of a stationary limit and the normalization condition of the populations $\int p_i(s,t)\, ds = 1,\ \forall t$ are no longer guaranteed.

The computation of the generalized coordinate s is carried out by means of eqn. (3.3) with the method reported in Section 3.1, while the diffusion tensor along the same $D_i(s)$ is carried out with the approach reported in Section 3.2. The main theory and equations underlying the DVR approach are reported in Chapter 2. Here we recall and summarize for clarity the main

steps in order to apply DVR to the system of coupled reactive Smoluchowski equations:

1. Using eqn. (2.6) we express Γ_i in a more convenient way, allowing the evaluation of large values of $V_i(s)$ with no numerical problems

$$\begin{aligned}\Gamma_i &= D_i(s)\left[\frac{\partial^2}{\partial s^2}+\frac{\partial}{\partial s}\frac{V_i(s)}{k_BT}\frac{\partial}{\partial s}+\frac{\partial^2}{\partial s^2}\frac{V_i(s)}{k_BT}\right]\\ &\quad+\frac{\partial}{\partial s}D_i(s)\frac{\partial}{\partial s}+\frac{\partial}{\partial s}D_i(s)\frac{\partial}{\partial s}\frac{V_i(s)}{k_BT}\end{aligned} \tag{4.3}$$

2. We express the operators acting on $p_i(s,t)$ and $p_j(s,t)$ in the DVR matrix form by using product approximation, making use of approximate resolution of the identity and recalling the DVR matrix representation of first and second derivative operators (respectively $\mathbf{D}^{(1)\,\mathrm{DVR}}$ and $\mathbf{D}^{(2)\,\mathrm{DVR}}$) for bounded and periodic potentials see eqns. (2.16, 2.17, 2.20, 2.21) in Section 2.2,

$$\begin{aligned}\mathbf{M}_i^{\mathrm{DVR}} &= \mathbf{D}_i^{\mathrm{DVR}}\left[\mathbf{D}^{(2)\,\mathrm{DVR}}+\beta\,\mathbf{V}_i'^{\mathrm{DVR}}\,\mathbf{D}^{(1)\,\mathrm{DVR}}+\beta\,\mathbf{V}_i''^{\mathrm{DVR}}\right]\\ &\quad+\mathbf{D}_i'^{\mathrm{DVR}}\,\mathbf{D}^{(1)\,\mathrm{DVR}}+\beta\,\mathbf{D}_i'^{\mathrm{DVR}}\,\mathbf{V}_i'^{\mathrm{DVR}}\\ &\quad-\left[\mathbf{l}_i^{\mathrm{DVR}}+\sum_{j\neq i}^{n}\mathbf{k}_{ij}^{\mathrm{DVR}}\right]\end{aligned} \tag{4.4}$$

3. Choosing the same DVR grid points $\{s_\alpha\}$ for the generalized coordinate s we construct the total DVR matrix $\mathbf{M}^{\mathrm{DVR}}$;

$$\frac{\partial}{\partial t}\begin{pmatrix}\mathbf{p}_1\\ \vdots\\ \mathbf{p}_i\\ \vdots\\ \mathbf{p}_n\end{pmatrix}=-\underbrace{\begin{pmatrix}\mathbf{M}_1^{\mathrm{DVR}} & \cdots & -\mathbf{k}_{i1}^{\mathrm{DVR}} & \cdots & -\mathbf{k}_{n1}^{\mathrm{DVR}}\\ \vdots & & \vdots & & \vdots\\ -\mathbf{k}_{1i}^{\mathrm{DVR}} & \cdots & \mathbf{M}_i^{\mathrm{DVR}} & \cdots & -\mathbf{k}_{ni}^{\mathrm{DVR}}\\ \vdots & & \vdots & & \vdots\\ -\mathbf{k}_{1n}^{\mathrm{DVR}} & \cdots & -\mathbf{k}_{in}^{\mathrm{DVR}} & \cdots & \mathbf{M}_n^{\mathrm{DVR}}\end{pmatrix}}_{\mathbf{M}^{\mathrm{DVR}}}\begin{pmatrix}\mathbf{p}_1\\ \vdots\\ \mathbf{p}_i\\ \vdots\\ \mathbf{p}_n\end{pmatrix} \tag{4.5}$$

4. Eigenvalues and eigenfunctions are then calculated from the numerical diagonalization of $\mathbf{M}^{\mathrm{DVR}}$. Given the initial distributions $p_i(s,0)$, the

profiles $p_i(s,t)$ are built expanding upon DVR functions calculated at DVR points $\{s_\alpha\}$.

Code details

The code has been written in a modular fashion inside the previously implemented framework for the diffusion tensor, in the same development version of the Gaussian code [49]. After the user has chosen the system of interest, he/she must specify the number n of coupled states upon which the population relaxes under the combined effect of diffusion and reaction. Also he/she must specify the number α of DVR grid points $\{s_\alpha\}$ and the endpoints $[a,b]$ of the generalized coordinate domain. Finally reactivity information, *i.e.* all $l_i(s)$ and $k_{ij}(s)$ functions, must be given as input numerical files.

Supplementary input information, such as the number of time steps upon which the profile is calculated, the initial and final time of propagation, hydrodynamical parameters for the diffusion function calculation must be given.

From the relaxed or rigid scan calculation (respectively, the molecular geometry is optimized at each scan step, the molecular geometry is not optimized at each scan step) the generalized coordinate s is calculated and the energetics $V_i(s)$ and the diffusion functions $D_i(s)$ are automatically retrieved from the program. The code, thanks to a built-in FORTRAN interpreter, can also retrieve these information from numerical input files prepared from the output of other computational chemistry tools.

Since $\mathbf{M}^{\mathrm{DVR}}$ is not hermitian and computations with complex numbers are required, all the linear algebra calculations are carried out using standard LAPACK and BLAS routines [99], optimized for such goal.

We are currently trying to merge the calculation of rate constants and sink terms, still not available in Gaussian, inside our framework (*vide infra*). Also many efforts are being done in order to ease the tedious input stage via a Guided User Interface (GUI) in the framework of the Virtual Multi-frequency Spectrometer (VMS) project [55, 100, 101].

4.2 Test-case

In this Section we show the reliability of the program by comparing the results obtained for a specific case where analytical solution is available. In particular this is the case for one state with a parabolic potential $V(s) = c_1 s^2$, constant diffusion coefficient D, and a parabolic sink term $l(s) = c_2 s^2$ for a chosen normalized initial distribution (here we have chosen $p(s,0) \equiv p_{eq}(s)$). For this case the survival probability $Q(t)$ defined as

$$Q(t) = \int_a^b p(s,t)\, ds \tag{4.6}$$

is analytical, and it reads [102]

$$Q(t) = \frac{\sqrt{8\gamma}\, e^{-Dc_1(2-\gamma)t/\gamma}}{\sqrt{(2+\gamma)^2 - (2-\gamma)^2\, e^{-4Dc_1 t/\gamma}}} \tag{4.7}$$

where γ is defined as

$$\gamma = \frac{2}{\sqrt{1 + \frac{c_2}{Dc_1^2}}} \tag{4.8}$$

The survival probability gives information about the cumulative probability of not reacting till time t.
The potential $V(s)$ is always expressed in $k_B T$ units (multiplied by β) for a constant temperature of 300 K.
We have chosen $c_1 = 0.25$, $c_2 = 0.5$, $D = 10^{-6}$ s^{-1} and the number of DVR grid points is $\alpha = 100$, in the domain $[-4.0, 4.0]$. In Figure 4.1 we compare the resulting profile of $Q(t)$ and the analytical one, eqn. (4.7). The two profiles are identical, confirming the consistency of our approach. The agreement has been verified also for steeper potential (higher values of c_1), different diffusion and sink magnitudes and diffusional space domains. Here we have shown the limit in which both diffusion and reaction take place, that is one of the most problematic case where space-dependent sink term is present. The reliability of the method in the case of free diffusion and/or no reactivity [1] has been shown in Chapter 2, guaranteeing the performance also in other simpler limits.

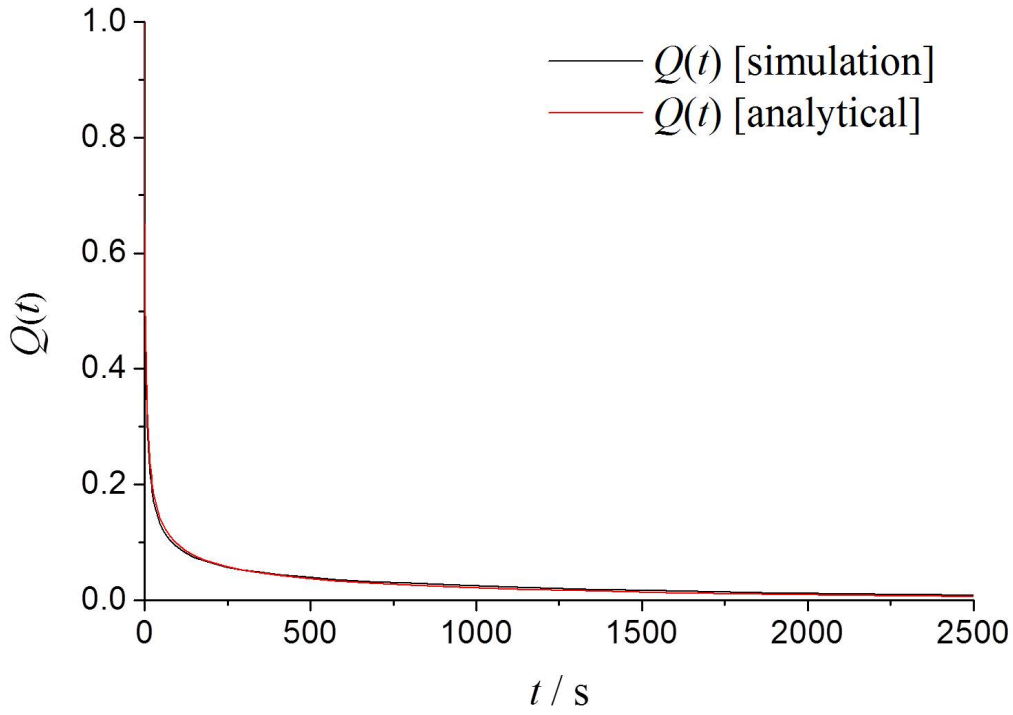

Figure 4.1: Plot of the survival probability for the test-case. The black line is the calculated survival probability with our code, while the red line is the analytical one, eqn. (4.7). The physical and diffusional parameters are reported in the text.

4.3 Application

In this Section we apply the whole framework presented till here to a specific case-study of chemical interest. We focused on the prototype TICT system of (N, N-dimethylamino)benzonitrile (DMABN) molecule depicted in Figure 4.2, studied with similar approaches in the past by Polimeno and coworkers, ref. [98]. This system and in general TICT systems are characterized by a high dipole moment in the excited singlet state S_1 when excited from the ground state S_0 minimum. The system then undergoes relaxation via the intramolecular rotation of the dimethyl group along the C–N bond (dihedral angle θ in Figure 4.2) reaching a potential minimum. Inversely, in this situation the dipole reaches its maximum value, and this state is known as TICT state. In the singlet excited state and in particular in the twisted situation, charge-transfer from S_1 occurs via a deactivation decay mechanism (both radiative and non-radiative in nature).

Inspired by the previous work of Pedone and coworkers, ref. [6], our objective is to determine the excited state dynamics of the population density $p_{\mathrm{ES}}(s,t)$ from which it is possible to calculate the time resolved emission spectra. By using our established modular framework we performed a relaxed scan calculation for both ground and excited states along the θ internal coordinate from which the generalized coordinate s, the ground $V_{\mathrm{GS}}(s)$ and excited state $V_{\mathrm{ES}}(s)$ potential energies and the diffusion functions, $D_{\mathrm{GS}}(s)$, $D_{\mathrm{ES}}(s)$ are calculated. Finally using quantum mechanical calculations (*vide infra*) we have calculated the reactive rate constant from the excited state to the ground state, $k_{\mathrm{ES,GS}}(s)$. We neglected the possibility of population disappearance and so we didn't consider the sink term $l_{\mathrm{ES}}(s)$. Also, since our focus is on the excited state dynamics and since the laser pulse is not continued after the instantaneous irradiation, the rate constant from the ground state to the excited state, $k_{\mathrm{GS,ES}}(s)$ is assumed to be zero.

S_0 and S_1 energetic and diffusion properties have been calculated by means of density functional theory (DFT) and time dependent (TD)-DFT [103] relaxed scan computations done with a development version of Gaussian, [49] employing hybrid exchange-correlation functional CAM-B3LYP

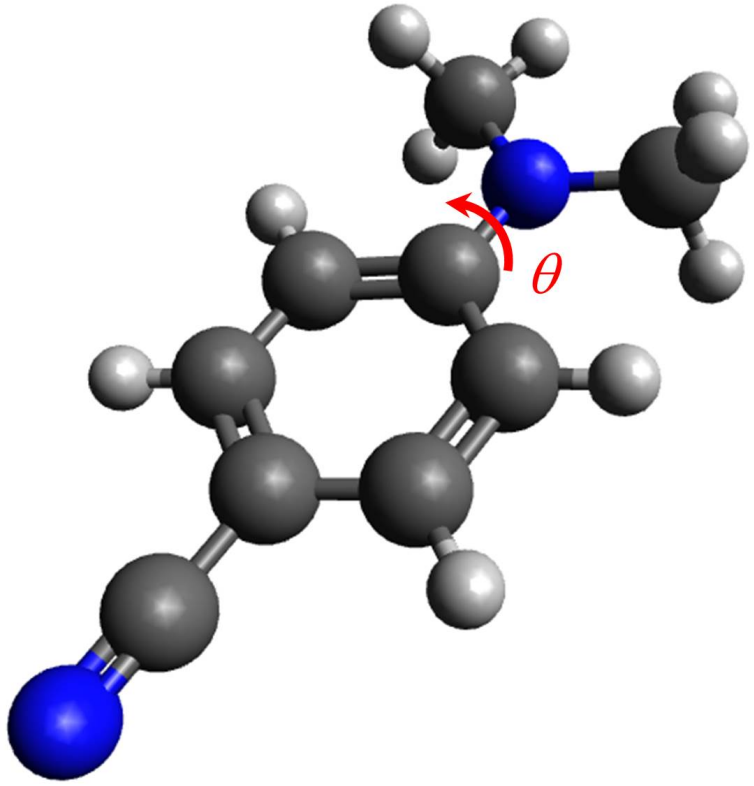

(a)

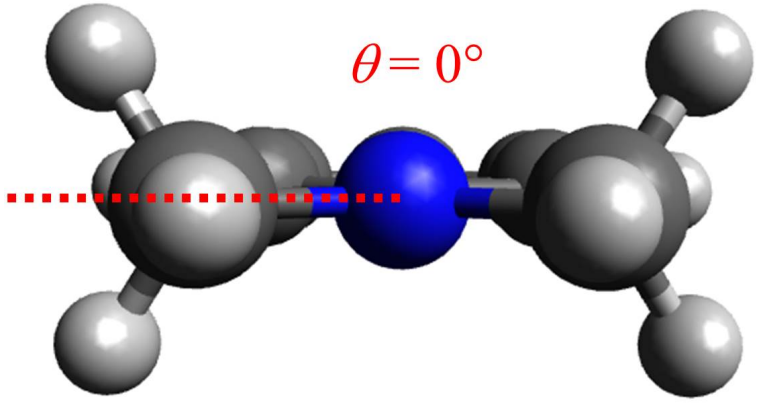

(b)

Figure 4.2: Panel a; sketch of the DMABN molecule depicting the optimized ground state geometry calculated at the level of CAM-B3LYP/6-31+G* in water. Panel b; starting conformation for the scan along the highlighted internal coordinate θ.

[104] and using 6-31+G* basis set. We chose the long-range corrected CAM-B3LYP functional because it is known that B3LYP functional [76] overestimates the energies of charge transfer states, for example as seen in the work of Pedone and coworkers for coumarin derivatives. Bulk solvent effects of water have been included by means of the polarizable continuum model (PCM) [73].

In panel a of Figure 4.3 we report $V_{\mathrm{GS}}(s)$ and $V_{\mathrm{ES}}(s)$ profiles, while in panel b we report the oscillator strength for the $S_0 \rightarrow S_1$ transition as a function of the generalized coordinate s. The ground state has a minimum at $\theta = 0°$, while at the same angle, the excited state has a maximum, corresponding to the locally excited (LE) state. Specular to this, the situation is inverted at $\theta = 90°$, where the excited state has now a minimum that is the TICT state, separated from the LE state by 9.018 $k_B T$ units. Just to have an idea, this is the order of magnitude of rotation barriers in common alkanes, *e.g.* n-butane [2, 105]. The oscillator strength is widely affected by the twist of the angle θ reaching its minimum at $\theta = 90°$; this suggests that at room temperature, the TICT state should not be populated.

Figure 4.4a shows the diffusion function profiles along the generalized coordinate, for the two states. Since there is no direct correlation between energetics and diffusion, providing quantitative inferences about the profiles' shape is not trivial. Qualitatively, we can state that they reflect the geometry change of the system step by step during the relaxed scan. In particular the irregularities in $D_{\mathrm{ES}}(s)$ profile reflect the geometry changing in the excited state and they are not directly explicable. In order to check the reliability of this profile we performed the same calculation extending the domain of the internal coordinate θ, from 0° to 180°. In the domain $[90°, 180°]$ we retrieved the specular profile of $D_{\mathrm{ES}}(s)$ reported in Figure 4.4a (also for $D_{\mathrm{GS}}(s)$). This is a first indication that the computed $D_{\mathrm{ES}}(s)$ profile is reliable and together with the good results obtained from the calculation of fluorescence lifetime (*vide infra*) we can state *a posteriori* that $D_{\mathrm{ES}}(s)$ profile is trustworthy and we believe that there are not numerical artifacts in the diffusion computation. In Figure 4.4b we see the plot of the dipole moment μ in the excited state; as expected, the LE state has a lower dipole moment around 14.6 D that

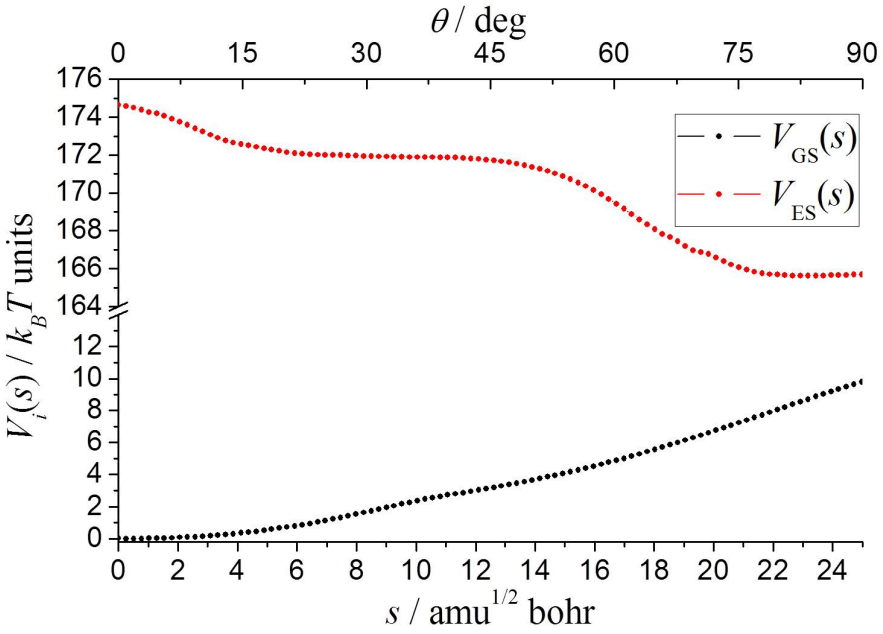

(a)

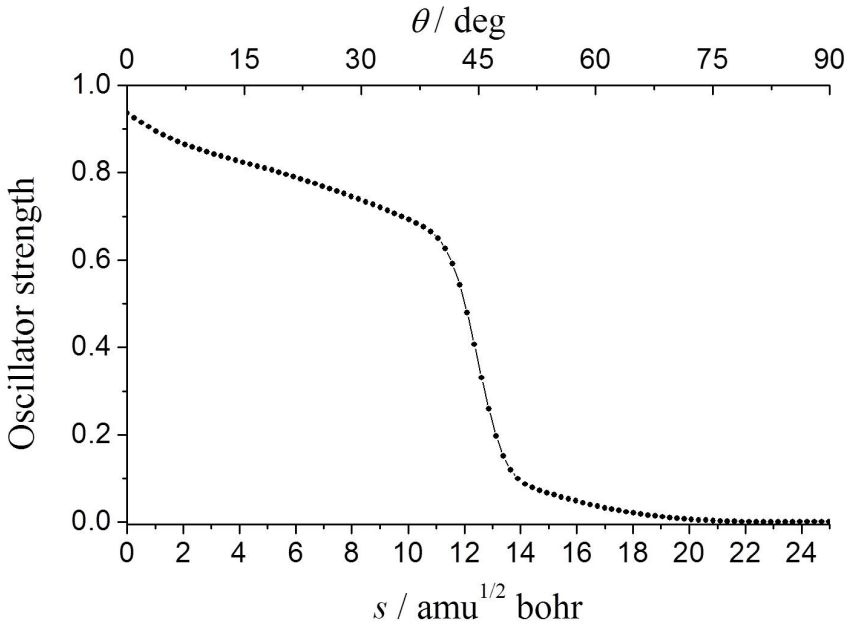

(b)

Figure 4.3: Panel a; calculated potential energies of S_0 (black line) and S_1 (red line) states, of DMABN from the relaxed scan in water. Panel b, oscillator strength plot for the $S_0 \rightarrow S_1$ transition. In the upper axis is shown the corresponding internal coordinate θ along which the scan is performed. ($T = 300K$) As expected, the oscillator strength falls from the LE to the TICT state, which is dark.

increases till its maximum (19.8 D) in the TICT state. The dipole moment at the ground state minimum is 10.4 D.

The rate constant term $k_{\mathrm{ES,GS}}(s)$ accounts for the continuous depletion of the excited state population due to radiative and non-radiative decay.

$$k_{\mathrm{ES,GS}}(s) = k^{\mathrm{r}}_{\mathrm{ES,GS}}(s) + k^{\mathrm{nr}}_{\mathrm{ES,GS}}(s) \tag{4.9}$$

These two separated contributions have been calculated using Fermi's golden rule (main theory and equations here used are reported in Appendix C). In Figure 4.5 we show the computed profiles of the radiative and non-radiative rate constants ($k^{\mathrm{r}}_{\mathrm{ES,GS}}(s)$ and $k^{\mathrm{nr}}_{\mathrm{ES,GS}}(s)$) as a function of the generalized coordinate. The non-radiative contribution dominates over the radiative one by a factor around 72. This compares fairly well to the ratio of 30 between the two for DMABN in *n*-butyl chloride at 150 K. [98] As expected, the emission rate is near zero at the charge transfer state conformation, because of orbital symmetry. Symmetrically, the non-radiative rate is lower at the LE state and reach a maximum around the TICT state.

After we have calculated all the above mentioned energetic, diffusion and reaction input parameters, we followed the excited state population dynamics $p_{\mathrm{ES}}(s,t)$ by means of eqn. (4.1). Just before the radiation pulse excitation, the ground state population is assumed to be at equilibrium, and after the laser pulse excitation the excited state population resembles the ground state one. Consequently, as initial population we have chosen

$$p_{\mathrm{ES}}(s,0) = p_{eq,\mathrm{GS}}(s) \tag{4.10}$$

In other words, the ground state energetics provides the initial distribution function on the excited state, after photon excitation.

In Figure 4.6 we plot the calculated probability density profile for the excited state, $p_{\mathrm{ES}}(s,t)$ as a function of the generalized coordinate s and time t, while in panel b we report the same computed at several times. The initial population quickly diffuses towards the TICT state and after 15 ps it is redistributed at the minimum; at the same time, it is disappearing due

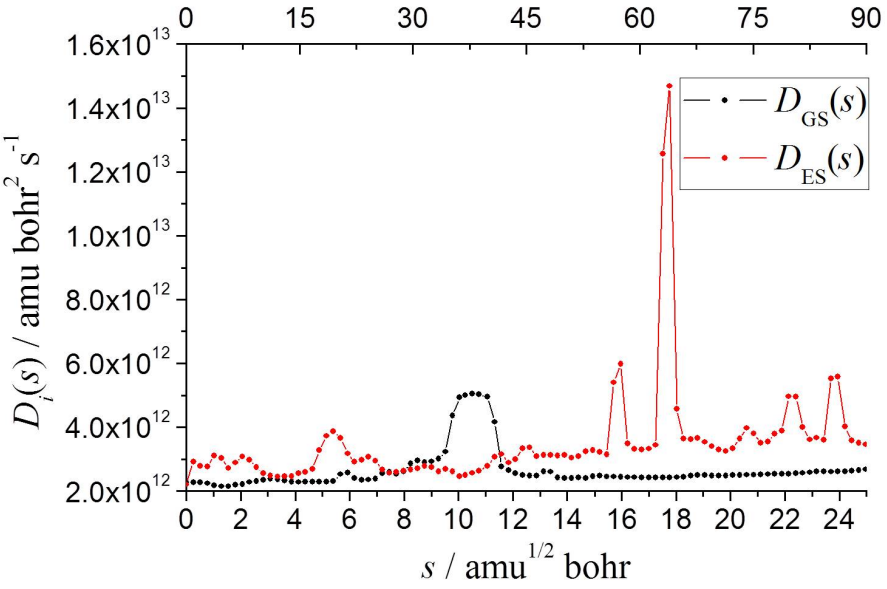

(a)

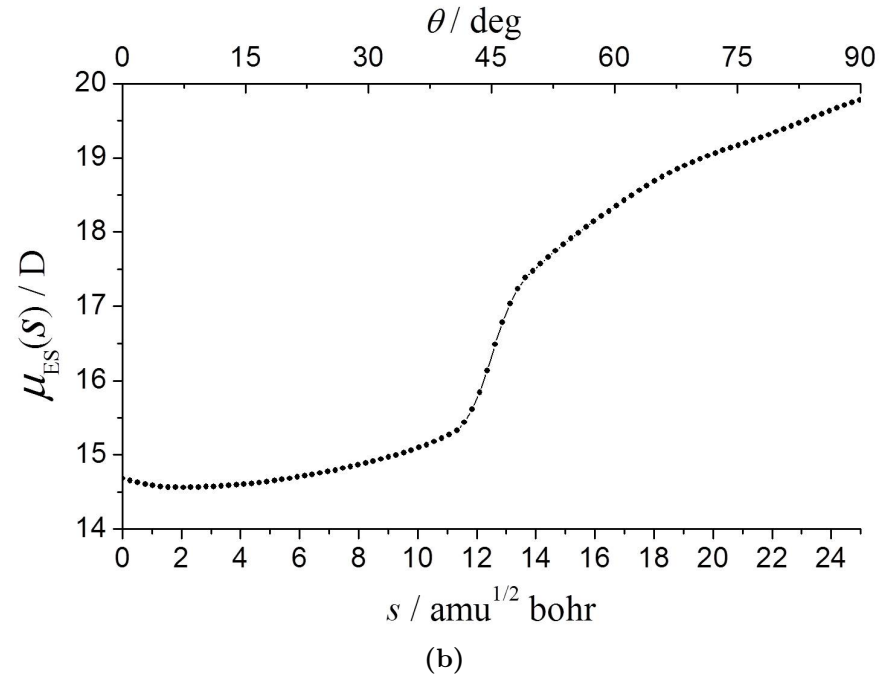

(b)

Figure 4.4: Panel a; diffusion function along the generalized coordinate for both the ground and excited states. Panel b; variation of the dipole moment of the S_1 state along the generalized coordinate. In the upper axis is shown the corresponding internal coordinate θ along which the scan is performed. ($T = 300K$) The dipole moment increases by approximately 5 D from the LE to the TICT state.

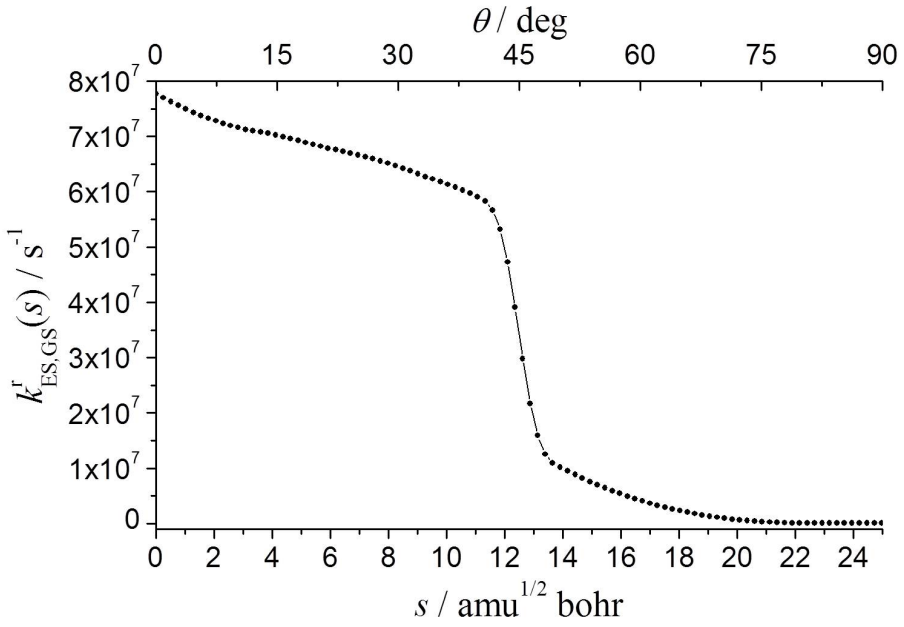

(a)

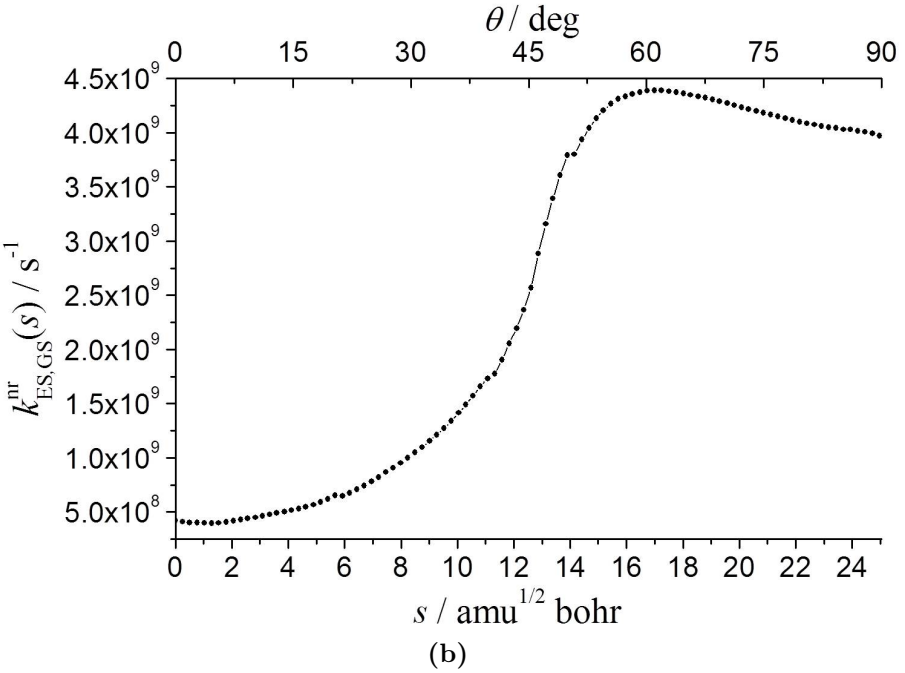

(b)

Figure 4.5: Panel a; radiative rate constant along the generalized coordinate; $k^{\mathrm{r}}_{\mathrm{ES,GS}}(s)$ falls sharply from the LE to the TICT state. Panel b; non-radiative rate constant along the generalized coordinate; $k^{\mathrm{nr}}_{\mathrm{ES,GS}}(s)$ increases from LE to TICT state which is predominantly a dark state. In the upper axis is shown the corresponding internal coordinate θ along which the scan is performed.

to the combined effect of reactive contribution and after 50 ps it relaxes back completely to the ground state. The migration to the TICT dark state (radiative contribution is approximately zero in this conformation) decreases the fluorescent population. The rate of this decay is affected both by diffusion and reaction.

In order to better state this effect we have calculated the time resolved emission spectrum of DMABN molecule using $p_{\mathrm{ES}}(s,t)$ using the relations reported in Appendix D. In panel a of Figure 4.7 we report the calculated time resolved fluorescence spectra as a function of the frequency ν and time t, while in panel b we report the same computed at several times. The parameters used for the line shape function, g are the asymmetry parameter $\gamma = -0.4$ and the bandwidth $\Delta = 3300$ cm^{-1}, while the electronic transition moment, $M(z)$ is collected from the Gaussian scan calculation output. It can be seen that the peak position shifts to red and the fluorescence intensity gradually decreases till a total loss of fluorescence emission occurs. In Figure 4.8 we have collected the peak intensities as a function of time (black dots and line) and fitted the peak intensity decay with a mono-exponential function (red line) in order to retrieve an approximate life time; $\tau = 12.98$ ps. This value is in good agreement with the measured life time of 15 ps of DMABN in water [106].

We also performed a similar set of calculations in n-hexane solution to determine the variation of the radiative and non-radiative rates with the rotation of the dimethyl group along the C–N bond. Hexane, being a non-polar solvent; results in a more pronounced character of the LE state and therefore, the relative variation of the radiative and non-radiative rates between the LE and TICT states is different from that in water.
For example, we see that the dipole moments of both states are lower by about 4 to 5 D in hexane, compared to those in the highly polar solvent water. The transition dipole moment shows an initial increase corresponding to the LE state and then from $\theta \sim 30°$, starts falling steadily to zero, as expected for the TICT state. This leads to an initial increase in the rate of radiative decay (in the order of 10^7 s^{-1}), followed by a steady decay to zero. This agrees very well to the already-mentioned fact that the TICT state is

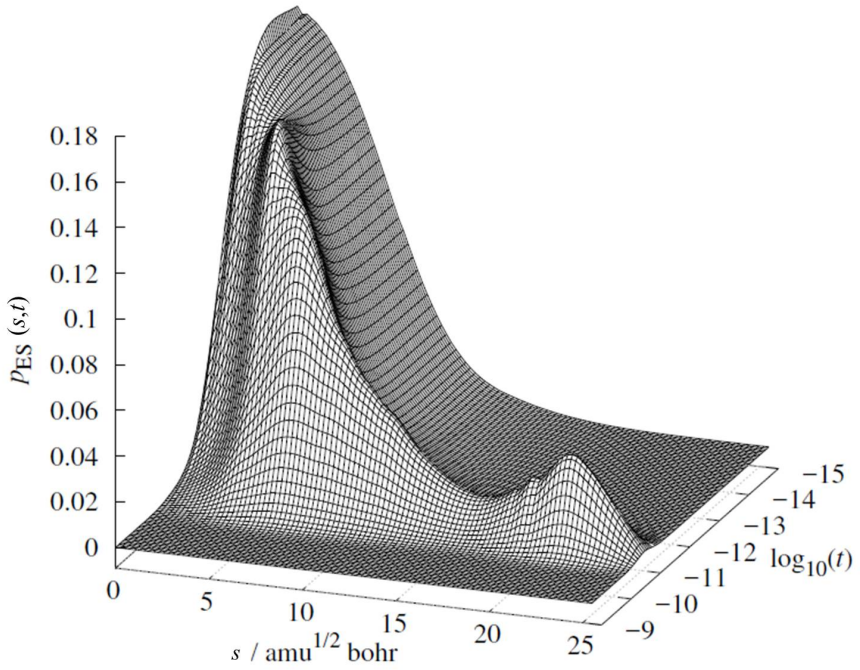

(a)

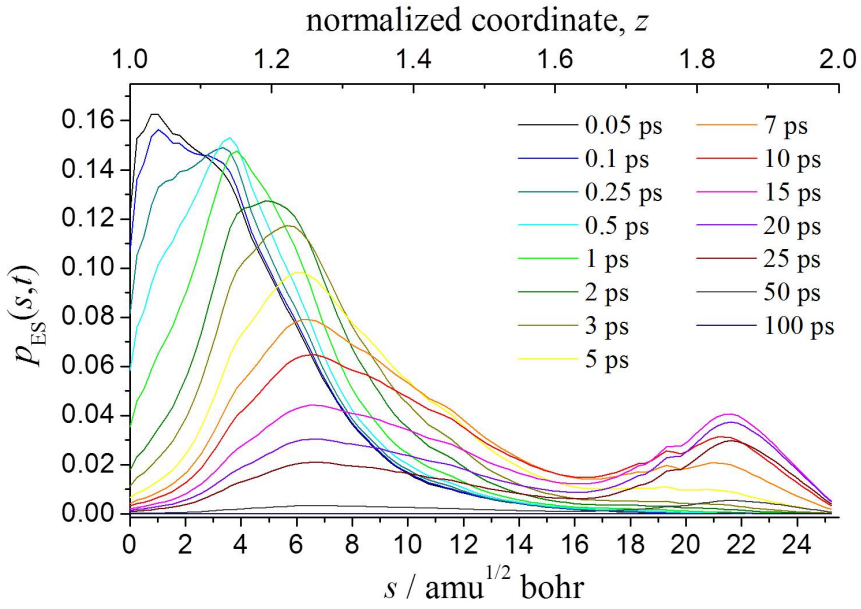

(b)

Figure 4.6: Panel a; calculated probability density profile along the generalized coordinate and along time. Panel b; The same probability density profile extrapolated at several times; in the upper axis is shown the corresponding normalized coordinate z used in the time resolved emission spectra calculation (see Appendix D).

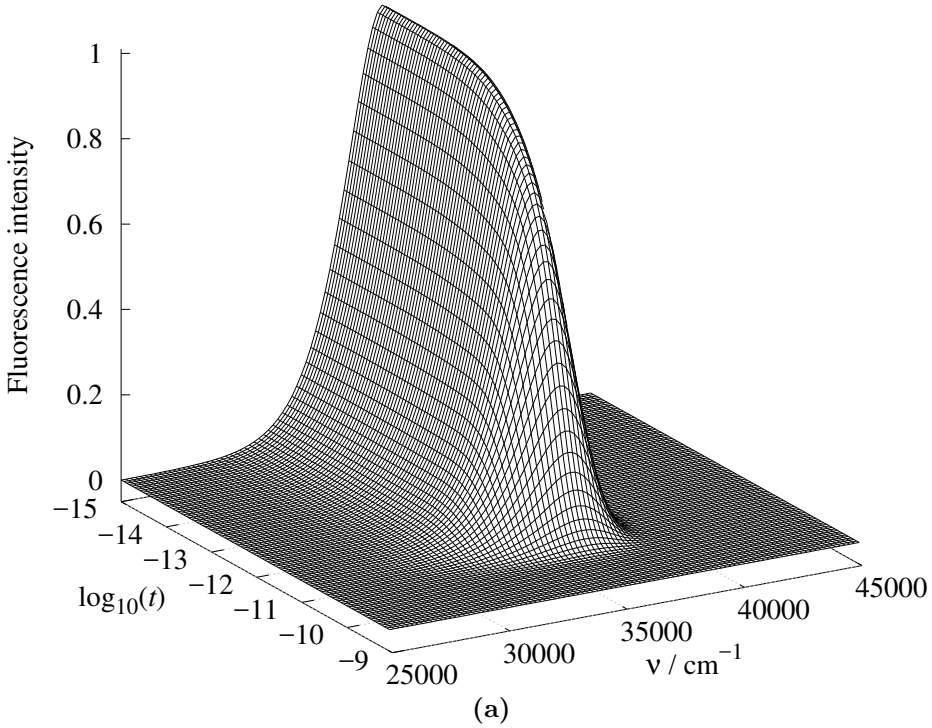

(a)

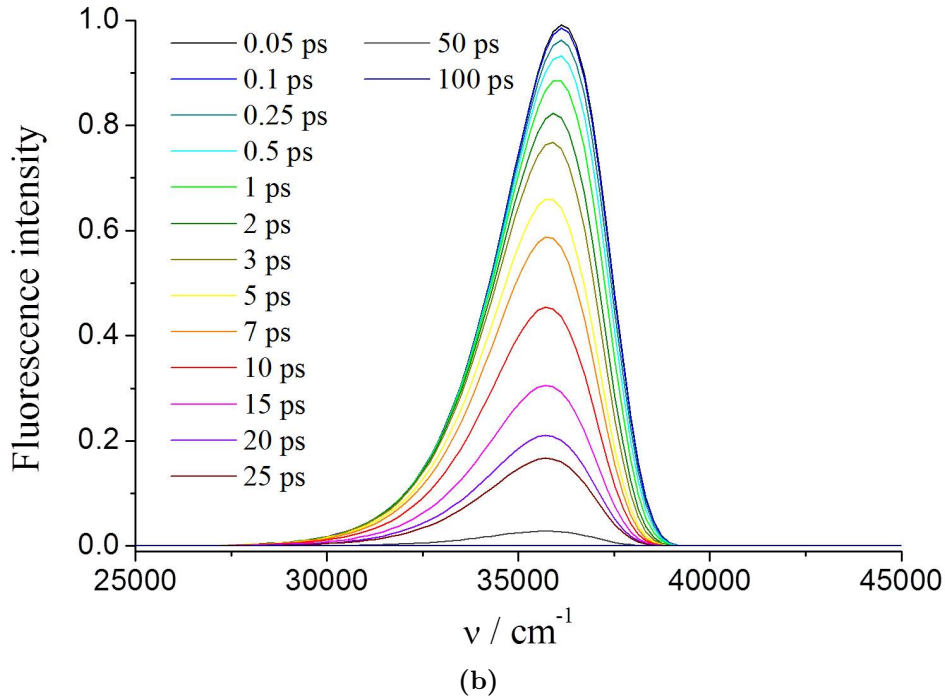

(b)

Figure 4.7: Panel a; calculated time resolved emission spectra. Panel b; The same spectra extrapolated at several times.

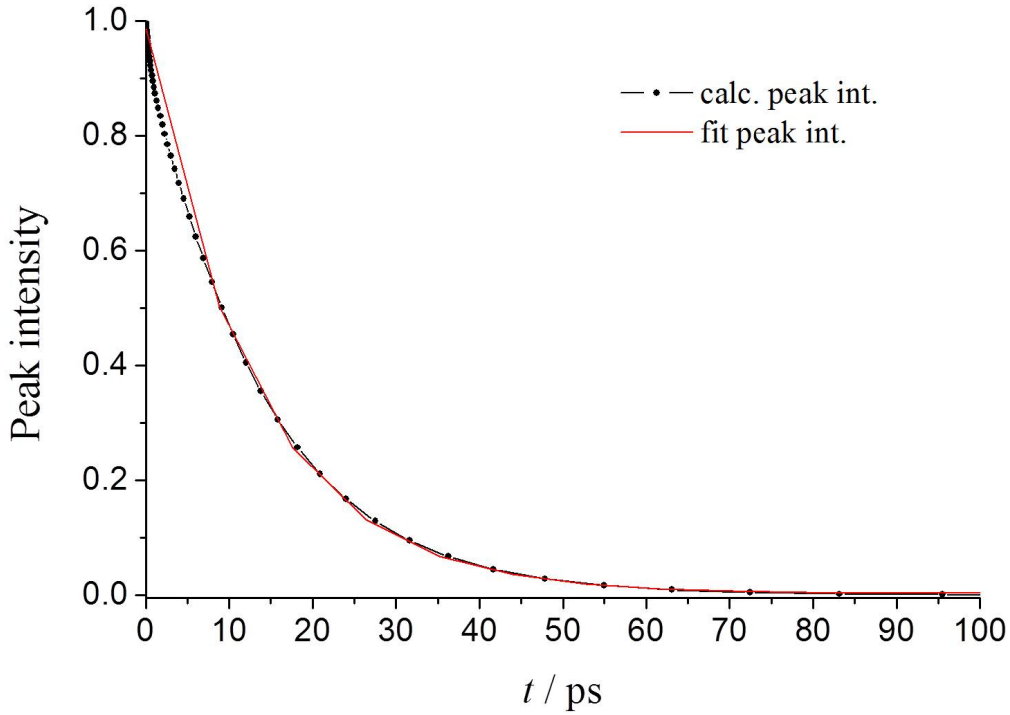

Figure 4.8: Calculated peak intensities of the DMABN time resolved spectrum along time (black dots and line) and mono-exponential fit (red line).

dark.
On the other hand, the rate of non-radiative decay shows a slow increase till $\theta = 30°$, from around 7.6×10^8 s^{-1} to 1.7×10^9 s^{-1}, and then shows a more pronounced increase till 3.2×10^9 s^{-1} corresponding to the dark TICT state. The data agree fairly well to previously reported data for DMABN in n-butyl chloride at 150 K, as also observed before for our simulations performed in water [98].

Existing literature on fluorescence quantum yields of DMABN in different solvents suggest that the effect of solvent relaxation on the same is not a very prominent one [107, 108, 109]. Polimeno and coworkers [98] suggest that fast relaxing solvents can alter the rate constant by a factor of about 0.82. In the methodology we followed, the solvent relaxation energy, can, in principle, be computed as a difference of the vertical excitation energies using the state-specific solvation scheme of the polarizable continuum model, within the equilibrium and non-equilibrium regimes. However, this means that two additional computations have to be performed at each of the scan geometries, which will increase considerably the computation time for medium sized systems such as DMABN. Although explicit consideration of dielectric friction is outside the scope of this work, we believe that since dielectric friction plays an important role in the kinetics of ionic systems or electrolytic solutions, for a neutral molecule such as DMABN, we can intuitively comment that the effect of dielectric friction can be neglected in the present scope of this work.

4.4 Final remarks

In this Chapter we have presented a general approach for the solution of coupled reactive one-dimensional Smoluchowski equations. This updated approach embedded in the Gaussian framework covers a wide class of chemical problems and overcomes the limitations of previous models. It allows for a generic treatment of diffusion coupled to reactivity coupled also to different possible diffusional states. The reliability of the solution is guaranteed by the consolidated numerical method of DVR presented and the inclusion of a generalized coordinate along which the system is evolving across more

general paths give access to more detailed information.

We have shown the robustness of our implementation with a test case, by comparing the calculated survival probability with an analytical one for a specific diffusional problem. Then we have considered a concrete example of chemical interest that is the fluorescence intensity decay for a TICT molecule. The computed evolution of the probability density of the excited state coupled to the ground state with a specific rate constant gives access to the spectra calculation. The modularity of the implemented code allows the integration of scan calculations with the computation of the generalized coordinate and the diffusion tensor along the same, reducing the input stage efforts for the generic user. If needed, these information can also be given manually.

A recent diabatization approach based on the dipole moments of the electronic states and the corresponding transition dipole moments was used to compute the rates of radiative and non-radiative transitions for the depletion of the excited state population. A definitive implementation of such theory in the above mentioned framework is currently under work in our group.

There are encouraging perspectives about the extension of the approach to more than one internal generalized coordinate leading to multidimensional coupled reactive Smoluchowski equations; this will be the main objective of our future investigations. Also a more versatile graphical input format interface, using the VMS software, is currently under implementation. It will facilitate the creation of complicated input files for diffusional computations and the understanding of difficult output files, allowing direct visualization of the results. The modularity of the software constructed as an integrated environment for electronic and magnetic spectroscopies will function as a base for future comparisons between collected experimental results and theoretical ones. The embedded scientific data visualizer for the analysis and processing of data will then ease the interpretation of results with the aid of different graphical tools.

In conclusion, apart from the further improvements and developments mentioned above, we think that, we already have at our disposal a quite powerful "black-box" machinery allowing us to complement experimental

and theoretical studies for a number of diffusional problems of fundamental and applicative interests.

Chapter 5

Conclusions

The research activity done in these years of my Ph.D. were focused on learning and understanding the basic concepts about stochastic dynamics of single molecules in liquid phases, and methods to practically treat the equations underlying the description of these processes. The work was constituted by the development of a part of formal elaboration over the manipulation of algebraic structures of the Smoluchowski equation in conjunction with the application of a new numerical method based on DVR. New approaches like the inclusion of a generalized coordinate and the computation of variable diffusion tensor along the same has opened the road for the development of a general and complete framework to set up and solve the one-dimensional Smoluchowski equation and more complicated descriptions like the system of coupled reactive Smoluchowski equations. Then we applied these instruments to the study of simple case models. The chosen cases were focused on the conformational dynamics of single molecules in liquid phase, this choice was mainly dictated by the fact that they are simple and good systems to perform preliminary tests. Also these molecular systems with few internal degrees of freedom have been widely studied over the past decades by means of Molecular Dynamics simulations, and this line of research seemed to be exhausted at the beginning of the nineties. By the way, the interest for such rapid conformational dynamics has been recently renewed thanks to the advancement of "fast" spectroscopic techniques that give access to experimen-

tal investigations over time scales of teens of ps. The results here presented open encouraging possibilities for dealing with more complicated systems, for example when multidimensional treatments are needed and traditional methods often become unfeasible. Apart from the chemical systems presented in this thesis, we believe that the approaches here presented can be applied to other areas of interest currently under study. In particular they could support the modern description of molecular motors where the conformational fluctuation is coupled to reactive events; *e.g.* photo-excitations, localized ATP hydrolysis, etc., [110]. The theoretical and numerical background is robust and general enough to allow extensions in several directions (*e.g.*, solution of Fokker-Planck or stochastic Liouville equations, multidimensional problems, free-energy rather than electronic-energy driven processes). To the best of our knowledge, there are no such works in the current literature, by the way, the ambitious target to apply the whole machinery to more complicated equations as Fokker-Planck and/or stochastic Liouville equation is not a trivial task. Methodological difficulties can be encountered when translating the concept of generalized coordinate and diffusion tensor along the same to the above mentioned equations. The passage to multidimensional cases implies the construction of multiple generalized coordinates carrying all the problematics mentioned in Section 3.5. In particular we want to remark that Markovian properties are not assured for complex system characterized by more than one degree of freedom and this represent still an open problem.

Appendix A

General theory of DVR

The theory that underlies DVR finds its mathematical roots upon the theory of Gaussian quadratures which is in turn intimately linked with the theory of orthogonal polynomials, even if it is possible to construct DVR starting from other orthogonal functions, like the sinc-DVR built from the Fourier basis (see below). Consider a set of polynomials $\rho(x)$ orthogonal with respect to a weight function $w(x) \geq 0$ on the interval $[a, b]$ (where a and b may be $\pm\infty$), with a scalar product defined as:

$$\langle \rho_m | \rho_n \rangle = \int_a^b dx\, w(x)\, \rho_m(x)\, \rho_n(x) = \delta_{mn} \tag{A.1}$$

The integral

$$I[f] = \int_a^b dx\, w(x)\, f(x) \tag{A.2}$$

may be written as

$$I[f] = \langle \rho_0 | f \rangle \tag{A.3}$$

with $\rho_0(x) \equiv 1$. An N-point quadrature approximation to the integral is defined by N points $\{x_1, \ldots, x_N\}$ and weights $\{w_1, \ldots, w_N\}$

$$I[f] = \sum_{i=1}^{N} w_i\, f(x_i) \tag{A.4}$$

and is exact for the first $2N$ orthogonal polynomials $\rho_0, \ldots, \rho_{2N-1}$. This is possible because there are precisely $2N$ parameters (x_i, w_i) that may be chosen. We want to eliminate the weight function from the definition of the scalar product, and in order to do so we introduce the functions

$$\phi_n(x) = \sqrt{w(x)}\,\rho_{n-1}(x), \qquad n = 1, \ldots, N \tag{A.5}$$

where we have absorbed the square root of the weight function. Then the orthonormality relations are given exactly by the quadrature

$$\langle \phi_m | \phi_n \rangle = \int_a^b dx\, \phi_m^*(x)\, \phi_n(x) = \delta_{mn} = \sum_{i=1}^{N} \frac{w_i}{w(x_i)}\, \phi_m^*(x_i) \phi_n(x_i) \tag{A.6}$$

and because of the Gaussian quadrature is exact for polynomials of degree $2N-1$ we also find that the quadrature approximations of the matrix elements

$$X_{mn} = \langle \phi_m | x | \phi_n \rangle = \sum_{i=1}^{N} \frac{w_i}{w(x_i)}\, \phi_m^*(x_i) x_i\, \phi_n(x_i) \tag{A.7}$$

are exact. If now we define the elements of the transformation matrix $\mathbf{U}$ as

$$U_{im} = \sqrt{\frac{w_i}{w(x_i)}}\, \phi_m(x_i) \tag{A.8}$$

we can easily see that $\mathbf{U}$ is a unitary matrix

$$(\mathbf{U}^\dagger \mathbf{U})_{mn} = \sum_{i=1}^{N} U_{im}^* U_{in} = \sum_{i=1}^{N} \frac{w_i}{w(x_i)}\, \phi_m^*(x_i)\, \phi_n(x_i) = \delta_{mn} \tag{A.9}$$

and that eqn. (A.7) can be rewritten in matrix form as

$$\mathbf{X} = \mathbf{U}^\dagger\, \mathbf{X}^{\mathrm{DVR}}\, \mathbf{U} \tag{A.10}$$

where $\mathbf{X}^{\mathrm{DVR}}$ is a diagonal matrix of DVR points $\{x_i\}$. Since $\mathbf{U}$ is unitary, eqn. (A.10) also states that DVR points can be found diagonalizing the coordinate matrix $\mathbf{X}$:

$$\mathbf{U}\, \mathbf{X}\, \mathbf{U}^\dagger = \mathbf{X}^{\mathrm{DVR}} \tag{A.11}$$

Thus the Gaussian quadrature points are the DVR points and $\mathbf{U}$ is the transformation between the so called Finite Basis Representation (FBR) and DVR. The idea of a DVR, is to apply the unitary transformation to the basis $\{\phi_1(x), \ldots, \phi_n(x)\}$

$$\theta_i(x) = \sum_{i=1}^{N} U^*_{im} \phi_m(x) \tag{A.12}$$

in order to have basis functions localized on grid points x_i

$$\theta_i(x_j) = \sum_{i=1}^{N} U^*_{im} \phi_m(x_j) = \sum_{i=1}^{N} \sqrt{\frac{w(x_j)}{w_j}}\, U^*_{im} U_{jm} = \sqrt{\frac{w(x_j)}{w_j}}\, \delta_{ij} \tag{A.13}$$

Thus, any multiplicative operator (*e.g.* $G(x)$ here) will be diagonal in this basis if quadrature approximation is used

$$(\mathbf{G}^{\mathrm{DVR}})_{jk} = \langle \theta_j | G(x) | \theta_k \rangle = \sum_{i=1}^{N} \frac{w_i}{w(x_i)}\, \theta^*_j(x_i)\, G(x_i)\, \theta_k(x_i) = G(x_i)\, \delta_{jk} \tag{A.14}$$

It is clear that different kind of operators, such as derivative operators ($\frac{d}{dx}, \frac{d^2}{dx^2}, \ldots$), will not be diagonal in a DVR and it will be necessary to find their representation in the chosen DVR basis, ($\mathbf{D}^{\mathrm{DVR}}$ in the text).

sinc-DVR

This DVR is constructed starting from Fourier basis; following Tannor [19] we show the similarity between this DVR and the ones built from a set of orthogonal polynomials. We consider the band limited Fourier orthogonal basis functions, *i.e.* functions that have no component of $|k|$ beyond K, and in the infinite x space range the basis functions are of the form

$$\phi_k(x) = \frac{e^{ikx}}{\sqrt{2\pi}}\ , \qquad -K \leq k \leq K\ , \qquad -\infty < x < \infty \tag{A.15}$$

The orthogonality relation is now expressed as

$$\begin{aligned}\langle\phi_{k'}|\phi_k\rangle &= \int_{-\infty}^{\infty} dx\, \phi^*_{k'}(x)\, \phi_k(x) = \int_{-\infty}^{\infty} dx\, \frac{e^{i(k-k')x}}{2\pi} = \delta(k-k') \\ &= \sum_{j=-\infty}^{\infty} \Delta x\, \phi^*_{k'}(x_j)\, \phi_k(x_j) = \sum_{j=-\infty}^{\infty} \Phi^*_{k'}(x_j)\, \Phi_k(x_j) \end{aligned} \tag{A.16}$$

Taking $\Delta x = \frac{2\pi}{2K}$, $x_j = j\Delta x = \frac{j\pi}{K}$, the basis orthogonality relation is exact for

$$\Phi_k(x_j) = \frac{e^{ikx_j}}{\sqrt{2K}} \tag{A.17}$$

In order to construct the DVR basis we perform a Fourier transform on the basis set, obtaining a basis that is complete for all band limited functions

$$\begin{aligned}\int_{-K}^{K} dk\, \Phi^*_k(x_j)\, \phi_k(x) = \theta_j(x) &= \int_{-K}^{K} dk\, \frac{e^{-ikx_j}}{\sqrt{2K}}\, \frac{e^{ikx}}{\sqrt{2\pi}} \\ &= \frac{\sin(K(x-x_j))}{\sqrt{\pi K}(x-x_j)} = \sqrt{\frac{K}{\pi}}\, \mathrm{sinc}[K(x-x_j)] \end{aligned} \tag{A.18}$$

It is readily seen that each sinc function is centered on a different grid point for a uniform grid, $x_j = j\Delta x$, with $\Delta x = \frac{\pi}{K}$; cfn. eqn. (2.14) in the text. Another simple derivation of this sinc-DVR starting with particle-in-a-box basis eqn. (2.15) is presented in Appendix A of ref. [14].

Appendix B

Finite difference scheme

The one-dimensional Smoluchowski equation (eqn. (2.5) in the text) can be compacted introducing the probability flux $J(x,t)$ as

$$\frac{\partial}{\partial t}\, p(x,t) = -\frac{\partial J(x,t)}{\partial x} \tag{B.1}$$

with

$$\frac{\partial J(x,t)}{\partial x} = -D(x)\, p_{eq}(x)\, \frac{\partial}{\partial x}\, p_{eq}^{-1}(x)\, p(x,t) \tag{B.2}$$

Given that x varies between the endpoints $x_{\min}$ and $x_{\max}$, we partition the domain $[x_{\min}, x_{\max}]$ into N intervals (here $N \equiv N_{\text{points}}$ in the text), each one labeled by the central point x_n belonging to the same interval and by its endpoints, respectively $x_n^- \equiv x_{n-1}^+$ (left) and $x_n^+ \equiv x_{n+1}^-$ (right). The intervals length is chosen to be the same; *i.e.* $\Delta x = \frac{x_{\min} - x_{\max}}{N}$. Eqn. (B.1) evaluated in the generic point x_n can be approximated as incremental ratio

$$\frac{\partial}{\partial t}\, p(x_n,t) = -\frac{\partial J(x_n,t)}{\partial x} \simeq -\frac{J(x_n^+,t) - J(x_n^-,t)}{\Delta x} \tag{B.3}$$

It is possible to set out the fluxes evaluated at the n-th interval endpoints using eqn. (B.2) and approximating again the derivative as incremental ratio. Collecting the factors and introducing the column vector $\mathbf{P}(t)$ with elements $P_n(t) = p(x_n,t)$ $(n = 1, 2, \ldots, N)$ one obtains the following matrix relation

$$\dot{\mathbf{P}}(t) = -\mathbf{\Gamma}(t)\, \mathbf{P}(t) \tag{B.4}$$

where $\mathbf{\Gamma}(t)$ is a tridiagonal matrix with elements

$$\Gamma_{n,m}(t) = \begin{cases} \delta_{m,n} \frac{p_{eq}^{-1}(x_n)}{\Delta x^2} \left[D(x_n^+)\, p_{eq}(x_n^+) + D(x_n^-)\, p_{eq}(x_n^-) \right] \\ -\delta_{m,n+1} \frac{p_{eq}^{-1}(x_{n+1})}{\Delta x^2} D(x_n^+)\, p_{eq}(x_n^+) \\ -\delta_{m,n-1} \frac{p_{eq}^{-1}(x_{n-1})}{\Delta x^2} D(x_n^-)\, p_{eq}(x_n^-) \end{cases} \tag{B.5}$$

To complete the procedure it is necessary to set the proper boundary conditions on fluxes in correspondence with the domain endpoints $x_{\min}, x_{\max} \equiv x_1^-, x_N^+$. For reflective boundary conditions, the flux at the endpoints must vanish

$$J(x_1^-, t) = 0 \quad \text{and} \quad J(x_N^+, t) = 0 \tag{B.6}$$

at any t. This implies that

$$\begin{aligned} \Gamma_{1,1}(t) &= \frac{p_{eq}^{-1}(x_1)}{\Delta x^2} D(x_1^+)\, p_{eq}(x_1^+) \\ \Gamma_{N,N}(t) &= \frac{p_{eq}^{-1}(x_N)}{\Delta x^2} D(x_N^-)\, p_{eq}(x_N^-) \end{aligned} \tag{B.7}$$

On the other hand, for periodic boundary conditions, it must be

$$J(x_1^-, t) = J(x_N^+, t) \tag{B.8}$$

at any t. This implies that

$$\begin{aligned} \Gamma_{1,1}(t) &= \frac{p_{eq}^{-1}(x_1)}{\Delta x^2} \left[D(x_1^+)\, p_{eq}(x_1^+) + D(x_1^-)\, p_{eq}(x_1^-) \right] \\ \Gamma_{1,N}(t) &= -\frac{p_{eq}^{-1}(x_N)}{\Delta x^2} D(x_1^-)\, p_{eq}(x_1^-) \\ \Gamma_{N,1}(t) &= -\frac{p_{eq}^{-1}(x_1)}{\Delta x^2} D(x_N^+)\, p_{eq}(x_N^+) \\ \Gamma_{N,N}(t) &= \frac{p_{eq}^{-1}(x_N)}{\Delta x^2} \left[D(x_N^+)\, p_{eq}(x_N^+) + D(x_N^-)\, p_{eq}(x_N^-) \right] \end{aligned} \tag{B.9}$$

Finally the eigenvalues λ^{FD}'s are found by diagonalizing $\mathbf{\Gamma}$.

Appendix C

Rate of internal conversion using adiabatic and diabatic electronic states

The first order rate constants of fluorescence (radiative) and internal conversion (non-radiative) between the S_1 and S_0 states have been computed from Fermi's golden rule as [111]

$$k = \frac{2\pi}{\hbar}\, V^2 f(\Delta E, T) \tag{C.1}$$

where V is the electronic coupling between the two states and ΔE is the adiabatic energy difference between them. The Franck-Condon weighted density of states $f(\Delta E, T)$ has been computed as the Fourier transform of a time-dependent correlation function $\chi(t)$; in the so-called time domain, the rate expression becomes [111]

$$k = V^2 Z^{-1} \int_{-\infty}^{\infty} dt\; e^{i\Delta E t}\; \chi(t) \tag{C.2}$$

where Z is the thermal vibrational partition function of the initial state.
For fluorescence, V is given by the square of the magnitude of the transition electric dipole moment $\boldsymbol{\mu}_{12}$.
For internal conversion, V has been computed using a diabatic representation

of the electronic states, as a function of the altering dihedral. This has been done to avoid possible singularities of the non-adiabatic coupling introduced by the nuclear kinetic energy operator, which brings about internal conversion between adiabatic states.

Diabatic states (Ψ_i^{dia}) can be expressed as a linear combination of adiabatic ones (Ψ_j^{adia}): [112]

$$\Psi_i^{\text{dia}} = \sum_{j=1}^{N} T_{ij} \Psi_j^{\text{adia}} \tag{C.3}$$

where $\mathbf{T}$ is an orthogonal transformation matrix. For transitions between two electronic states, the transformation matrix is obtained from a rotation angle θ as follows: [112]

$$\begin{pmatrix} \Psi_1^{\text{dia}} \\ \Psi_2^{\text{dia}} \end{pmatrix} = \begin{pmatrix} \cos\theta & \sin\theta \\ -\sin\theta & \cos\theta \end{pmatrix} \begin{pmatrix} \Psi_1^{\text{adia}} \\ \Psi_2^{\text{adia}} \end{pmatrix} \tag{C.4}$$

The recently developed dipole-quadrupole (DQ)-diabatization scheme by Truhlar and coworkers has been used to compute the rotation angle [112]. As the name suggests, the dipole- and quadrupole moments of the two electronic states and the corresponding transition moments are used to compute θ. For states involving distinctly different dipole moments, or excited states with charge transfer character, such as the TICT state for DMABN, the dipole moments are sufficient for diabatization. Here, the diabatic states are selected so that the following function f_D is maximized:

$$f_D = |\boldsymbol{\mu}_{11}|^2 + |\boldsymbol{\mu}_{22}|^2 + \quad P + \sqrt{(P^2 + Q^2)} \cos\left(4(\theta - \gamma)\right) \tag{C.5}$$

where P and Q are computed from the state and transition dipole moments,

$$Q = \boldsymbol{\mu}_{11} \cdot \boldsymbol{\mu}_{12} - \boldsymbol{\mu}_{12} \cdot \boldsymbol{\mu}_{22} \tag{C.6}$$

and

$$P = -\frac{|\boldsymbol{\mu}_{11}|^2 + |\boldsymbol{\mu}_{22}|^2}{4} + |\boldsymbol{\mu}_{12}|^2 + \frac{\boldsymbol{\mu}_{11} \cdot \boldsymbol{\mu}_{22}}{2} \tag{C.7}$$

with

$$\gamma = \arctan(-Q/P) \tag{C.8}$$

From eqn. (C.5), it can be easily shown that f_D is maximized when [112]

$$\theta = \gamma, \gamma + \pi/2, \ldots \tag{C.9}$$

Under the harmonic approximation, the time-dependent autocorrelation function can be evaluated analytically [111, 113]

$$\begin{aligned} \chi(t) &= \sqrt{\frac{\det(\bar{\mathbf{a}}\ \bar{\bar{\mathbf{a}}})}{\det(\mathbf{B})\ \det(\mathbf{B} - \mathbf{A}\mathbf{B^{-1}}\mathbf{A})}} \\ &\quad \times \exp\left[(i/\hbar)\left(\mathbf{K}^T\ (\bar{\mathbf{b}} - \bar{\mathbf{a}})\ \mathbf{J}(\mathbf{B} - \mathbf{A})^{-1}(\bar{\bar{\mathbf{b}}} - \bar{\bar{\mathbf{a}}})\ \mathbf{J}^T\ \mathbf{K}\right)\right] \end{aligned} \tag{C.10}$$

The matrices $\mathbf{A}$ and $\mathbf{B}$ are given as

$$\begin{aligned} \mathbf{A} &= \bar{\bar{\mathbf{a}}} + \mathbf{J}^T\ \bar{\mathbf{a}}\ \mathbf{J} \\ \mathbf{B} &= \bar{\bar{\mathbf{b}}} + \mathbf{J}^T\ \bar{\mathbf{b}}\ \mathbf{J} \end{aligned} \tag{C.11}$$

$\mathbf{J}$ is the Duschinsky matrix and $\mathbf{K}$ is the shift vector between the normal modes of the states.
The diagonal matrices $\bar{\mathbf{a}}$, $\bar{\bar{\mathbf{a}}}$, $\bar{\mathbf{b}}$ and $\bar{\bar{\mathbf{b}}}$ have elements

$$\begin{aligned} \bar{\mathrm{a}}_{\mathrm{jj}} &= \frac{\bar{\omega}_j}{\sin(\hbar\bar{\tau}\bar{\omega}_j)} \quad \bar{\bar{\mathrm{a}}}_{\mathrm{jj}} = \frac{\bar{\bar{\omega}}_j}{\sin(\hbar\bar{\bar{\tau}}\bar{\bar{\omega}}_j)} \\ \bar{\mathrm{b}}_{\mathrm{jj}} &= \frac{\bar{\omega}_j}{\tan(\hbar\bar{\tau}\bar{\omega}_j)} \quad \bar{\bar{\mathrm{b}}}_{\mathrm{jj}} = \frac{\bar{\bar{\omega}}_j}{\tan(\hbar\bar{\bar{\tau}}\bar{\bar{\omega}}_j)} \end{aligned} \tag{C.12}$$

where

$$\begin{aligned} \bar{\tau} &= -\frac{i}{k_B T} - \frac{t}{\hbar} \\ \bar{\bar{\tau}} &= \frac{t}{\hbar}, \end{aligned} \tag{C.13}$$

At 0 K, $\bar{\mathbf{b}}$ is substituted by the diagonal matrix $\bar{\mathbf{\Gamma}}$ with elements

$$\bar{\Gamma}_{\mathrm{jj}} = \frac{i\bar{\omega}_j}{\hbar} \tag{C.14}$$

Additionally, $\bar{\mathbf{a}}$ is set to zero everywhere; in the determinant pre-factor of eqn. (C.10), it is set to $\bar{\mathbf{\Gamma}}$.

Here, we have used the so-called vertical gradient (VG) approximation [113] for the vibronic simulations, *i.e.*, the Duschinsky matrix has been assumed to be the identity matrix, thus neglecting mode-mixing effects and the excited state PES has been assumed to be identical to the ground state PES. The gradient of the PES and the normal modes and frequencies of the initial state are used to approximate the shift vector.

Appendix D

Time resolved emission spectra calculation

The calculation of time resolved fluorescence spectrum makes use of the main relations presented in the Glasbeek model for femtosecond fluorescence studies in liquid solution [114, 115] and previously used by others [116]. Initially a normalized coordinate z is calculated, in our case we have chosen it between $[1, 2]$ where the endpoints correspond respectively to $\theta = 0°$ and $\theta = 90°$. The fluorescence intensity can be expressed as

$$I_{\mathrm{fl}}(\nu, t) \propto \int g(\nu_0(z), \nu - \nu_0(z))\, |M(z)|^2\, p(z, t)\, \nu^3\, dz \tag{D.1}$$

where $g(\nu_0(z), \nu - \nu_0(z))$ is a line shape function characterizing the Franck-Condon factor, $M(z)$ is the coordinate dependent electronic transition moment between the ground and the excited states, $p(z, t)$ is the probability density from eqn. (4.1) and ν the frequency.
For the Franck-Condon line shape function g, we used the following log-normal function used in the works cited above

$$g(\nu) = h \begin{cases} e^{-\ln 2\,(\ln(1+\alpha)/\gamma)^2} & \alpha > -1 \\ 0 & \alpha \leq -1 \end{cases} \tag{D.2}$$

$$\alpha := 2\,\frac{\gamma(\nu - \nu_0(z))}{\Delta} \tag{D.3}$$

where $\nu_0(z)$ is the coordinate dependent energy gap between S_1 and S_0, γ is the asymmetry parameter and Δ represents the bandwidth.

Bibliography

[1] A. Piserchia, V. Barone. Discrete variable representation of the Smoluchowski equation using a sinc basis set. *Phys. Chem. Chem. Phys.* **2015**, *17*, 17362–17374.

[2] A. Piserchia, V. Barone. Toward a General Yet Effective Computational Approach for Diffusive Problems: Variable Diffusion Tensor and DVR Solution of the Smoluchowski Equation along a General One-Dimensional Coordinate. *J. Chem. Theory Comput.* **2016**, *12*, 3482–3490.

[3] C. W. Gardiner, *Handbook of Stochastic Methods: For Physics, Chemistry and the Natural Sciences*, of *Springer series in synergetics*, Springer-Verlag Berlin Heidelberg, Germany, **1985**.

[4] N. G. Van Kampen, *Stochastic Processes in Physics and Chemistry*, of *North-Holland Personal Library*, Elsevier Science, Oxford, UK, **2011**.

[5] R. Zwanzig, *Nonequilibrium Statistical Mechanics*, Oxford University Press, New York, **2001**.

[6] A. Pedone, E. Gambuzzi, V. Barone, S. Bonacchi, D. Genovese, E. Rampazzo, L. Prodi, M. Montalti. Understanding the photophysical properties of coumarin-based Pluronic-silica (PluS) nanoparticles by means of time-resolved emission spectroscopy and accurate TDDFT/stochastic calculations. *Phys. Chem. Chem. Phys.* **2013**, *15*, 12360–12372.

[7] N. Agmon, J. J. Hopfield. Transient kinetics of chemical reactions with bounded diffusion perpendicular to the reaction coordinate: Intramolecular processes with slow conformational changes. *J. Chem. Phys.* **1983**, *78*, 6947–6959.

[8] E. Pines, D. Huppert, N. Agmon. Geminate recombination in excited-state proton-transfer reactions: Numerical solution of the Debye-Smoluchowski equation with backreaction and comparison with experimental results. *J. Chem. Phys.* **1988**, *88*, 5620–5630.

[9] G. J. Moro, P. L. Nordio, A. Polimeno. Multivariate Diffusion Models of Dielectric Friction and TICT Transitions. *Mol. Phys.* **1989**, *68*, 1131–1141.

[10] N. Agmon, E. Pines, D. Huppert. Geminate Recombination in Proton-Transfer Reactions. II. Comparison of Diffusional and Kinetic Schemes. *J. Chem. Phys.* **1988**, *88*, 5631–5638.

[11] N. Agmon, J. J. Hopfield. CO Binding to Heme Proteins: A Model for Barrier Height Distributions and Slow Conformational Changes. *J. Chem. Phys.* **1983**, *79*, 2042–2053.

[12] P. Banushkina, M. Meuwly. Hierarchical Numerical Solution of Smoluchowski Equations with Rough Potentials. *J. Chem. Theory Comput.* **2005**, *1*, 208–214.

[13] J. Dunkel, W. Ebeling, L. Schimansky-Geier, P. Hänggi. Kramers problem in evolutionary strategies. *Phys. Rev. E* **2003**, *67*, 061118.

[14] D. T. Colbert, W. H. Miller. A novel discrete variable representation for quantum mechanical reactive scattering via the S-matrix Kohn method. *J. Chem. Phys.* **1992**, *96*, 1982–1991.

[15] G. H. Gardenier, M. A. Johnson, A. B. McCoy. Spectroscopic Study of the Ion-Radical H-Bond in $H_4O_2^+$. *J. Phys. Chem. A* **2009**, *113*, 4772–4779.

[16] H. Wei, T. Carrington. Discrete variable representations of complicated kinetic energy operators. *J. Chem. Phys.* **1994**, *101*, 1343–1360.

[17] G. C. Groenenboom, D. T. Colbert. Combining the discrete variable representation with the S-matrix Kohn method for quantum reactive scattering. *J. Chem. Phys.* **1993**, *99*, 9681–9696.

[18] D. Luckhaus. 6D vibrational quantum dynamics: Generalized coordinate discrete variable representation and (a)diabatic contraction. *J. Chem. Phys.* **2000**, *113*, 1329–1347.

[19] D. J. Tannor, *Introduction to Quantum Mechanics: A Time-dependent Perspective*, University Science Books, **2007**.

[20] J. C. Light, T. Carrington, *Discrete-Variable Representations and their Utilization*, *Vol. 114*, John Wiley & Sons, Inc., **2007**, pp. 263–310.

[21] V. Szalay. Discrete variable representations of differential operators. *J. Chem. Phys.* **1993**, *99*, 1978–1984.

[22] J. C. Light, I. P. Hamilton, J. V. Lill. Generalized discrete variable approximation in quantum mechanics. *J. Chem. Phys.* **1985**, *82*, 1400–1409.

[23] Z. Bačić, J. C. Light. Theoretical Methods for Rovibrational States of Floppy Molecules. *Annu. Rev. Phys. Chem.* **1989**, *40*, 469–498.

[24] G. E. Uhlenbeck, L. S. Ornstein. On the Theory of the Brownian Motion. *Phys. Rev.* **1930**, *36*, 823–841.

[25] H. Risken, *The Fokker-Planck Equation: Methods of Solution and Applications*, of *Lecture Notes in Mathematics*, Springer Berlin Heidelberg, **1996**.

[26] P. Hänggi, P. Talkner, M. Borkovec. Reaction-rate theory: fifty years after Kramers. *Rev. Mod. Phys.* **1990**, *62*, 251–341.

[27] H. Yu, A. N. Gupta, X. Liu, K. Neupane, A. M. Brigley, I. Sosova, M. T. Woodside. Energy landscape analysis of native folding of the prion protein yields the diffusion constant, transition path time, and rates. *Proc. Natl. Acad. Sci. USA* **2012**, *109*, 14452–14457.

[28] K. Neupane, A. P. Manuel, M. T. Woodside. Protein folding trajectories can be described quantitatively by one-dimensional diffusion over measured energy landscapes. *Nature Physics* **2016**, *12*, 700–703.

[29] H. A. Kramers. Brownian motion in a field of force and the diffusion model of chemical reactions. *Physica* **1940**, *7*, 284–304.

[30] O. Edholm, O. Leimar. The accuracy of Kramers' theory of chemical kinetics. *Physica* **1979**, *98A*, 313–324.

[31] V. Barone, M. Zerbetto, A. Polimeno. Hydrodynamic modeling of diffusion tensor properties of flexible molecules. *J. Comput. Chem.* **2009**, *30*, 2–13.

[32] J. Zheng, K. Kwak, J. Xie, M. D. Fayer. Ultrafast Carbon-Carbon Single-Bond Rotational Isomerization in Room-Temperature Solution. *Science* **2006**, *313*, 1951–1955.

[33] W. L. Jorgensen, J. D. Madura, C. J. Swenson. Optimized intermolecular potential functions for liquid hydrocarbons. *J. Am. Chem. Soc.* **1984**, *106*, 6638–6646.

[34] J. Huang, K. Hedberg. Conformational analysis. 14. The dihaloethanes $ClCH_2CH_2F$, $BrCH_2CH_2F$, and $BrCH_2CH_2Cl$. Investigations of the molecular structures, rotameric compositions, anti and gauche energy and entropy differences, and barriers hindering internal rotation by gas-phase electron diffraction augmented by rotational constants and ab initio calculation. *J. Am. Chem. Soc.* **1990**, *112*, 2070–2075.

[35] G. Moro, P. L. Nordio. Diffusive and jump description of hindered motions. *Mol. Phys.* **1985**, *56*, 255–269.

[36] G. Moro, P. L. Nordio. Diffusion between inequivalent sites. *Mol. Phys.* **1986**, *57*, 947–955.

[37] A. Ferrarini, G. Moro, P. L. Nordio. Conformational kinetics of aliphatic tails. *Mol. Phys.* **1988**, *63*, 225–247.

[38] B. Nigro, D. Di Stefano, A. Rassu, G. J. Moro. Cranklike conformational transitions in polyethylene. *J. Chem. Phys.* **2004**, *121*, 4364–4376.

[39] J. G. De La Torre, V. A. Bloomfield. Hydrodynamic properties of complex, rigid, biological macromolecules: theory and applications. *Q. Rev. Biophys.* **1981**, *14*, 81–139.

[40] J. G. De La Torre, M. L. Huertas, B. Carrasco. HYDRONMR: Prediction of {NMR} Relaxation of Globular Proteins from Atomic-Level Structures and Hydrodynamic Calculations. *J. Magn. Reson. B* **2000**, *147*, 138–146.

[41] K. Fukui. Formulation of the reaction coordinate. *J. Phys. Chem.* **1970**, *74*, 4161–4163.

[42] A. Amadei, A. B. M. Linssen, H. J. C. Berendsen. Essential dynamics of proteins. *Proteins: Struct., Funct., Bioinf.* **1993**, *17*, 412–425.

[43] V. Barone. Characterization of the potential energy surface of the HO_2 molecular system by a density functional approach. *J. Chem. Phys.* **1994**, *101*, 10666–10676.

[44] N. Rega, M. Cossi, V. Barone. Intrinsic and Environmental Effects in the Structure and Magnetic Properties of Glycine Radical in Aqueous Solution. *J. Am. Chem. Soc.* **1997**, *119*, 12962–12967.

[45] R. Improta, V. Barone. Interplay of Electronic, Environmental, and Vibrational Effects in Determining the Hyperfine Coupling Constants of Organic Free Radicals. *Chem. Rev.* **2004**, *104*, 1231–1254.

[46] D. Skouteris, D. Calderini, V. Barone. Methods for Calculating Partition Functions of Molecules Involving Large Amplitude and/or Anharmonic Motions. *J. Chem. Theory Comput.* **2016**, *12*, 1011–1018.

[47] K. Fukui. The path of chemical reactions - the IRC approach. *Acc. Chem. Res.* **1981**, *14*, 363–368.

[48] W. H. Miller, N. C. Handy, J. E. Adams. Reaction path Hamiltonian for polyatomic molecules. *J. Chem. Phys.* **1980**, *72*, 99–112.

[49] M. J. Frisch, G. W. Trucks, H. B. Schlegel, G. E. Scuseria, M. A. Robb, J. R. Cheeseman, G. Scalmani, V. Barone, B. Mennucci, G. A. Petersson, H. Nakatsuji, M. Caricato, X. Li, H. P. Hratchian, J. Bloino, B. G. Janesko, A. F. Izmaylov, F. Lipparini, G. Zheng, J. L. Sonnenberg, W. Liang, M. Hada, M. Ehara, K. Toyota, R. Fukuda, J. Hasegawa, M. Ishida, T. Nakajima, Y. Honda, O. Kitao, H. Nakai, T. Vreven, K. Throssell, J. A. Montgomery Jr., J. E. Peralta, F. Ogliaro, M. Bearpark, J. J. Heyd, E. Brothers, K. N. Kudin, V. N. Staroverov, T. Keith, R. Kobayashi, J. Normand, K. Raghavachari, A. Rendell, J. C. Burant, S. S. Iyengar, J. Tomasi, M. Cossi, N. Rega, J. M. Millam, M. Klene, J. E. Knox, J. B. Cross, V. Bakken, C. Adamo, J. Jaramillo, R. Gomperts, R. E. Stratmann, O. Yazyev, A. J. Austin, R. Cammi, C. Pomelli, J. W. Ochterski, R. L. Martin, K. Morokuma, V. G. Zakrzewski, G. A. Voth, P. Salvador, J. J. Dannenberg, S. Dapprich, P. V. Parandekar, N. J. Mayhall, A. D. Daniels, O. Farkas, J. B. Foresman, J. V. Ortiz, J. Cioslowski, D. J. Fox, *Gaussian Development Version, Revision I.03*, Gaussian, Inc., Wallingford, CT, **2015**.

[50] V. Barone, M. Brustolon, P. Cimino, A. Polimeno, M. Zerbetto, A. Zoleo. Development and Validation of an Integrated Computational Approach for the Modeling of cw-ESR Spectra of Free Radicals in Solution: p-(Methylthio)phenyl Nitronylnitroxide in Toluene as a Case Study. *J. Am. Chem. Soc.* **2006**, *128*, 15865–15873.

[51] S. Carlotto, P. Cimino, M. Zerbetto, L. Franco, C. Corvaja, M. Crisma, F. Formaggio, C. Toniolo, A. Polimeno, V. Barone. Unraveling Solvent-

Driven Equilibria between α- and 310-Helices through an Integrated Spin Labeling and Computational Approach. *J. Am. Chem. Soc.* **2007**, *129*, 11248–11258.

[52] M. Zerbetto, S. Carlotto, A. Polimeno, C. Corvaja, L. Franco, C. Toniolo, F. Formaggio, V. Barone, C. P. Ab Initio Modeling of CW-ESR Spectra of the Double Spin Labeled Peptide Fmoc-(Aib-Aib-TOAC)2-Aib-OMe in Acetonitrile. *J. Phys. Chem. B* **2007**, *111*, 2668–2674.

[53] M. Zerbetto, A. Polimeno, P. Cimino, V. Barone. On the interpretation of continuous wave electron spin resonance spectra of tempo-palmitate in 5-cyanobiphenyl. *J. Chem. Phys.* **2008**, *128*, 024501.

[54] M. Zerbetto, A. Polimeno, V. Barone. Simulation of electron spin resonance spectroscopy in diverse environments: An integrated approach. *Comput. Phys. Commun.* **2009**, *180*, 2680–2697.

[55] M. Zerbetto, D. Licari, V. Barone, A. Polimeno. Computational tools for the interpretation of electron spin resonance spectra in solution. *Mol. Phys.* **2013**, *111*, 2746–2756.

[56] M. Zerbetto, D. Kotsyubynskyy, J. Kowalewski, G. Widmalm, A. Polimeno. Stochastic Modeling of Flexible Biomolecules Applied to NMR Relaxation. I. Internal Dynamics of Cyclodextrins: γ-Cyclodextrin as a Case Study. *J. Phys. Chem. B* **2012**, *116*, 13159–13171.

[57] D. Kotsyubynskyy, M. Zerbetto, M. Soltesova, O. Engström, R. Pendrill, J. Kowalewski, G. Widmalm, A. Polimeno. Stochastic Modeling of Flexible Biomolecules Applied to NMR Relaxation. 2. Interpretation of Complex Dynamics in Linear Oligosaccharides. *J. Phys. Chem. B* **2012**, *116*, 14541–14555.

[58] A. Piserchia, M. Zerbetto, M. Salvia, G. Salassa, L. Gabrielli, F. Mancin, F. Rastrelli, D. Frezzato. Conformational Mobility in Monolayer-Protected Nanoparticles: From Torsional Free Energy Profiles to NMR Relaxation. *J. Phys. Chem. C* **2015**, *119*, 20100–20110.

[59] V. Szalay. Eckart-Sayvetz conditions revisited. *J. Chem. Phys.* **2014**, *140*, 234107–234119.

[60] G. R. Kneller. Superposition of Molecular Structures using Quaternions. *Mol. Simul.* **1991**, *7*, 113–119.

[61] G. Moro. Coupling of the overall molecular motion with the conformational transitions. II. The full rotational problem. *Chem. Phys.* **1987**, *118*, 181–197.

[62] H. Goldstein, C. P. Poole, J. L. Safko, *Classical Mechanics*, Addison Wesley, Boston, **2002**.

[63] H. B. Thompson. Calculation of Cartesian Coordinates and Their Derivatives from Internal Molecular Coordinates. *J. Chem. Phys.* **1967**, *47*, 3407–3410.

[64] J. G. Kirkwood, J. Riseman. The Intrinsic Viscosities and Diffusion Constants of Flexible Macromolecules in Solution. *J. Chem. Phys.* **1948**, *16*, 565–573.

[65] H. Yamakawa. Transport Properties of Polymer Chains in Dilute Solution: Hydrodynamic Interaction. *J. Chem. Phys.* **1970**, *53*, 436–443.

[66] J. Rotne, S. Prager. Variational Treatment of Hydrodynamic Interaction in Polymers. *J. Chem. Phys.* **1969**, *50*, 4831–4837.

[67] A. K. Rappe, C. J. Casewit, K. S. Colwell, W. A. Goddard III, W. M. Skiff. UFF, a full periodic table force field for molecular mechanics and molecular dynamics simulations. *J. Am. Chem. Soc.* **1992**, *114*, 10024–10035.

[68] S. Grimme. Semiempirical hybrid density functional with perturbative second-order correlation. *J. Chem. Phys.* **2006**, *124*, 034108.

[69] M. Biczysko, P. Panek, G. Scalmani, J. Bloino, V. Barone. Harmonic and Anharmonic Vibrational Frequency Calculations with the Double-

Hybrid B2PLYP Method: Analytic Second Derivatives and Benchmark Studies. *J. Chem. Theory Comput.* **2010**, *6*, 2115–2125.

[70] R. A. Kendall, T. H. Dunning, R. J. Harrison. Electron affinities of the first-row atoms revisited. Systematic basis sets and wave functions. *J. Chem. Phys.* **1992**, *96*, 6796–6806.

[71] S. Grimme, J. Antony, S. Ehrlich, H. Krieg. A consistent and accurate ab initio parametrization of density functional dispersion correction (DFT-D) for the 94 elements H-Pu. *J. Chem. Phys.* **2010**, *132*, 154104.

[72] M. Cossi, N. Rega, G. Scalmani, V. Barone. Energies, structures, and electronic properties of molecules in solution with the C-PCM solvation model. *J. Comput. Chem.* **2003**, *24*, 669–681.

[73] J. Tomasi, B. Mennucci, R. Cammi. Quantum Mechanical Continuum Solvation Models. *Chem. Rev.* **2005**, *105*, 2999–3094.

[74] R. Edberg, D. J. Evans, G. P. Morriss. Conformational kinetics in liquid butane by nonequilibrium molecular dynamics. *J. Chem. Phys.* **1987**, *87*, 5700–5708.

[75] C. L. Yaws, *Transport Properties of Chemicals and Hydrocarbons*, Elsevier Science, Oxford, UK, **2014**.

[76] A. D. Becke. Density-functional thermochemistry. III. The role of exact exchange. *J. Chem. Phys.* **1993**, *98*, 5648–5652.

[77] E. B. Krissinel', N. Agmon. Spherical symmetric diffusion problem. *J. Comput. Chem.* **1996**, *17*, 1085–1098.

[78] R. Gepshtein, D. Huppert, N. Agmon. Deactivation Mechanism of the Green Fluorescent Chromophore. *J. Phys. Chem. B* **2006**, *110*, 4434–4442.

[79] Y. Erez, Y. Liu, N. Amdursky, D. Huppert. Modeling the Nonradiative Decay Rate of Electronically Excited Thioflavin T. *J. Phys. Chem. A* **2011**, *115*, 8479–8487.

[80] T. Carrington, W. H. Miller. Reaction surface Hamiltonian for the dynamics of reactions in polyatomic systems. *J. Chem. Phys.* **1984**, *81*, 3942–3950.

[81] D. P. Tew, N. C. Handy, S. Carter. A reaction surface Hamiltonian study of malonaldehyde. *J. Chem. Phys.* **2006**, *125*, 084313i.

[82] R. Dawes, T. Carrington. A multidimensional discrete variable representation basis obtained by simultaneous diagonalization. *J. Chem. Phys.* **2004**, *121*, 726–736.

[83] I. Degani, D. J. Tannor. Calculating Multidimensional Discrete Variable Representations from Cubature Formulas. *J. Phys. Chem. A* **2006**, *110*, 5395–5410.

[84] A. Baiardi, J. Bloino, V. Barone. Accurate Simulation of Resonance-Raman Spectra of Flexible Molecules: An Internal Coordinates Approach. *J. Chem. Theory Comput.* **2015**, *11*, 3267–3280.

[85] A. Baiardi, J. Bloino, V. Barone. General formulation of vibronic spectroscopy in internal coordinates. *J. Chem. Phys.* **2016**, *144*, 084114.

[86] V. Barone. Vibrational zero-point energies and thermodynamic functions beyond the harmonic approximation. *J. Chem. Phys.* **2004**, *120*, 3059–3065.

[87] V. Barone, M. Biczysko, J. Bloino. Fully anharmonic IR and Raman spectra of medium-size molecular systems: accuracy and interpretation. *Phys. Chem. Chem. Phys.* **2014**, *16*, 1759–1787.

[88] S. A. Maluendes, M. Dupuis. A dynamic reaction coordinate approach to abinitio reaction pathways: Application to the 1,5 hexadiene Cope rearrangement. *J. Chem. Phys.* **1990**, *93*, 5902–5911.

[89] A. Laio, M. Parrinello. Escaping free-energy minima. *Proc. Natl. Acad. Sci. USA* **2002**, *99*, 12562–12566.

[90] C. Jarzynski. Equilibrium free-energy differences from nonequilibrium measurements: A master-equation approach. *Phys. Rev. E* **1997**, *56*, 5018–5035.

[91] G. E. Crooks. Path-ensemble averages in systems driven far from equilibrium. *Phys. Rev. E* **2000**, *61*, 2361–2366.

[92] J. C. Equalities and Inequalities: Irreversibility and the Second Law of Thermodynamics at the Nanoscale. *Annu. Rev. Condens. Matter Phys.* **2011**, *2*, 329–351.

[93] D. Collin, F. Ritort, C. Jarzynski, S. B. Smith, I. Tinoco, C. Bustamante. Verification of the Crooks fluctuation theorem and recovery of RNA folding free energies. *Nature Letters* **2005**, *437*, 231–234.

[94] C. Jarzynski. Nonequilibrium work relations: foundations and applications. *Eur. Phys. J. B* **2008**, *64*, 331–340.

[95] G. Giacometti, G. J. Moro, P. L. Nordio, A. Polimeno. Diffusive Coupling of Internal and Solvent Coordinates in Conformational Transitions Involving Electron Transfer. *J. Mol. Liq.* **1989**, *42*, 19–30.

[96] A. Barbon, P. L. Nordio, A. Polimeno. Intramolecular Electron Transfer Reaction in Dimethylaminobenzonitrile. *Mol. Cryst. Liq. Crys. A* **1993**, *234*, 69–78.

[97] N. Agmon, S. Rabinovich. Diffusive Dynamics on Potential Energy Surfaces: Nonequilibrium CO Binding to Heme Proteins. *J. Chem. Phys.* **1992**, *97*, 7270–7286.

[98] A. Polimeno, A. Barbon, P. L. Nordio, W. Rettig. Stochastic Model for Solvent-Assisted Intramolecular Charge-Transfer. *J. Phys. Chem.* **1994**, *98*, 12158–12168.

[99] *LAPACK Users' Guide 3rd ed.*, Society for Industrial and Applied Mathematics, Philadelphia, PA, **1999**.

[100] D. Licari, A. Baiardi, M. Biczysko, F. Egidi, C. Latouche, V. Barone. Implementation of a graphical user interface for the virtual multifrequency spectrometer: The VMS-Draw tool. *J. Comput. Chem.* **2015**, *36*, 321–334.

[101] V. Barone. The Virtual Multifrequency Spectrometer: a New Paradigm for Spectroscopy. *WIREs Comput. Mol. Sci.* **2016**, *6*, 86–110.

[102] G. H. Weiss. A Perturbation Analysis of the Wilemski–Fixman Approximation for Diffusion-Controlled Reactions. *J. Chem. Phys.* **1984**, *80*, 2880–2887.

[103] A. Dreuw, M. Head-Gordon. Single-Reference ab Initio Methods for the Calculation of Excited States of Large Molecules. *Chem. Rev.* **2005**, *105*, 4009–4037.

[104] T. Yanai, D. P. Tew, N. C. Handy. A new hybrid exchange-correlation functional using the Coulomb-attenuating method (CAM-B3LYP). *Chem. Phys. Lett.* **2004**, *393*, 51–57.

[105] J. P. Ryckaert, A. Bellemans. Molecular dynamics of liquid alkanes. *Faraday Discuss. Chem. Soc.* **1978**, *66*, 95–106.

[106] Y. H. Kim, D. W. Cho, M. Yoon, D. Kim. Observation of Hydrogen-Bonding Effects on Twisted Intramolecular Charge Transfer of p-(N,N-Diethylamino)benzoic Acid in Aqueous Cyclodextrin Solutions. *J. Phys. Chem.* **1996**, *100*, 15670–15676.

[107] M. Van der Auweraer, Z. R. Grabowski, W. Rettig. Molecular structure and the temperature-dependent radiative rates in Twisted Intramolecular Charge-Transfer and exciplex systems. *J. Phys. Chem.* **1991**, *95*, 2083–2092.

[108] T. C. Swinney, D. F. Kelley. Proton-transfer and solvent polarization dynamics in 3-hydroxyflavone. 2. Mixed solvents. *J. Phys. Chem.* **1991**, *95*, 10369–10373.

[109] P. J. Stiles, J. B. Hubbard, R. F. Kayser. Dielectric saturation and dielectric friction in electrolyte solutions. *J. Chem. Phys.* **1982**, *77*, 6189–6196.

[110] A. B. Kolomeisky, M. B. Fisher. Molecular Motors: A Theorist's Perspective. *Annu. Rev. Phys. Chem.* **2007**, *58*, 675–695.

[111] S. Banerjee, A. Baiardi, J. Bloino, V. Barone. Temperature Dependence of Radiative and Nonradiative Rates from Time-Dependent Correlation Function Methods. *J. Chem. Theory Comput.* **2016**, *12*, 774–786.

[112] C. E. Hoyer, X. Xu, D. Ma, L. Gagliardi, D. G. Truhlar. Diabatization based on the dipole and quadrupole: The DQ method. *J. Chem. Phys.* **2014**, *141*, 114104.

[113] A. Baiardi, J. Bloino, V. Barone. General Time Dependent Approach to Vibronic Spectroscopy Including Franck-Condon, Herzberg-Teller, and Duschinsky Effects. *J. Chem. Theory Comput.* **2013**, *9*, 4097–4115.

[114] M. J. Van der Meer, H. Zhang, M. Glasbeek. Femtosecond fluorescence upconversion studies of barrierless bond twisting of auramine in solution. *J. Chem. Phys.* **2000**, *112*, 2878–2887.

[115] M. Glasbeek, H. Zhang. Femtosecond Studies of Solvation and Intramolecular Configurational Dynamics of Fluorophores in Liquid Solution. *Chem. Rev.* **2004**, *104*, 1929–1954.

[116] K. Tominaga, G. C. Walker, W. Jarzeba, P. F. Barbara. Ultrafast charge separation in ADMA: experiment, simulation, and theoretical issues. *J. Phys. Chem.* **1991**, *95*, 10475–10485.